

University of Louisville

ThinkIR: The University of Louisville's Institutional Repository

Electronic Theses and Dissertations

12-2022

The role of MMP-3 in copper oxide nanoparticle-induced pulmonary inflammation and fibrosis.

Yuanbao Zhang
University of Louisville

Follow this and additional works at: <https://ir.library.louisville.edu/etd>



Part of the [Environmental Public Health Commons](#)

Recommended Citation

Zhang, Yuanbao, "The role of MMP-3 in copper oxide nanoparticle-induced pulmonary inflammation and fibrosis." (2022). *Electronic Theses and Dissertations*. Paper 4017.
<https://doi.org/10.18297/etd/4017>

This Doctoral Dissertation is brought to you for free and open access by ThinkIR: The University of Louisville's Institutional Repository. It has been accepted for inclusion in Electronic Theses and Dissertations by an authorized administrator of ThinkIR: The University of Louisville's Institutional Repository. This title appears here courtesy of the author, who has retained all other copyrights. For more information, please contact thinkir@louisville.edu.

THE ROLE OF MMP-3 IN COPPER OXIDE NANOPARTICLE-INDUCED
PULMONARY INFLAMMATION AND FIBROSIS

By

Yuanbao Zhang

B.S., Anhui Medical University, 2012

M.S., Beijing Municipal Institute of Labor Protection, 2015

A Dissertation

Submitted to the Faculty of the

School of Public Health and Information Sciences of the University of Louisville

In Partial Fulfillment of the Requirements

for the Degree of

Doctor of Philosophy

in Public Health Sciences

Department of Environmental and Occupational Health Sciences

Department of Epidemiology and Population Health

University of Louisville

Louisville, Kentucky

December 2022

Copyright 2022 by Yuanbao Zhang

All Rights Reserved

THE ROLE OF MMP-3 IN COPPER OXIDE NANOPARTICLE-INDUCED
PULMONARY INFLAMMATION AND FIBROSIS

By

Yuanbao Zhang
B.S., Anhui Medical University, 2012
M.S., Beijing Municipal Institute of Labor Protection, 2015

Dissertation Approved on

November 17, 2022

By the following Dissertation Committee

Qunwei Zhang, Ph.D.

Shao-yu Chen, Ph.D.

Gary W. Hoyle, Ph.D.

Rachel Neal, Ph.D.

Jerry Yu, Ph.D.

DEDICATION

This dissertation is dedicated to

My parents

Mr. Guanbiao Zhang

&

Ms. Faxia Du

who have given me endless love, encouragement, and support.

ACKNOWLEDGEMENTS

I would like to express my deep gratitude to my mentor, Dr. Qunwei Zhang, for his professional guidance and endless support during my stay over the past four years. I am especially grateful to benefit from his personality and diligence, which will guide me for the rest of my life.

I would also like to thank my committee members, Dr. Shao-yu Chen, Dr. Gary W. Hoyle, Dr. Rachel Neal, and Dr. Jerry Yu, for their suggestions and support over the past two years. They have provided me with helpful guidance and valuable advice. I express my heartfelt appreciation to them for their patience and time in serving on my dissertation committee.

Many thanks also go to the members in Dr. Zhang's lab. I truly appreciate Dr. Yiqun Mo for everything she has taught and trained me, and I hope to continue learning from her. I thank Dr. Jiali Yuan and other former members for all their help in life and study.

My appreciation also goes to Ms. Barbara J. Parker, for her valuable help and kindness during my study in Louisville. I also thank Ms. Robin L. Newlon, Dr. Robert R. Jacobs, and other members in the former Department of Environmental and Occupational Health Sciences and Department of Epidemiology and Population Health for all their help.

I must thank my wife, Yueyue, for her encouragement and support. Last but not the least, I would like to thank my beloved parents, my baby daughter, and other members of my family, for their endless love and support.

ABSTRACT

THE ROLE OF MMP-3 IN COPPER OXIDE NANOPARTICLE-INDUCED PULMONARY INFLAMMATION AND FIBROSIS

Yuanbao Zhang

November 17, 2022

Copper oxide nanoparticles (Nano-CuO) are widely used in medical and industrial fields and our daily necessities. However, the biosafety assessment of Nano-CuO is far behind their rapid development. This study was to investigate the potential mechanisms underlying Nano-CuO-induced pulmonary inflammation and fibrosis, especially to determine whether Nano-CuO exposure could dysregulate MMP-3, an important mediator in pulmonary fibrosis, and its roles in Nano-CuO-induced pulmonary inflammation and fibrosis.

Aim 1 was to investigate whether exposure to Nano-CuO caused MMP-3 dysregulation in lung epithelial cells and the role of MMP-3 in Nano-CuO-induced alteration of cell junction-associated proteins. The potential mechanisms that might be involved in these effects were also explored. The results demonstrated that exposure to Nano-CuO, but not Nano-TiO₂, caused increased ROS generation, MAPKs activation, and MMP-3 expression. Nano-CuO-induced ROS generation was not observed in mitochondrial DNA-depleted BEAS-2B ρ⁰ cells, indicating that

mitochondria may be the main source of Nano-CuO-induced ROS generation, which was also confirmed by pretreatment of cells with Mito-TEMPO, a specific mitochondrial ROS inhibitor. In addition, pretreatment of cells with ROS scavengers or inhibitors or depleting mitochondrial DNA significantly attenuated Nano-CuO-induced MAPKs activation and MMP-3 upregulation, and pretreatment of cells with MAPKs inhibitors abolished Nano-CuO-induced MMP-3 upregulation, suggesting Nano-CuO-induced MMP-3 upregulation is through Nano-CuO-induced ROS generation and MAPKs activation. Moreover, exposure of BEAS-2B cells to Nano-CuO for 48 h resulted in decreased expression of tight junction-associated proteins such as zonula occludens protein-1 (ZO-1), occludin, and claudin-1, and adherens junction-associated protein E-cadherin, which were inhibited by MMP-3 siRNA transfection, suggesting an important role of MMP-3 in Nano-CuO-induced alterations of cell junction-associated proteins.

Aim 2 was to examine whether Nano-CuO exposure could activate fibroblasts and the role of MMP-3 and OPN in this process. The results showed that exposure to non-cytotoxic doses of Nano-CuO caused a dose-dependent increase in MMP-3 expression and activity and OPN expression in both BEAS-2B cells and PMA-differentiated U937 macrophages (U937*), but not in MRC-5 fibroblasts. Nano-CuO exposure also increased the production of MMP-3-cleaved OPN fragment, and the cleavage of OPN was abolished by MMP-3 siRNA transfection in BEAS-2B and U937* cells. Conditioned media from Nano-CuO-exposed BEAS-2B, U937*, or the co-culture of BEAS-2B and U937* caused activation of unexposed MRC-5 fibroblasts, which was reflected by increased

expression of α -smooth muscle actin (α -SMA), Col1A1, and fibronectin. However, direct exposure to Nano-CuO did not induce the activation of MRC-5 fibroblasts. In a triple co-culture system, exposure of BEAS-2B and U937* cells to Nano-CuO caused activation of unexposed MRC-5 fibroblasts, while transfection of MMP-3 siRNA in BEAS-2B and U937* cells significantly inhibited the activation and migration of MRC-5 fibroblasts, suggesting that MMP-3 released from Nano-CuO-exposed BEAS-2B and U937* cells may play a key role in Nano-CuO-induced activation of MRC-5 fibroblasts. Furthermore, pretreated MRC-5 fibroblasts with GRGDSP, an RGD-containing peptide that interrupts the binding of MMP-3-cleaved OPN to its cell surface receptors, attenuated Nano-CuO-induced activation and migration of fibroblasts in the triple co-culture system, indicating that MMP-3-cleaved OPN is engaged in the activation of MRC-5 fibroblasts caused by Nano-CuO.

Aim 3 was to investigate the role of MMP-3 in Nano-CuO-induced lung injury and fibrosis *in vivo*. Our results demonstrated that mice intratracheally exposed to Nano-CuO (0, 25, 50, 100 μ g per mouse) resulted in a dose-dependent increase in acute lung inflammation at day 3 after exposure, which was evidenced by elevated neutrophil count, and the levels of total protein and LDH in BALF. Nano-CuO-induced acute lung inflammation was further confirmed histologically by the infiltration of excessive neutrophils into lung alveolar space and interstitial tissues. In the time-course study, Nano-CuO exposure caused increases in the neutrophil count, and the levels of total protein and LDH in BALF, which appeared as early as day 1 after exposure, peaked at day 3 and then declined. Although the total cell

count, macrophage count, and LDH level in BALF decreased from day 14 after exposure, their levels were still higher than those in the control group at days 28 and 42 post-exposure, suggesting that Nano-CuO exposure caused chronic inflammation in mouse lungs. Nano-CuO-caused fibrosis were observed in the lung sections evidenced by trichrome staining at days 14, 28, and 42 post-exposure. Nano-CuO-induced fibrosis was further confirmed by increased hydroxyproline content and fibrosis-related proteins, such as α -SMA, Col1A1, and fibronectin. Nano-CuO exposure also caused persistent expression of MMP-3 in mouse lungs from day 1 to day 42 post-exposure. Elevated MMP-3 protein levels in BALF were confirmed by Western blot. To explore the role of MMP-3 in Nano-CuO-induced lung inflammation and fibrosis, mouse Ambion® *In vivo* Pre-designed MMP-3 siRNA was chosen. MMP-3 siRNA treatment significantly ameliorated the acute lung inflammation and injury caused by Nano-CuO. MMP-3 siRNA treatment also restored the downregulated cell junction-associated proteins such as ZO-1, occludin, and E-cadherin in mouse lungs caused by Nano-CuO. Furthermore, MMP-3 siRNA treatment alleviated Nano-CuO-induced chronic inflammation and fibrosis in mouse lungs. These results suggest that MMP-3 plays important roles in Nano-CuO-induced pulmonary inflammation, injury, and fibrosis.

In summary, this study showed that exposure to Nano-CuO could cause ROS generation which further leads to MMP-3 production in lung epithelial cells. Increased MMP-3 production caused disruption of cell junction-associated proteins, initiating and promoting Nano-CuO-induced lung inflammation, injury, and fibrosis. Findings in this study could provide insights into the interventions that

prevent metal nanoparticle-induced lung injury and fibrosis. Findings in this study also provide the scientific basis to establish the exposure limits of metal oxide nanoparticles.

TABLE OF CONTENTS

	PAGE
ACKNOWLEDGEMENTS.....	iv
ABSTRACT	vi
LIST OF FIGURES	xvii
CHAPTER I: INTRODUCTION	1
1.1 Copper oxide nanoparticles.....	1
1.2 Lung toxicity of Nano-CuO	1
1.3 MMP-3 and pulmonary inflammation and fibrosis	4
1.4 MMP-3 and lung epithelial barrier.....	9
1.5 MMP-3 and fibroblast activation	13
1.6 Specific aims	15
CHAPTER II: DETERMINE WHETHER EXPOSURE TO NANO-CUO WOULD CAUSE MMP-3 PRODUCTION IN LUNG EPITHELIAL CELLS AND THE ROLE OF MMP-3 IN NANO-CUO-INDUCED ALTERATIONS OF CELL JUNCTION- ASSOCIATED PROTEINS	16
2.1 Introduction	16
2.2 Materials and methods	18
2.2.1 Nanoparticles and their characterization	18

2.2.2 Chemicals and reagents	18
2.2.3 Cell culture	19
2.2.4 Cytotoxicity of metal oxide nanoparticles	19
2.2.5 Detection of ROS generation	20
2.2.6 Generation of BEAS-2B Rho-0 (ρ^0) cells.....	21
2.2.7 Extraction of total RNA and real-time PCR	22
2.2.8 β -casein and gelatin zymography assays	24
2.2.9 Protein extraction and Western blot	25
2.2.10 Transfection of BEAS-2B cells with MMP-3 siRNA	26
2.2.11 Immunofluorescent staining	26
2.2.12 Statistical analysis.....	27
2.3 Results	28
2.3.1 Cytotoxicity of Nano-CuO and Nano-TiO ₂ in BEAS-2B cells.....	28
2.3.2 ROS generation in BEAS-2B cells exposed to Nano-CuO, but not to Nano-TiO ₂	28
2.3.3 Role of Nano-CuO-induced ROS on MAPKs activation	34
2.3.4 Effects of Nano-CuO on MMP-3 production.....	39
2.3.5 Effects of Nano-CuO-induced ROS and MAPKs activation on MMP-3 expression.....	43
2.3.6 Nano-CuO exposure caused downregulation of tight and adherens junction-associated proteins in lung epithelial BEAS-2B cells.....	48

2.3.7 The role of MMP-3 in Nano-CuO-induced downregulation of tight and adherens junction-associated proteins.....	53
2.4 Discussion.....	57
CHAPTER III: EXAMINE WHETHER NANO-CUO EXPOSURE WOULD ACTIVATE FIBROBLASTS AND THE ROLE OF MMP-3 AND OPN IN THIS PROCESS.....	
3.1 Introduction	64
3.2 Materials and methods	68
3.2.1 Nanoparticles and their characterization	68
3.2.2 Chemicals and reagents	68
3.2.3 Cell culture	69
3.2.4 Collection of conditioned media	69
3.2.5 Triple co-culture model.....	70
3.2.6 Cytotoxicity assays.....	71
3.2.7 Wound healing assay.....	71
3.2.8 β -casein zymography assay.....	72
3.2.9 Protein extraction and Western blot	72
3.2.10 Transfection of BEAS-2B and U937* cells with MMP-3 siRNA	72
3.2.11 Statistical analysis.....	73
3.3 Results	74
3.3.1 Cytotoxic effects of Nano-CuO on MRC-5, U937*, and BEAS-2B cells	74

3.3.2 Exposure to Nano-CuO increased the expression and activity of MMP-3 in BEAS-2B and U937* cells, but not in MRC-5 cells	76
3.3.3 Exposure to Nano-CuO caused upregulation of OPN in BEAS-2B and U937* cells, but not in MRC-5 cells.....	80
3.3.4 The role of MMP-3 in Nano-CuO-induced production of cleaved-OPN84	
3.3.5 Direct Nano-CuO exposure did not activate MRC-5 cells	86
3.3.6 Conditioned media from Nano-CuO-exposed BEAS-2B or U937* cells caused activation of unexposed MRC-5 fibroblasts	88
3.3.7 Conditioned media from Nano-CuO-exposed co-culture of BEAS-2B and U937* cells caused activation of unexposed MRC-5 fibroblasts	92
3.3.8 Exposure of BEAS-2B and U937* cells to Nano-CuO caused activation of unexposed MRC-5 fibroblasts in a triple co-culture system	95
3.3.9 The role of MMP-3 in Nano-CuO-induced activation of MRC-5 cells in the triple co-culture system	98
3.3.10 The role of MMP-3-cleaved OPN in activation of unexposed MRC-5 cells in triple co-culture system	102
3.4 Discussion.....	106
CHAPTER IV: INVESTIGATE THE ROLE OF MMP-3 IN NANO-CUO-INDUCED LUNG INFLAMMATION, INJURY, AND FIBROSIS <i>IN VIVO</i>	116
4.1 Introduction	116
4.2 Materials and methods	117
4.2.1 Nanoparticles and their characterization	117

4.2.2 Animals	117
4.2.3 Exposure of mice to Nano-CuO	118
4.2.4 MMP-3 siRNA delivery in mice.....	118
4.2.5 Preparation of bronchoalveolar lavage fluid (BALF).....	119
4.2.6 Biochemical analysis of BALF	120
4.2.7 Lung histology and trichrome staining.....	120
4.2.8 Hydroxyproline assay.....	121
4.2.9 Total RNA extraction and real-time PCR.....	122
4.2.10 Protein isolation and Western blot.....	123
4.2.11 Statistical analysis.....	124
4.3 Results	125
4.3.1 Dose- and time- response studies after Nano-CuO exposure.....	125
4.3.2 Nano-CuO exposure upregulated MMP-3 in mouse lungs.....	130
4.3.3 Nano-CuO exposure downregulated cell junction-associated proteins in mouse lungs.....	132
4.3.4 Nano-CuO exposure induced overexpression of pro-inflammatory cytokines and fibrosis-related genes.....	134
4.3.5 Nano-CuO exposure induced lung inflammation and fibrosis in mice	136
4.3.6 Knocking-down MMP-3 ameliorated Nano-CuO-induced acute lung inflammation and injury in mice.....	142
4.3.7 Knocking-down MMP-3 ameliorated Nano-CuO-induced downregulation of cell junction-associated proteins in mouse lungs	148

4.3.8 Knocking-down MMP-3 alleviated Nano-CuO-caused chronic lung inflammation and fibrosis in mice	150
4.4 Discussion.....	155
CHAPTER V: SUMMARY AND CONCLUSION	162
REFERENCES	166
CURRICULUM VITAE	181

LIST OF FIGURES

Figure 1. Cytotoxicity of Nano-CuO and Nano-TiO ₂ on human lung epithelial (BEAS-2B) cells.	30
Figure 2. Effects of Nano-CuO and Nano-TiO ₂ on ROS generation in BEAS-2B cells, and the effects of ROS scavengers, mitochondria-targeted ROS inhibitor, or mitochondrial DNA depletion on Nano-CuO-induced ROS generation.	31
Figure 3. Validation of the depletion of mtDNA in BEAS-2B ρ^0 cells.	33
Figure 4. Dose- and time- dependent activation of MAPKs in BEAS-2B cells exposed to Nano-CuO.	35
Figure 5. Effects of ROS scavenger or mitochondrial DNA depletion on Nano-CuO-induced MAPKs activation in human lung epithelial cells.	37
Figure 6. Dose- and time- dependent induction of MMP-3 in BEAS-2B cells exposed to metal oxide nanoparticles.	40
Figure 7. Dose- and time- dependent studies of TIMP-1 and TIMP-4 mRNA expression in BEAS-2B cells exposed to Nano-CuO.	42
Figure 8. Effects of ROS scavengers or inhibitors, and mitochondrial DNA depletion on Nano-CuO-induced MMP-3 expression.	45

Figure 9. Effects of MAPKs inhibitors on Nano-CuO-induced MMP-3 upregulation in BEAS-2B cells.....	47
Figure 10. Dose- and time-dependent effects of Nano-CuO exposure on tight junction-associated proteins in BEAS-2B cells.....	49
Figure 11. Dose- and time- dependent effects of Nano-CuO exposure on adherens junction-associated protein E-cadherin in BEAS-2B cells.	51
Figure 12. The efficiency of MMP-3 siRNA transfection and the effects of MMP-3 siRNA on MMP-2 and MMP-9 activities in BEAS-2B cells.	54
Figure 13. The role of MMP-3 on Nano-CuO-induced downregulation of tight junction-associated proteins in BEAS-2B cells.....	55
Figure 14. The role of MMP-3 on Nano-CuO-induced downregulation of adherens junction-associated protein E-cadherin in BEAS-2B cells.	56
Figure 15. Cytotoxicity of Nano-CuO on human MRC-5 fibroblasts and U937-derived macrophages.	75
Figure 16. Increased secretion of MMP-3 in BEAS-2B cells and U937* macrophages exposed to Nano-CuO.....	78
Figure 17. Increased MMP-3 activity in BEAS-2B and U937* cells exposed to Nano-CuO.....	79
Figure 18. Increased expression of OPN in BEAS-2B cells and U937* macrophages exposed to Nano-CuO.....	81
Figure 19 Increased production of cleaved-OPN in BEAS-2B cells and U937* macrophages exposed to Nano-CuO.....	83

Figure 20. The role of MMP-3 on Nano-CuO-induced production of cleaved-OPN in BEAS-2B cells and U937* macrophages.	85
Figure 21. Direct Nano-CuO exposure had no effects on activation of MRC-5 fibroblasts.....	87
Figure 22. Conditioned media from Nano-CuO-exposed BEAS-2B or U937* cells caused activation of unexposed MRC-5 fibroblasts.	89
Figure 23. Conditioned media from Nano-CuO-exposed BEAS-2B or U937* cells enhanced migration of unexposed MRC-5 fibroblasts.	91
Figure 24. Conditioned media from Nano-CuO-exposed co-culture of BEAS-2B and U937* cells caused activation of unexposed MRC-5 fibroblasts.	93
Figure 25. Exposure of BEAS-2B and U937* cells to Nano-CuO caused activation of unexposed MRC-5 fibroblasts in a triple co-culture system.	96
Figure 26. The role of MMP-3 on Nano-CuO-induced activation of MRC-5 fibroblasts in the triple co-culture system.	99
Figure 27 MMP-3 siRNA transfection attenuated Nano-CuO-induced migration of MRC-5 fibroblasts in the triple co-culture system.....	100
Figure 28. The role of MMP-3-cleaved OPN in Nano-CuO-induced activation of MRC-5 fibroblasts in the triple co-culture system.....	103
Figure 29. Pretreatment of GRGDSP peptides inhibited Nano-CuO-induced migration of MRC-5 fibroblasts in the triple co-culture system.	104
Figure 30. Exposure to Nano-CuO did not cause upregulation of TGF- β 1 in BEAS-2B cells and U937* macrophages.	115

Figure 31. Dose-response results of cellular and biochemical constituents in BALF from mice after Nano-CuO exposure.	127
Figure 32. Time-response results of cellular and biochemical constituents in BALF from mice after Nano-CuO exposure.	128
Figure 33. Increased MMP-3 protein level in BALF from mice after Nano-CuO exposure.	131
Figure 34. Nano-CuO exposure downregulated cell junction-associated proteins in mouse lungs.	133
Figure 35. Upregulation of pro-inflammatory and fibrosis-related genes after Nano-CuO exposure.	135
Figure 36. Histology of mouse lungs after Nano-CuO exposure.	138
Figure 37. Nano-CuO exposure increased the hydroxyproline content and fibrosis-associated proteins in mouse lungs.	140
Figure 38. The efficiency of MMP-3 siRNA treatment in mouse lungs.	144
Figure 39. MMP-3 siRNA treatment significantly decreased the cellular and biochemical constituents in BALF caused by Nano-CuO exposure.	145
Figure 40. Knocking-down MMP-3 ameliorated Nano-CuO-caused acute lung injury and inflammation in mice.	147
Figure 41. MMP-3 knockdown significantly restored the decreased expression of cell junction-associated proteins caused by Nano-CuO exposure in mouse lungs.	149
Figure 42. Knocking-down of MMP-3 ameliorated Nano-CuO-caused chronic lung inflammation and fibrosis in mice.	152

Figure 43. MMP-3 siRNA treatment reduced the increases of hydroxyproline content and fibrosis-related proteins caused by Nano-CuO in mouse lungs.

..... 153

CHAPTER I: INTRODUCTION

1.1 Copper oxide nanoparticles

Copper oxide nanoparticles (Nano-CuO) are one of important classes of metal oxide nanoparticles, which are widely used in a range of applications such as catalysts, solar cells, wood-protection, electronics, and antimicrobial productions due to their high surface reactivity, chemical stability, thermoelectric properties, and superconductivity (Bhaumik et al. 2014; Evans et al. 2008; Maqsood et al. 2014; Ren et al. 2009; Tal Ben-Moshe 2009). They are also used in inks as an additive and in food packages as a coating material (Longano et al. 2012; Soltani et al. 2016). It is estimated that the global production of Nano-CuO by the year of 2025 will be 1600 tons (Future Markets Inc. 2015). The increasing use of Nano-CuO calls for a full understanding of their potential effects on human and environmental health.

1.2 Lung toxicity of Nano-CuO

Lungs are constantly in contact with ambient environment; thus they are one major portal to exposure of microbes, environmental pollution and nanoparticles. Noxious effects caused by copper (oxide) particles were reported in human. A case reported that in an enclosed, poorly ventilated steam condenser,

twenty-six workers got metal fume fever after cutting brass pipes with electric cutting torches(Armstrong et al. 1983). And the copper (oxide) dusts induced acute adverse effects include fever, dyspnea, chills, headache, and nausea in exposed workers. These symptoms appeared less than 5 h after exposure and excessive urine copper levels were confirmed in five of twelve exposed workers (Armstrong et al. 1983).

Nanoparticles can easily enter and deposit into lungs compared to micro-sized particles (Ilves et al. 2019; Juganson et al. 2015). Therefore, cells in first defend line of lungs against exogenous materials, such as epithelial cells, would be firstly exposed to nanoparticles after inhalation. Nano-CuO-induced toxicity in airway epithelial cells has been demonstrated in many *in vitro* studies. A previous study showed that Nano-CuO is more toxic than its bulk counterparts (micro-size CuO)(Strauch et al. 2017), and exposure of human bronchial epithelial BEAS-2B cells to 1 µg/mL and higher doses of Nano-CuO for 24 h resulted in a remarkable induction of oxidative stress-sensitive and pro-inflammatory genes, as well as those coding for cyclin-dependent kinase inhibitor 1 (p21^{Cip1}) and the apoptosis-related proteins Noxa and DR5 (Strauch et al. 2017). Nano-CuO exposure in BEAS-2B cells also activated DNA damage inducible genes, however, genes coding for distinct DNA repair factors were downregulated (Strauch et al. 2017). Nano-CuO exposure induced mitochondrial depolarization, reactive oxygen species (ROS) generation, DNA damage, and cell death in airway epithelial HEp-2 cells and human lung carcinoma epithelial A549 cells (Fahmy and Cormier 2009; Karlsson et al. 2008; Wang et al. 2012b). Exposure of Human bronchial epithelial

cells (HBEC) and A549 cells to Nano-CuO also caused lactate dehydrogenase (LDH) release, IL-8 production, and the activation of the pro-inflammatory transcription factors AP-1 and NF- κ B (Cho et al. 2012; Horie et al. 2018; Jing et al. 2015). Similarly, exposure of human airway epithelial H292 cells to Nano-CuO resulted in increased expression of pro-inflammatory cytokines such as IL-6 and TNF- α , and pro-fibrotic factor transforming growth factor- β 1 (TGF- β 1), as well as collagen I (Ko et al. 2018).

Lung inflammation induced by Nano-CuO has been shown in several animal models. A previous study demonstrated that inhalation exposure of rats to Nano-CuO for 5 consecutive days (6 h per day) caused dose-dependent alveolitis, bronchiolitis, vacuolation of the respiratory epithelium, and emphysema in the lungs; and limited inflammation was still observed at day 22 post-exposure at the highest exposure dose of 13.2 mg/m³ (Gosens et al. 2016). Wistar rats intratracheally instilled with 515 μ g of Nano-CuO exhibited elevated LDH, total protein, pro-inflammatory mediator IL-1 β , and MIP-2 in bronchoalveolar lavage fluid (BALF), and severe neutrophilic inflammation in alveoli and peribronchial and perivascular regions at 24 h post-exposure. At day 28 post-exposure, granulomatous inflammation in the rat lungs was observed (Cho et al. 2010). In addition, in an ovalbumin (OVA)-induced asthma mouse model, Nano-CuO exposure aggravated the airway hyper-responsiveness, and caused increased mucus secretion, ROS generation, inflammatory cell count, proinflammatory cytokines, and immunoglobulin E induced by OVA at 48 h post-exposure (Park et al. 2016). Similarly, in OVA-challenged BALB/c mice, exposure to Nano-CuO

exacerbated the allergic airway inflammation via excessive neutrophil infiltration in the lungs (Ilves et al. 2019).

Several studies have investigated the long-term effects of Nano-CuO exposure on lungs. Lai and colleagues reported that exposure of C57BL/6 mice to 5 mg/kg of Nano-CuO resulted in myofibroblast activation, collagen accumulation, and increased expression of progressive fibrosis marker α -SMA, suggesting that Nano-CuO induced fibrosis in the lung tissues at day 28 post-exposure (Lai et al. 2018). Female Wistar rats exposed to 515 μ g of Nano-CuO caused interstitial fibrosis in the rat lungs at day 28 after exposure (Cho et al. 2010).

Taken together, these studies demonstrated that Nano-CuO exposure caused epithelial damage, inflammation, injury, and fibrosis in lungs. However, the mechanisms underlying Nano-CuO-caused pulmonary injury and fibrosis are still not well known.

1.3 MMP-3 and pulmonary inflammation and fibrosis

Matrix metalloproteinases (MMPs) were initially described in 1962 in a study of tissue remodeling during anuran tadpole metamorphosis (Gross and Lapiere 1962). Up to date, 28 MMPs have been found in vertebrates and plants. In human, there are 24 MMPs genes encoding 23 secreted and membrane associated MMPs (Jablonska-Trypuc et al. 2016; Laronha and Caldeira 2020). Matrix metalloproteinases are a larger family of endopeptidases that belong to the metzincin superfamily. MMPs are able to degrade all kinds of extracellular matrix proteins. They are crucial in many physiological processes such as morphogenesis

and tissue repair; they are also associated with many pathological events such as inflammation, fibrosis, cancer, etc. (Apte and Parks 2015; Shay et al. 2015). Matrix metalloproteinase-3 (MMP-3), also named stromelysin-1, is an important member of matrix metalloproteinases family. MMP-3 is secreted as an inactive proprotein which consists of three basic parts: a propeptide, a metalloproteinase catalytic domain, and a hemopexin-like C-terminal domain (Gomis-Ruth et al. 1997). MMP-3 can degrade extracellular matrix proteins, such as collagen, fibronectin, laminin, and elastin, and cleave and activate other MMPs and cytokines, rendering MMP-3 crucial in many physiological and pathological processes (Fingleton 2017; Wan et al. 2021; Ye et al. 1996).

Inflammation, a complex biological part of immune responding to harmful stimuli, is one of the most fundamental and pronounced reactions to eliminate the stimuli and initiate repair process (Ferrero-Miliani et al. 2007; Netea et al. 2017). During the inflammatory response, proteolysis is a key process to enable tissue remodeling and healing (Keller et al. 2013). MMPs are such one big family of endopeptidases that can degrade extracellular matrix and basement membrane, making MMPs inevitably involved in the regulation of inflammation. MMPs can regulate inflammatory responses through alteration of vessel permeability and regulation of cytokine activities (Chang and Werb 2001; Fingleton 2017; Mittal et al. 2016). For example, in 12-O-tetradecanoylphorbol-13-acetate (TPA)-induced mouse skin inflammation model, elevated MMP-2 cleaved and inactivated complement 1 (C1) inhibitor, which further increased activation of complement 1 and generation of bradykinin by plasma kallikrein, finally resulting in an increase in

vessel permeability in wild-type mice. Whereas in MMP-2 knockout (KO) mice, the vessel permeability was significantly lower as compared to that in wild-type mice (Keller et al. 2013). Similarly, in lipopolysaccharide-induced uveitis mouse model, systemic administration of lipopolysaccharide caused increased expression of MMP-3 in the posterior of eyes, leukocyte adhesion and infiltration in vitreous cavity, and upregulation of intercellular adhesion molecule 1 and IL-6 mRNA in retina and retinal pigment epithelium. However, in MMP-3 KO mice, these effects were significantly suppressed (Van Hove et al. 2016).

MMP-3 has been reported to be engaged in lung inflammation. For example, in immunoglobulin G immune complexes-mediated acute lung injury mouse model, distinct increase of MMP-3 activity was observed in wild-type mouse lungs, however, in MMP-3 KO mice, the IgG complexes-mediated acute alveolitis was markedly decreased which was reflected by reduced protein content and leukocyte count in BALF (Warner et al. 2001). Similarly, a less degree of MIP-2-induced lung inflammation was observed in MMP-3 KO mice as compared to that in wild-type mice (Nerusu et al. 2007). Furthermore, lacking MMP-3 expression also protects mice from lipopolysaccharide- or hydrochloric acid-induced lung injury. (Puntorieri et al. 2016). Recently, increased MMP-3 in serum of 108 hospitalized COVID-19 patients was observed as compared to that in control patients, and the level of MMP-3 was correlated with the disease severity (Gelzo et al. 2022). The above studies suggest that MMP-3 plays important roles in pulmonary inflammatory responses.

Pulmonary fibrosis is a typical disease state that results from dysfunctional remedy responding to lung tissue injury caused by various particles, infections, allergens, chemicals, and other hazard factors (Giannandrea and Parks 2014; Tran et al. 2022; Zhao et al. 2022). It is characterized by the excessive extracellular matrix deposition and thickened alveolar walls. The progression of lung fibrosis leads to the reduction of lung compliance and capacity, lung dysfunction and failure, and ultimately death (Tran et al. 2022; Zhao et al. 2022; Zhao et al. 2020). To date, there is no cure for pulmonary fibrosis. Understanding of the mechanisms underlying pulmonary fibrosis may provide new therapeutic strategies to treat the patients with lung fibrosis.

The mechanisms underlying pulmonary fibrosis may be complex due to its various etiologies. Previous studies have revealed that many biological molecules and multiple mechanistic elements are involved in this process (Bonnans et al. 2014; Giannandrea and Parks 2014; Wynn 2008; Wynn and Ramalingam 2012; Zhao et al. 2022; Zhao et al. 2020). Among them, one family of molecules are considered to play important roles in fibrosis that are matrix metalloproteinases, also called matrixins (Nagase and Woessner 1999; Nagase and Brew 2002; Sternlicht and Werb 2001; Visse and Nagase 2003).

In normal physiological condition, the expression and activity of MMPs are precisely regulated by transcriptional factors and cytokines to interact with extracellular matrix (ECM) and are balanced by endogenous inhibitors called tissue inhibitors of metalloproteinases (TIMPs) (Balkowiec et al. 2018; Cui et al. 2017). Loss of balance or control between MMPs and TIMPs may lead to

basement membrane disruption and invasion of fibroblasts to normal alveolar space where they aberrantly proliferate and produce unusual amount of ECM proteins like collagens, finally result in the diseases such as fibrosis (Brew et al. 2000; Garcia-de-Alba et al. 2010; Gomez et al. 1997; Herrera et al. 2013; Woessner 1998; Yu et al. 2012). Our previous studies have shown that MMPs, such as MMP-2 and MMP-9, are involved in metal nanoparticle-induced lung inflammation and fibrosis (Mo et al. 2019; Mo et al. 2020b; Wan et al. 2008; Wan et al. 2011; Wan et al. 2017). Previous studies also demonstrated that MMP-3, another type of MMPs, was upregulated in fibrotic diseases including idiopathic pulmonary fibrosis (IPF), bleomycin-induced pulmonary fibrosis, and liver fibrosis (Ra and Parks 2007; Suhaimi et al. 2020; Yamashita et al. 2011; Yamashita et al. 2014; Ye et al. 1996). For example, in the lungs of patients with idiopathic pulmonary fibrosis, both MMP-3 mRNA and protein expression levels were increased (Yamashita et al. 2011). And MMP-3 was found overexpressed in various kinds of cells in the lungs of IPF patients including alveolar macrophages, alveolar and bronchial epithelial cells, interstitial fibroblasts, and intravascular leukocytes by immunohistochemical staining (Yamashita et al. 2011). Moreover, forced overexpression of MMP-3 caused pulmonary fibrosis in rats, while MMP-3 KO mice were protected from bleomycin-induced pulmonary fibrosis (Yamashita et al. 2011). MMP-3 also mediates the progress of fibrotic response in other organs such as kidney (Rao et al. 2005; Yamashita et al. 2014). Meanwhile, MMP-3 could promote epithelial-mesenchymal transition (EMT), an important process contributing to the formation of fibrosis, both *in vitro* and *in vivo*, and in MMP-3

transgenic mice, moderate or severe fibrosis was observed (Sternlicht et al. 1999; Zhang et al. 2021b). These results suggest that MMP-3 overexpression may contribute to the formation of lung fibrosis.

1.4 MMP-3 and lung epithelial barrier

In lungs, the physical barrier constituted by airway epithelium is continually challenged by external environmental agents, including noxious stimuli such as allergens, virus, and microbes, and other environmental and occupational pollutions such as metal (oxide) nanoparticles. The integrity of epithelial barrier is essential to provide an effective protection for lungs, which depends on cell junctions, such as tight junctions, adherens junctions, gap junctions, and other junctions. Tight junction, one important component in apical junctional complex which lock the epithelial cells into a stable layer and functions as the barrier, plays important role in protecting and separating different compartments within organism and regulating the diffusion of ions and solutes based on size and charge (Tepass 2003; Zihni et al. 2016). Tight junction is a multiple protein complex which is situated between the epithelial, endothelial, and myelinated cells. To date, more than 40 different tight junction proteins have been identified, including transmembrane proteins occludin, claudin-1, and cytoplasmic protein ZO-1 [20]. Adherens junction is another protein complex that occurs at cell-cell junctions in epithelium (Guo et al. 2007), and usually locates below tight junctions. One important component of adherens junction is E-cadherin. E-cadherin is a transmembrane glycoprotein and consists of an extracellular domain that forms

adhesions between epithelial cells and a cytoplasmic domain that is bound by the anchor proteins p120 catenin or β -catenin and stabilized to actin cytoskeleton (Leckband and Prakasam 2006; Pokutta and Weis 2007; Yuksel et al. 2021).

Alteration of these junction proteins would affect the integrity of epithelial barrier and further result in lung injury. A growing body of studies showed that disruption of airway epithelial junctions is involved in human lung diseases, such as chronic obstructive pulmonary disease (COPD) and asthma. (Brune et al. 2015; Lappi-Blanco et al. 2013; Ohta et al. 2012; Zou et al. 2020). For example, the expression of tight junction-associated proteins, such as ZO-1 and occludin, were significantly decreased both in lungs of COPD patients and in the air-liquid interface (ALI) culture of COPD patients-derived airway epithelial cells (Carlier et al. 2021; Heijink et al. 2014; Russell et al. 2002). Meantime, the expression of adherens protein E-cadherin was also reduced in ALI culture of COPD patients-derived airway epithelial cells (François Carlier 2022). And inhaled corticosteroid treatment-induced lung function improvement in COPD was related with upregulation of genes enriched for epithelial junctions (van den Berge et al. 2014). Similarly, increasing evidence suggests that disruption of pulmonary epithelial junctions is also involved in the pathogenesis of pulmonary fibrosis. A case highlighted that a young man with a known genetic defect that leads to loss of epithelial junction developed severe lung fibrosis (Kulkarni et al. 2016). Increased permeability was also observed in the lungs of patients with IPF, suggesting that dysfunction of cell junction in lung epithelium is involved in the development of lung injury and fibrosis (McKeown et al. 2009).

Many factors have been shown to be involved in the dysfunction of epithelial junctions (Brune et al. 2015). Among them, MMPs are considered to play roles in the regulation of epithelial barrier due to their capability to degrade extracellular matrix proteins and basement membrane. In the bronchoalveolar lavage fluid (BALF) obtained from IPF patients, elevated MMPs expression and activities were observed (Henry et al. 2002), and the elevated levels of MMPs were correlated with an increased permeability index (McKeown et al. 2009). MMPs, such as MMP-2 and MMP-9, have been reported to cause disruption of tight junction-associated proteins. It was reported that MMP-9 was involved in the decrease of occludin expression in BEAS-2B cells after silicon dioxide nanoparticles exposure, and this effect was inhibited by pretreatment with an MMP inhibitor (Liu et al. 2020). Overexpression of MMP-2 and MMP-9 could degrade tight junction-associated protein ZO-1 and increase blood-brain barrier (BBB) permeability, which were inhibited by pre-treatment of MMP-2/9 inhibitor SB-3CT *in vitro* (Zhang et al. 2018). Our previous study also showed that MMP-2 and MMP-9 were involved in Nano-Ni-induced downregulation of tight junction-associated proteins, including ZO-1, occludin, and claudin-1, in human keratinocytes (Yuan et al. 2021).

Recently, growing studies showed that MMP-3 is involved in the alteration of cell junctions. In IPF patients, elevated MMP-3 level is associated with the increased lung permeability (McKeown et al. 2009). In animal models, overexpression of MMP-3 was observed after spinal cord injury, and enhanced expression of MMP-3 caused blood-spinal cord barrier (BSCB) disruption, which was reflected by the decrease in tight junction-associated proteins ZO-1 and

occludin. Transfection of MMP-3 siRNA into the cells or treatment with an MMP-3 inhibitor, N-isobutyl-N-(4-methoxyphenylsulfonyl)glycyl hydroxamic acid (NNGH), significantly reduced the permeability of BSCB and increased the protein levels of ZO-1 and occludin. Similarly, the levels of tight junction-associated proteins were higher in MMP-3 KO mice than in wild-type mice after spinal cord injury. Furthermore, exogenous injection of an active MMP-3 recombinant enzyme into normal spinal cord increased BSCB permeability (Lee et al. 2014). In another study, isoflurane anesthesia and dye extravasation from brain were performed to evaluate the effects of MMP-3 on blood-brain barrier (BBB) permeability *in vivo*. Their results showed that both the isoflurane usage and anesthesia induction time were higher in MMP-3 KO mice than those in wild-type mice that had been administrated with MMP3 recombinant protein (wild-type+MMP-3), and the anesthesia emergence times were reported shorter in MMP-3 KO mice than that in wild-type+MMP-3 mice. Meantime, dye extravasation from brain was significant lower in MMP-3 KO mice than wild-type-MMP-3 mice (Zhang et al. 2021a). The transendothelial electrical resistance (TEER) results demonstrated that MMP-3 KO or inhibition significantly increased, while MMP-3 treatment decreased the barrier integrity of brain microvascular endothelial cells (BMVECs) monolayers. Their study further demonstrated that increased MMP-3 activity reduced the abundance of tight junction-associated proteins occludin, ZO-1, and claudin-5, as well as the adherens junction-associated protein E-cadherin in BMVECs (Zhang et al. 2021a). However, no studies have investigated the role of MMP-3 in the regulation of lung epithelial barrier after metal oxide nanoparticle exposure.

1.5 MMP-3 and fibroblast activation

A hallmark of fibrosis is the excess production and deposition of extracellular matrix into normal lung tissues. Fibroblasts, as well as other mesenchymal cells, are the principal cell types to regulate ECM homeostasis (Bonnans et al. 2014; Darby and Hewitson 2007; Zhao et al. 2020). Activated fibroblasts have a high capacity to produce extracellular matrix proteins and express α -SMA, which contribute to the form of fibrotic foci and contraction of fibrotic tissues (Darby and Hewitson 2007; Dong and Ma 2017). A variety of cytokines such as TGF- β , IL-1, and tumor necrosis factor (TNF), growth factors such as connective tissue growth factor (CTGF), and platelet-derived growth factor (PDGF), and matrix factors such as MMPs and ECM proteins are involved in the activation and proliferation of fibroblasts (Bassiouni et al. 2021; Bonnans et al. 2014; Hynes 2009; Mo et al. 2020b; Wynn and Ramalingam 2012; Zhao et al. 2020). Among them, the role of matrix factors in regulation of fibroblast activation is gaining more and more attention (Berrier and Yamada 2007; Hynes 2009; Hynes 2002; Zhao et al. 2020).

Osteopontin (OPN), also named secreted phosphoprotein 1 (SPP1), is an extracellular structural protein, as well as an important cytokine, playing key roles in many physiological and pathological progress, including inflammation, cancer, COPD, asthma, and fibrosis (O'Regan and Berman 2000; Pang et al. 2019; Sodek et al. 2000; Thompson et al. 2014; Wang and Denhardt 2008). OPN is secreted by many kinds of cells including macrophages, epithelial cells, endothelial cells, and fibroblasts (Mori et al. 2008). Human OPN has two well-known integrin-binding

motifs: a typical RGD motif and a SVVYGLR integrin-binding site, through which it binds to the cell surface receptors (Mori et al. 2008; O'Regan 2003; Ophascharoensuk et al. 1999; Pardo et al. 2005). The receptors for OPN include integrins family (such as $\alpha V\beta 3$) and CD44 which are expressed in most cell types. It is reported that OPN could promote the activation, migration, and un-controlled proliferation of fibroblasts (Burdo et al. 2007; Crawford et al. 1998; Denhardt et al. 2001; Lin et al. 2000; Lin and Yang-Yen 2001; Mori et al. 2008; Ophascharoensuk et al. 1999; Pardo et al. 2005; Scatena et al. 1998). Increased OPN level is related to the severity of lung diseases, such as asthma and IPF (Mangum et al. 2004; Samitas et al. 2011; Samitas et al. 2013; Simoes et al. 2009). Previous studies showed that exposure to single-walled carbon nanotube caused increased OPN expression and contributed to single walled carbon nanotube-induced pulmonary fibrosis (Dong and Ma 2017; Mangum et al. 2006). However, whether exposure to metal oxide nanoparticles could cause upregulation of OPN, which further contributes to lung inflammation and fibrosis, is still unclear.

Though intact OPN shows some physiological function, the modification of OPN after secretion is needed for its bioactivity (Christensen et al. 2010; Leitner et al. 2015). Proteolytic cleavage could modulate the biological activities of OPN and enhance its integrin-binding ability (Agnihotri et al. 2001; Helluin et al. 2000; Kennon and Stewart 2021; Kon et al. 2014; Lindsey et al. 2015; Scatena et al. 2007; Yokasaki and Sheppard 2000). OPN is a substrate of MMP-3 and has at least 3 MMP-3-cleavage sites in the full-length protein. It has been observed that MMP-3 cleaved the OPN to be a more affinity fragment and MMP-3-mediated

cleavage of OPN potentiated the bioactivity of OPN (Agnihotri et al. 2001). Interestingly, MMP-3 is always co-expressed with OPN in fibrotic responses (Agnihotri et al. 2001; Craig et al. 2015; Szalay et al. 2009), suggesting that MMP-3-OPN interaction may play roles in the development of pulmonary fibrosis. However, the role of MMP-3-cleaved OPN in the activation of fibroblasts is unclear.

1.6 Specific aims

In this study, the objective was to investigate the role of MMP-3 in Nano-CuO-induced lung injury and fibrosis. Understanding how metal nanoparticles activate MMPs system that results in lung injury and fibrosis may lead to interventions that prevent metal nanoparticle-induced lung injury and fibrosis.

The hypothesis was that exposure to Nano-CuO would cause ROS generation which might further lead to MMP-3 production in lung epithelial cells, which might alter cell junction-associated proteins, initiating and promoting Nano-CuO-induced lung inflammation, injury, and fibrosis. This study will pursue the following three Specific Aims.

1. Determine whether exposure to Nano-CuO would cause MMP-3 production in lung epithelial cells and the role of MMP-3 in Nano-CuO-induced alteration of cell junction-associated proteins.

2. Examine whether Nano-CuO exposure would activate fibroblasts and the role of MMP-3 and OPN in this process.

3. Investigate the role of MMP-3 in Nano-CuO-induced lung inflammation, injury, and fibrosis *in vivo*.

CHAPTER II: DETERMINE WHETHER EXPOSURE TO NANO-CUO WOULD CAUSE MMP-3 PRODUCTION IN LUNG EPITHELIAL CELLS AND THE ROLE OF MMP-3 IN NANO-CUO-INDUCED ALTERATIONS OF CELL JUNCTION-ASSOCIATED PROTEINS

2.1 Introduction

In lungs, the epithelial barrier is the initial site of contact for all inhaled substances, playing as both a physical and an immunological shelter to protect the subepithelial tissues. Dysfunction of the barrier is considered as a critical factor in the development of lung inflammation and subsequent fibrosis (Brune et al. 2015; Carlier et al. 2021; Ohta et al. 2012). Epithelial junctions, such as tight junction, adherens junction, and other cell junctions, which lock the epithelial cells into a stable layer, contribute to the integrity of lung epithelial barrier. Previous studies have demonstrated that exposure to some nanoparticles disrupted the expression of tight junction-associated proteins, such as ZO-1, claudin, and adherens junction-associated protein E-cadherin in lung endothelial and epithelial cells or brain endothelial cells (Chen et al. 2020; Chen et al. 2016; Liu et al. 2020; Xu et al. 2015). Our previous study demonstrated that exposure to nickel nanoparticles caused downregulation of tight junction-associated proteins, such as ZO-1, occludin, and claudin-1 in epidermal keratinocytes (Yuan et al. 2021). However,

knowledge of the effects of Nano-CuO on lung epithelial junction-associated proteins is still limited.

Matrix metalloproteinases (MMPs) belong to a large family of endopeptidases that are able to degrade extracellular matrix proteins and basement membrane. MMPs are crucial in many physiological processes such as morphogenesis and tissue repair; they are also associated with many pathological events such as inflammation, cancer, and fibrosis etc. (Apte and Parks 2015; Shay et al. 2015). MMPs, such as MMP-2 and MMP-9, have been shown to be involved in metal nanoparticle-induced dysregulation of tight junction-associated proteins (Yuan et al. 2021). Previous studies also showed that MMP-3, another type of MMPs, was involved in the dysregulation of cell junction-associated proteins in blood-spinal cord barrier or blood-brain barrier, while knocking-out or knocking-down MMP-3 restored the abundance of tight junction-associated proteins and adherens junction-associated protein E-cadherin (Lee et al. 2014; Zhang et al. 2021a). This raises the intriguing possibility that MMP-3 may be involved in metal nanoparticle-induced pulmonary epithelial barrier dysfunction.

In the present study, we examined whether exposure to Nano-CuO altered the expression and activity of MMP-3 and its role in Nano-CuO-induced downregulation of epithelial junction-associated proteins in normal human bronchial epithelial BEAS-2B cells. We also explored the potential mechanisms that might be involved in these effects.

2.2 Materials and methods

2.2.1 Nanoparticles and their characterization

Copper (II) oxide nano-powder (Nano-CuO) was purchased from Sigma-Aldrich (St. Louis, MO) and Nano-TiO₂ was provided by INABTA and Co., Ltd., Vacuum Metallurgical Co., Ltd. (Japan). The characteristics of Nano-CuO and Nano-TiO₂ were described in our and other previous studies (Karlsson et al. 2008; Yu et al. 2010). Briefly, the mean diameters of Nano-CuO and Nano-TiO₂ in the powder are 42 nm and 28 nm determined by transmission electron microscopy (TEM), and their mean hydrodynamic sizes are 220 nm and 280 nm determined by dynamic light scattering (DLS). The specific surface area is 23 m²/g for Nano-CuO and 45.0 m²/g for Nano-TiO₂. The metal nanoparticles were suspended in normal saline in a concentration of 100 µg/mL. To reduce agglomeration, metal nanoparticle suspensions were ultrasonicated by an ultrasonic cleaner FS30 (Fisher Scientific, Pittsburg, PA) for at least 10 min prior to each experiment.

2.2.2 Chemicals and reagents

Catalase (CAT) was purchased from MP Biomedicals (Solon, OH). N-acetyl-L(+)-cysteine (NAC) and MitoSOX™ Red reagent were from Fisher (Fair Lawn, NJ). Trolox, Mito-TEMPO, and MMP-3 substrate β-casein were from SIGMA (Saint Louis, MO). TRIzol™ Reagent was purchased from Invitrogen (Carlsbad, CA). SB203580 was from TOCRIS (Ellisville, MO), PD98059 from Cell Signaling Technology (Beverly, MA), and SP600125 from Thermo Fisher (Ward Hill, MA).

Antibodies against β -actin (cat.# 58169), total p38 (cat.# 9212), phospho-p38 (cat.# 9215), total ERK1/2 (cat.# 9107), phospho-ERK1/2 (cat.# 9101), total JNK2 (cat.# 9258), phospho-JNK (cat.# 4668), E-cadherin (cat.# 3195), claudin-1 (cat.# 4933s), horseradish peroxidase (HRP)-conjugated horse anti-mouse IgG (cat.# 7076), and goat anti-rabbit IgG (cat.# 7074) were obtained from Cell Signaling Technology (Beverly, MA). Anti-MMP-3 antibody (cat.# 53015) was from abcam (Cambridge, MA). Anti-ZO-1 antibody (cat.# bs-1329R) was purchased from Bioss Antibodies (Woburn, MA). Anti-occludin antibody (cat.# NBP1-77037) was obtained from Novus Biologicals (Littleton, CO). All other chemicals were purchased from Fisher Scientific (Waltham, MA) except when otherwise stated. All chemicals used were of analytical grade.

2.2.3 Cell culture

Normal human bronchial epithelial cells BEAS-2B were purchased from American Type Culture Collection (ATCC, Cat.# CRL-9609, Manassas, VA) and maintained in RPMI 1640 medium with L-glutamine, supplemented with 10% FBS, 100 U/mL penicillin, and 100 μ g/mL streptomycin (Corning, Manassas, VA) in a humidified atmosphere at 37 °C and 5% CO₂.

2.2.4 Cytotoxicity of metal oxide nanoparticles

The cytotoxicity of Nano-CuO and Nano-TiO₂ in BEAS-2B cells were determined by both CellTiter 96[®] AQueous Non-Radioactive Cell Proliferation Assay (MTS assay) (Promega, Madison, WI) and alamarBlue Cell Viability

Reagent (AlamarBlue assay) (Invitrogen, Eugene, OR) as described in our previous studies (Mo et al. 2009a; Yu et al. 2010). Briefly, 3×10^3 BEAS-2B cells per well were seeded in 96-well plates. After 12 h incubation, cells were treated with different doses of Nano-CuO or Nano-TiO₂ (0, 0.5, 1.0, 1.5, 2.0, and 5.0 µg/mL) in a total volume of 200 µL per well. Cells without treatment were used as control. After 24 h treatment, the cytotoxicity was determined by recording the colorimetric absorbance at 490 nm for MTS assay and fluorescence at ex530/em590 for AlamarBlue assay. The cell viability was presented as the percentage as compared to the control.

2.2.5 Detection of ROS generation

ROS generation was tested using 2', 7'-dichlorodihydrofluorescein diacetate (H₂-DCFDA) (Molecular Probes, Eugene, OR). H₂-DCFDA is a non-fluorescent compound. It can rapidly permeate through cell membranes and is hydrolyzed by the intracellular esterases and oxidized by intracellular oxidants to be a high fluorescent DCF, with a fluorescent intensity proportional to the intracellular ROS. Briefly, BEAS-2B cells were seeded into 96-well plate overnight and pretreated with 5 µM of H₂-DCFDA for 2 h, followed by different doses of Nano-TiO₂ or Nano-CuO treatment for multiple times. Cells without treatment were used as control. The fluorescence was detected by Synergy HT microreader (BioTek, Winooski, VT) at ex485/em528. To determine the effects of ROS scavengers or inhibitors on Nano-CuO-induced ROS production in BEAS-2B cells, catalase (CAT, 2,000 U), N-acetyl-L(+)-cysteine (NAC, 20 mM), and Trolox (100 µM) were

added 2 h prior to adding H₂-DCFDA, followed by exposure to 1 µg/mL of Nano-CuO for 24 h.

For detection of mitochondrial ROS generation, MitoSOX™ Red Reagent (5 µM), a mitochondria-specific superoxide indicator, was used according to the manufacturer's instruction. Briefly, the cells were pretreated with MitoSOX™ for 2 h prior to exposure to 1 µg/mL of Nano-CuO. The fluorescence at ex530/em590 was recorded by Synergy HT microreader (BioTek, Winooski, VT). A specific mitochondrial superoxide scavenger, Mito-TEMPO (10 µM), was used to observe whether Nano-CuO-induced ROS generation was from mitochondria. For images of MitoSOX™ staining, cells were treated with Nano-CuO (1 µg/mL) for 6 h and MitoSOX™ (5 µM) for another 30 min. The images were captured by fluorescence microscopy (Nikon, Japan).

2.2.6 Generation of BEAS-2B Rho-0 (ρ⁰) cells

To obtain BEAS-2B ρ⁰ cells, parental BEAS-2B cells were chronically exposed to low dose of ethidium bromide (EtBr) as described previously (Fernandez-Moreno et al. 2016; Hashiguchi and Zhang-Akiyama 2009). Briefly, 1x10⁴ BEAS-2B cells per flask were seeded in 75 cm² flasks in complete media. After 12 h incubation, the medium was replaced with fresh complete medium supplemented with 50 ng/mL EtBr, 50 µg/mL uridine, and 100 µg/mL sodium pyruvate. After one week of culture, the medium was refreshed every other day. Usually after approximately one month following the initial addition of EtBr, ρ⁰ cell colonies were visible. To verify the depletion of mitochondrial DNA (mtDNA) in

BEAS-2B ρ^0 cells, genomic DNA was isolated from the cells as described previously (Blin and Stafford 1976). mtDNA level was quantified by qPCR using primers for mitochondrial encoded D-loop gene and normalized to nuclear encoded beta-2-microglobulin (B2M) gene. The PCR primers for D-loop gene were: forward 5'-CATCTGGTTCCTACTTCAGGG-3' and reverse 5'-TGAGTGGTTAATAGGGTGATAGA-3'. The primers for B2M gene (as a positive control and internal reference) were: forward 5'-TGCTGTCTCCATGTTTGATGTATCT-3' and reverse 5'-TCTCTGCTCCCCACCTCTAAGT-3'. qPCR was performed using a Bio-Rad iQ5 iCycler (Bio-Rad, Hercules, CA). Briefly, 100 ng genomic DNA was used in a total of 20 μ L reaction mix which contains 1 μ L of forward/reverse primer (5 μ M) and 10 μ L of 2 \times iTaq Universal SYBR Green Supermix. The mixture was preheated and denatured at 95 $^{\circ}$ C for 3 min, followed by 50 cycles of denaturation at 95 $^{\circ}$ C for 30 s, annealing at 54 $^{\circ}$ C for 1 min, and extension at 72 $^{\circ}$ C for 30 s. The failure of mitochondrial ROS production in BEAS-2B ρ^0 cells induced by Nano-CuO exposure was confirmed by using MitoSOXTM Red Reagent staining as described above.

2.2.7 Extraction of total RNA and real-time PCR

Total RNA was isolated from BEAS-2B or BEAS-2B ρ^0 cells by using TRIzol Reagent according to the manufacturer's instruction. Total RNA concentration and purity were determined by DU730 Spectrophotometer (Beckman Coulter, Fullerton, CA) at absorbance of 260 nm and 280 nm.

To quantify the expression levels of MMP-3, TIMP-1, and TIMP-4, RT-qPCR was performed using a Mastercycler (Eppendorf, Westbury, NY) and a Bio-Rad iQ5 iCycler as previously described (Mo et al. 2009a; Mo et al. 2012; Yu et al. 2010). Briefly, total RNA (2 µg) was reverse-transcribed into cDNA using 1 µL M-MLV reverse transcriptase (Promega, Madison, WI) in a total volume of 25 µL which contains 2 µL of 0.5 µg/µL oligo(dT)₁₈ primer, 1.25 µL of 10 mM dNTP, 0.75 µL RNasin Ribonuclease inhibitor, and 5 µL of 5 × M-MLV reaction buffer. Real-time PCR was performed using iTaq Universal SYBR Green Supermix (Bio-Rad, Hercules, CA). Briefly, 1 µL cDNA was used in a total of 20 µL reaction mix which contains 1 µL of forward/reverse primer (5 µM) and 10 µL of iTaq Universal SYBR Green Supermix. The mixture was denatured at 95 °C for 3 min, followed by 50 cycles of denaturation at 95 °C for 10 s, annealing at 58 °C for 30 s, and extension at 72 °C for 30 s. The melting curve was analyzed at last to confirm the single amplification product during the process. The primers for human MMP-3, TIMP-1, TIMP-4, and β-actin were:

MMP-3 forward 5'-CTCACAGACCTGACTCGGTT-3';

MMP-3 reverse 5'-CACGCCTGAAGGAAGAGATG-3';

TIMP-1 forward 5'-AATTCCGACCTCGTCATCAG-3';

TIMP-1 reverse 5'-GTTTGCAGGGGATGGATAAA-3';

TIMP-4 forward 5'-CTTGGTGCAGAGGGAAAGTC-3';

TIMP-4 reverse 5'-GCCGTCAACATGCTTCATAC-3';

β-actin forward 5'-CATCGAGCACGGCATCGTCA -3';

and β -actin reverse 5'-TAGCACAGCCTGGATAGCAAC -3'. The RT-qPCR results were recorded as threshold cycle numbers (Ct) and calculated by the $2^{-\Delta\Delta C_t}$ method (Livak and Schmittgen 2001) with normalization against β -actin mRNA level in the same sample.

2.2.8 β -casein and gelatin zymography assays

MMP-3 activity was measured by β -casein zymography assay while MMP-2 and MMP-9 activity by gelatin zymography assay as described previously with modifications (Mo et al. 2019; Wan et al. 2011; Yamashita et al. 2011). Briefly, cells were seeded in 6-well plates in serum-free RPMI1640. After Nano-CuO or Nano-TiO₂ treatment, the conditioned medium was collected. For β -casein zymography assay, the conditioned medium was concentrated by Amicon[®] Ultra centrifugal filter devices (with Ultracel-10K membrane, Millipore, Billerica, MA) for 10 times. Electrophoresis was performed on 10% SDS-polyacrylamide gel with 1 mg/mL β -casein or 0.5 mg/mL gelatin under non-reducing conditions. After electrophoresis, the gels were washed twice (30 min each) in 2.5% Triton X-100 solution, and incubated in calcium assay buffer (pH 7.5) containing NaCl (150 mM), CaCl₂ (10 mM), ZnCl₂ (5 μ M), and 1% Triton X-100 at 37 °C for 36 h. After staining with 0.1% Coomassie Brilliant Blue R-250 (Bio-Rad, Hercules, CA), the gels were destained in 10% acetic acid until clear bands were observed against the background of Coomassie blue-stained gel.

2.2.9 Protein extraction and Western blot

Proteins were extracted using RIPA lysis buffer supplemented with PMSF, protease inhibitor cocktail, and sodium orthovanadate (Santa Cruz, CA). Cell samples were lysed in RIPA buffer for 30 min on ice. After centrifugation at 10,000 g and 4 °C for 15 min, the supernatant containing total proteins was collected and the protein concentration was determined by Bradford protein assay (Bio-Rad). Western blot was performed as described previously (Long et al. 2019; Mo et al. 2009a; Yu et al. 2010). Proteins were separated on SDS-PAGE, transferred on to Immun-Blot™ polyvinylidene fluoride (PVDF) membrane (Bio-Rad), blocked in 5% fat-free milk in 1 × TBS with 0.05% tween-20 for 1-2 h at room temperature, and incubated with primary antibody in 5% BSA at 4 °C overnight with gentle shaking. After washing, the membrane was incubated with HRP-conjugated secondary antibody for 1-2 h at room temperature. The bands were detected by using SuperSignal™ West Pico PLUS Chemiluminescent Substrate (Thermo Scientific, Rockford, IL) followed by exposure to CL-XPosure™ film (Thermo Scientific). Films were scanned by using a HP Officejet Pro8500 printer and quantified by using NIH ImageJ software (<https://imagej.nih.gov/ij/>). To determine the secreted MMP-3, supernatant of the conditioned medium was collected for electrophoresis. A gel stained with 0.1% Coomassie Brilliant Blue R-250 (Bio-Rad, Hercules, CA) was used as loading reference.

2.2.10 Transfection of BEAS-2B cells with MMP-3 siRNA

Transfection was performed following the protocol provided by Thermo Fisher with modifications. Briefly, 1.5×10^5 BEAS-2B cells per well were seeded into six-well plates in antibiotic-free RPMI1640 supplemented with 10% FBS. The cells were incubated until 70-80% confluency. Cells were then transfected with a mixture of 6 μ L of TurboFectin 8.0 Transfection Reagent (Origene, Rockville, MD) and 30 nM of MMP-3 siRNA (Ambion, Carlsbad, CA) in a total volume of 1 mL antibiotic-free and FBS-free RPMI 1640 medium for 6 h. After transfection, the cells were treated with Nano-CuO for another 48 h. The transfection efficiency was determined by MMP-3 expression by Western blot, and the cells were also harvested for Western blot. Silencer™ Select Negative Control No. 2 siRNA (Ambion, Carlsbad, CA) was used as a negative control.

2.2.11 Immunofluorescent staining

Immunofluorescent staining was performed based on the methods described previously (Mo et al. 2015; Yuan et al. 2021). Briefly, cells were seeded into 4-well LAB-TEK® II chamber slides (Nalge Nunc International, IL). After exposure to Nano-CuO for 48 h, cells were fixed with 10% neutral buffered formalin for 10 min and rinsed with 1x PBS three times (5 min each). Then cells were incubated in a blocking solution (3.26% of BSA, 5% of normal goat serum, and 0.3% Triton X-100) for 1 h at room temperature for cell permeabilization and blocking of the nonspecific protein binding. After incubation with anti-E-cadherin (1:200) and anti-ZO-1 (1:200) antibodies overnight at 4 °C, the cells were

incubated with Alexa Fluor[®] 488-conjugated goat anti-rabbit IgG (Invitrogen, Carlsbad, CA) for 1 h at room temperature. The slides were mounted with Prolong Gold Antifade Reagent with DAPI (Invitrogen, Carlsbad, CA) and images were captured under fluorescence microscopy (Nikon, Japan).

2.2.12 Statistical analysis

Results were expressed as the mean \pm standard error (SE). The differences among groups with one independent variable were evaluated by one-way analysis of variance (ANOVA) with Bonferroni post-hoc test. The differences among groups with two independent variables were evaluated by two-way analysis of variance (ANOVA) with Holm-Sidak test. All analyses were carried out using SigmaPlot 13.0 software (Systat Software, San Jose, CA). In all statistical analyses, a p -value < 0.05 was deemed statistically significant.

2.3 Results

2.3.1 Cytotoxicity of Nano-CuO and Nano-TiO₂ in BEAS-2B cells

The cytotoxicity of different concentrations of Nano-CuO or Nano-TiO₂ on BEAS-2B cells was shown in Figure 1. The results of MTS assay showed that exposure to 1.5 µg/mL or higher concentrations of Nano-CuO for 24 h caused significant cytotoxic effects on BEAS-2B cells (Figure 1A). However, exposure of the cells to Nano-TiO₂ for 24 h did not cause any cytotoxic effects at all experimental doses (Figure 1A). The results were confirmed by using alamarBlue assay (Figure 1B). Non-cytotoxic doses were chosen for the following experiments.

2.3.2 ROS generation in BEAS-2B cells exposed to Nano-CuO, but not to Nano-TiO₂

Exposure of BEAS-2B cells to Nano-CuO caused a dose- and a time-dependent increase in ROS production reflected by the increased DCF fluorescence intensity (Figure 2A, B). Exposure to 0.5 and 1 µg/mL of Nano-CuO for 24 h induced a significant increase in ROS generation compared to the control (Figure 2A), and the production of ROS appeared as early as 3 h after 1 µg/mL of Nano-CuO exposure (Figure 2B). However, treatment with the same doses of Nano-TiO₂ did not cause any changes in DCF fluorescence in BEAS-2B cells (Figure 2A).

Pre-treatment of cells with ROS scavengers or inhibitors, including N-acetyl-l(+)-cysteine (NAC, 20 mM), catalase (2000 U), and Trolox (100 µM), significantly abolished Nano-CuO-induced ROS generation (Figure 2C). In addition, Nano-

CuO-induced ROS was abolished by pretreatment of the cells with Mito-TEMPO, a specific mitochondrial ROS inhibitor (Figure 2D), but not by NADPH oxidase inhibitor, DPI (20 nM) (data not shown). To further determine whether mitochondria was the potential source of Nano-CuO-induced ROS generation, BEAS-2B ρ^0 cells which lack mitochondrial DNA and dysfunction in oxidative phosphorylation were generated and the depletion of mitochondrial DNA in BEAS-2B ρ^0 cells was validated by qPCR (Figure 3). MitoSOX™ Red Reagent, a mitochondria-specific fluorogenic dye in living cells, was used to detect the production of mitochondrial specific ROS. It is rapidly oxidized by mitochondrial superoxide rather than other ROS and the oxidized product is highly fluorescent. The results showed that Nano-CuO-induced ROS generation was significantly attenuated in BEAS-2B ρ^0 cells (Figure 2D, E). Those results suggest that mitochondria may be the key source of ROS generation in the BEAS-2B cells exposed to Nano-CuO.

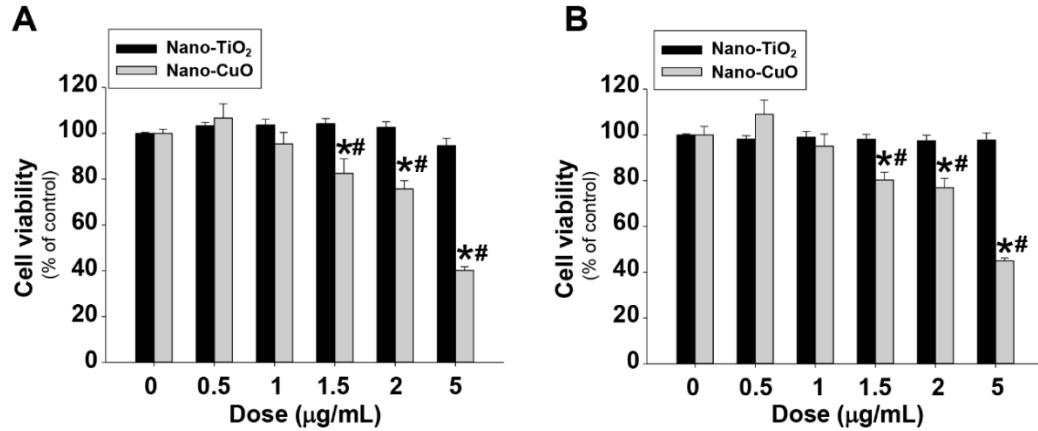


Figure 1. Cytotoxicity of Nano-CuO and Nano-TiO₂ on human lung epithelial (BEAS-2B) cells.

BEAS-2B cells were seeded into 96-well plates and treated with different doses of Nano-CuO or Nano-TiO₂ for 24 h. The cytotoxicity was determined by MTS assay (A) and alamarBlue assay (B). Cells without treatment were used as control. Data represent mean \pm SE (n=6). * Significant difference as compared to the control group, $p < 0.05$; # Significant difference as compared to the equal dose of Nano-TiO₂-treated group, $p < 0.05$.

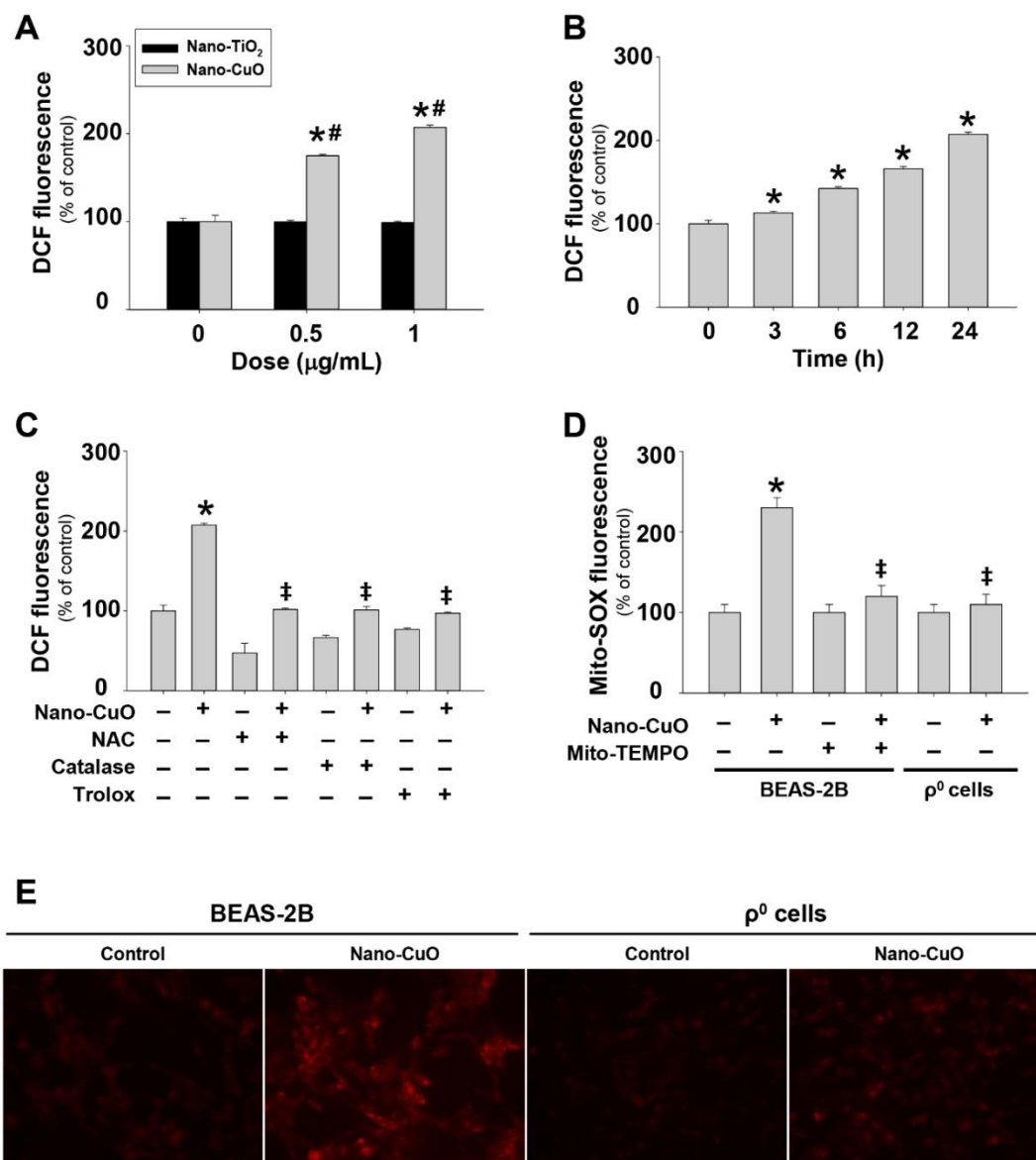


Figure 2. Effects of Nano-CuO and Nano-TiO₂ on ROS generation in BEAS-2B cells, and the effects of ROS scavengers, mitochondria-targeted ROS inhibitor, or mitochondrial DNA depletion on Nano-CuO-induced ROS generation.

BEAS-2B cells were pretreated with 5 µM H₂-DCFDA for 2 h, then were treated with different doses of Nano-CuO and Nano-TiO₂ for 24 h (A) or 1 µg/mL of Nano-CuO for 0, 3, 6, 12, 24 h (B). After treatment, the fluorescence at ex485/em528

was recorded. **(C)** For antioxidant experiments, ROS scavengers or inhibitors NAC (20 mM), CAT (2000 U), and Trolox (100 μ M) were added 2 h prior to adding H₂-DCFDA for 2 h and 1 μ g/mL of Nano-CuO for another 24 h. **(D)** Mito-TEMPO (10 μ M) was added 2 h prior to treating MitoSOX™ for 2 h and 1 μ g/mL of Nano-CuO for 24 h. **(E)** For images of stained cells, cells were incubated with Nano-CuO (1 μ g/mL) for 6 h and MitoSOX™ (5 μ M) for 30 min. Cells without treatment were used as control. Data represent mean \pm SE (n=6). * Significant difference as compared to the control group, $p < 0.05$; # Significant difference as compared to the equal dose of Nano-TiO₂-treated group, $p < 0.05$; ‡ Significant difference as compared to Nano-CuO-treated alone group, $p < 0.05$.

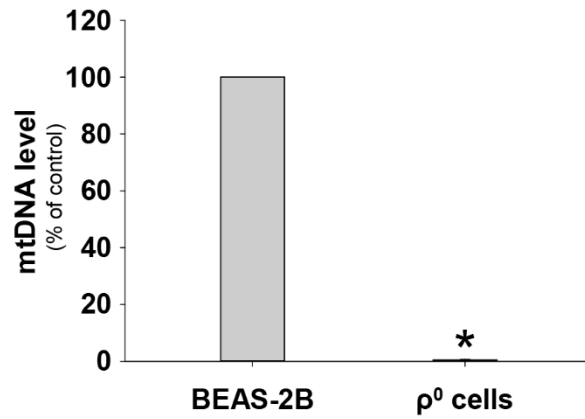


Figure 3. Validation of the depletion of mtDNA in BEAS-2B ρ⁰ cells.

mtDNA level was quantified by qPCR using primers for mitochondrial encoded D-loop gene and normalized to the level of a nuclear gene, beta-2-microglobulin (B2M). Data represent mean \pm SE (n=3). * Significant difference as compared to their parental control BEAS-2B cells, $p < 0.05$.

2.3.3 Role of Nano-CuO-induced ROS on MAPKs activation

To examine whether Nano-CuO-induced ROS generation could activate mitogen-activated protein kinases (MAPKs) cascade, the expression of p38, Erk1/2 and JNK in BEAS-2B cells were determined by Western blot. The results demonstrated that exposure to 0, 0.5 and 1 $\mu\text{g/mL}$ of Nano-CuO for 3 h caused a dose-dependent increase in phosphorylation of p38, Erk1/2 and JNK (Figure 4A, B). For the time-course study, BEAS-2B cells were exposed to 1 $\mu\text{g/mL}$ of Nano-CuO for 0, 3, 6, 12 and 24 h. The results showed that Nano-CuO caused increased phosphorylation of p38, Erk1/2 and JNK, which peaked at 6 or 12 h after treatment (Figure 4C, D). To further investigate the role of ROS generation on Nano-CuO-induced activation of MAPKs, BEAS-2B cells were pre-treatment with ROS inhibitor, NAC (20 mM), for 2 h prior to exposure to 1 $\mu\text{g/mL}$ of Nano-CuO for another 6 h. The results showed that NAC significantly suppressed Nano-CuO-induced increased phosphorylation of p38, Erk1/2 and JNK (Figure 5A-D). Nano-CuO also induced significant lower phosphorylation of MAPKs in BEAS-2B ρ^0 cells as compared to that in their parental cells (Figure 5A-D). These results indicated that ROS generation in BEAS-2B cells exposed to Nano-CuO was involved in Nano-CuO-induced activation of MAPKs.

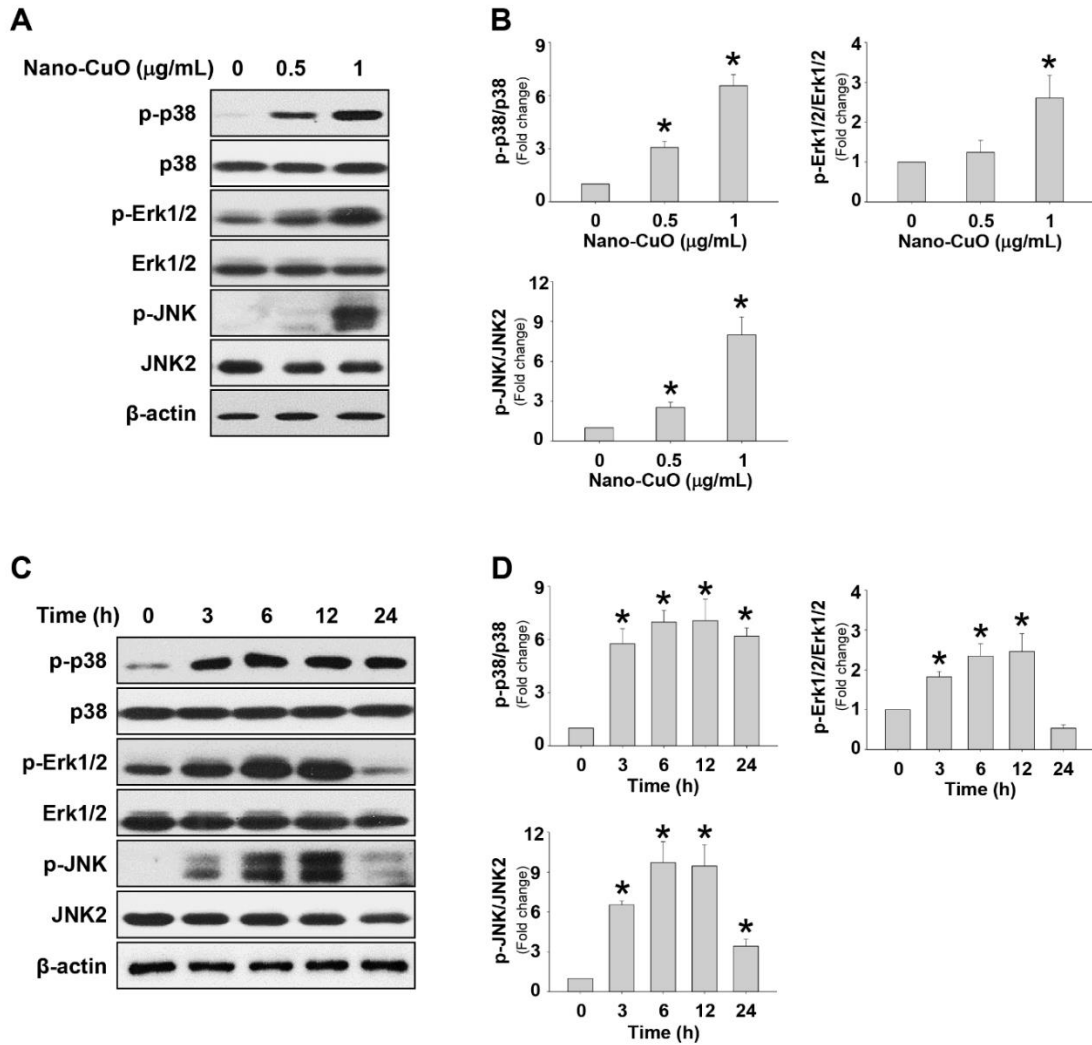


Figure 4. Dose- and time- dependent activation of MAPKs in BEAS-2B cells exposed to Nano-CuO.

For dose-response study, BEAS-2B cells were treated with 0.5 and 1 $\mu\text{g/mL}$ of Nano-CuO for 3 h (**A, B**). For time-course study, BEAS-2B cells were treated with 1 $\mu\text{g/mL}$ of Nano-CuO for 0, 3, 6, 12 and 24 h (**C, D**). **A** and **C** were the results of a single Western blot experiment. **B** and **D** were the average expression level of phospho-MAPKs (p-p38, p-Erk1/2, p-JNK) normalized to the expression level of

corresponding total MAPKs (p38, Erk1/2, JNK). Data represent mean \pm SE (n=3).

* Significant difference as compared to the control group, $p < 0.05$.

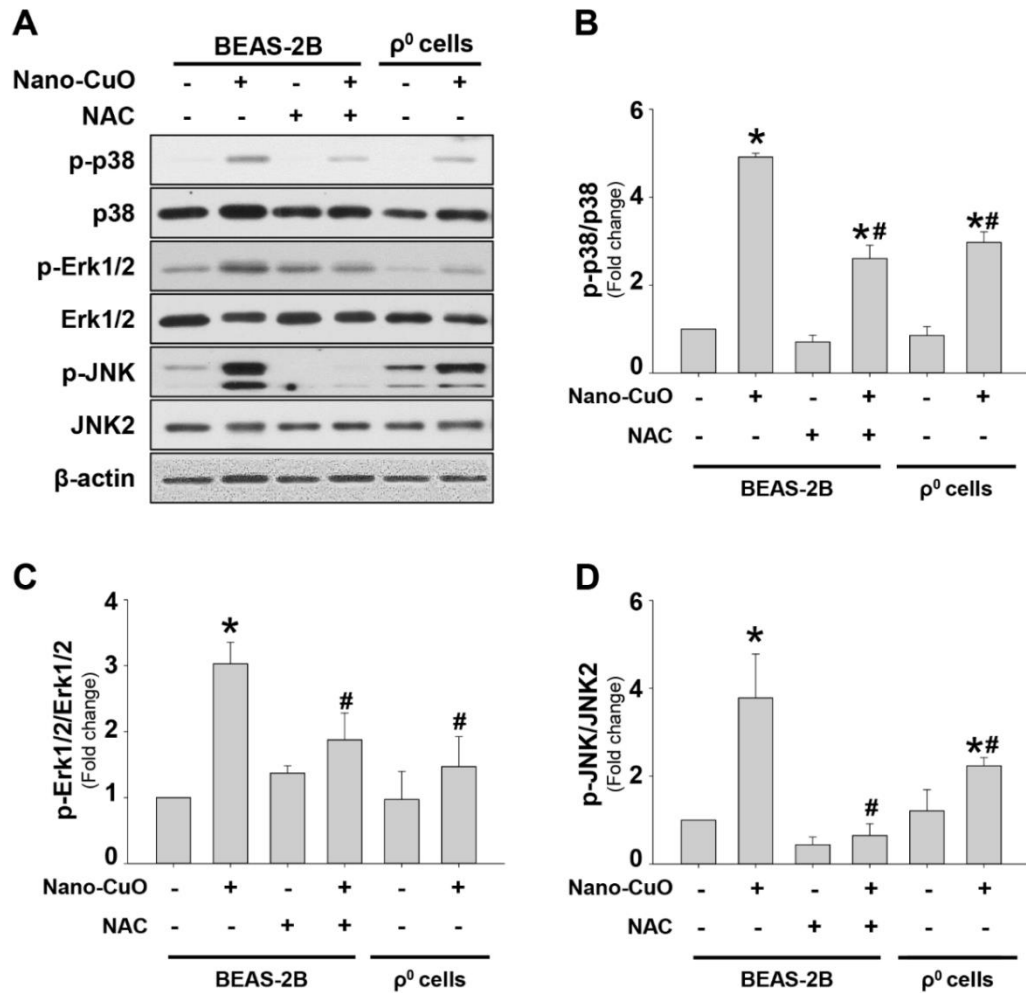


Figure 5. Effects of ROS scavenger or mitochondrial DNA depletion on Nano-CuO-induced MAPKs activation in human lung epithelial cells.

Protein was collected from the cells after exposure to 1 $\mu\text{g}/\text{mL}$ of Nano-CuO for 6 h with/without pre-treatment with NAC (20 mM) for 2 h. Cells without treatment were used as control. **(A)** The result of a single Western blot experiment. **(B, C, D)** The average expression level of phospho-MAPKs (p-p38, p-Erk1/2, p-JNK) normalized to the expression level of corresponding total MAPKs (p38, Erk1/2,

JNK). * Significant difference as compared to the control group, $p < 0.05$; # Significant difference as compared to Nano-CuO-treated alone group, $p < 0.05$.

2.3.4 Effects of Nano-CuO on MMP-3 production

To study whether exposure to Nano-CuO could cause the alteration of expression and activity of MMP-3, BEAS-2B cells were treated with 0, 0.5 or 1 $\mu\text{g/mL}$ of Nano-CuO for 6 h, or 1 $\mu\text{g/mL}$ of Nano-CuO for 0, 3, 6, 12 and 24 h. The results showed that exposure of BEAS-2B cells to Nano-CuO caused a significant dose-dependent increase in MMP-3 mRNA level (Figure 6A), and MMP-3 mRNA expression reached peak at 6 h after Nano-CuO exposure (Figure 6B). However, the mRNA levels of TIMP-1 or TIMP-4, which are considered as the endogenous inhibitors of MMP-3, did not change following Nano-CuO exposure (Figure 7). To further confirm the upregulation of MMP-3 by Nano-CuO at the protein level, Western blot was performed. Nano-CuO caused a dose-dependent increase in MMP-3 expression at protein level (Figure 6C, E), and the expression reached at the highest level at 12 h after Nano-CuO exposure (Figure 6D, F). MMP-3 activity results, detected by β -casein zymography, were consistent with its mRNA and protein expression results (Figure 6G, H). However, exposure of cells to Nano-TiO₂ did not cause any changes in the expression and activity of MMP-3 (Figure 6A, C, E, G). These results suggested that exposure of BEAS-2B cells to Nano-CuO caused upregulation of MMP-3, which might further cause an imbalance between MMP-3 and its inhibitors TIMP-1 and TIMP-4.

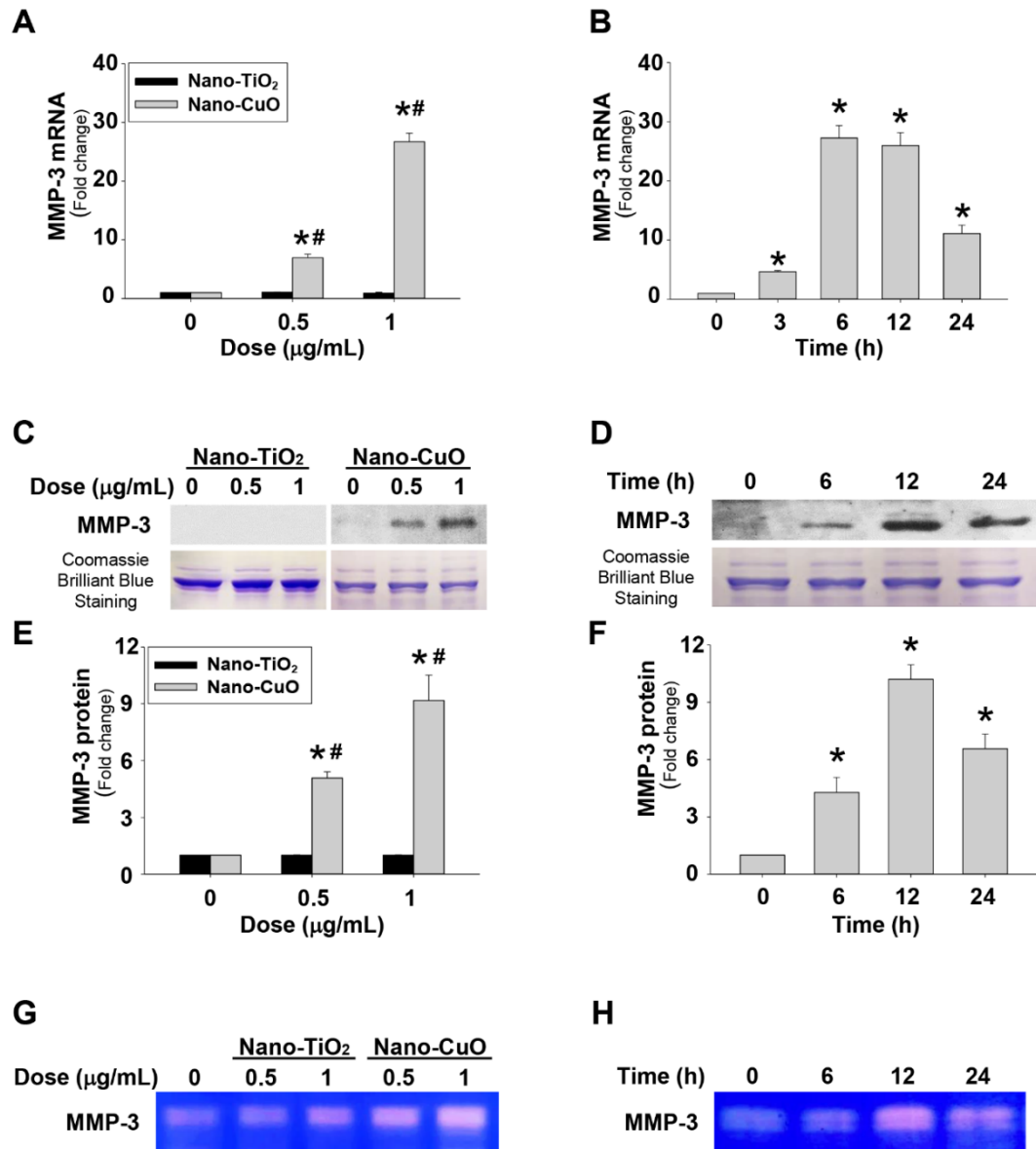


Figure 6. Dose- and time- dependent induction of MMP-3 in BEAS-2B cells exposed to metal oxide nanoparticles.

For dose-response study, BEAS-2B cells were exposed to 0.5 and 1 $\mu\text{g/mL}$ of Nano-CuO or Nano-TiO₂ for 6 h for MMP-3 mRNA (A) or 12 h for MMP-3 protein expression (C, E). For time-response study, the cells were exposed to 1 $\mu\text{g/mL}$ of

Nano-CuO for 0, 3, 6, 12 and 24 h for MMP-3 mRNA (**B**) or 0, 6, 12 and 24 h for MMP-3 protein expression (**D, F**). After treatment, the cells were collected for total RNA isolation, while the conditioned media were collected for Western blot. Cells without treatment were used as control. Equal protein loading was verified by Coomassie Brilliant Blue staining. **C** and **D** were the results of a single experiment, while **E** and **F** were normalized band densitometry readings averaged from three independent experiments. (**G, H**) MMP-3 activity was detected in the conditioned media by β -casein zymography. Data represent mean \pm SE (n=3). * Significant difference as compared to the control group, $p<0.05$; # Significant difference as compared to equal dose of Nano-TiO₂-treated group, $p<0.05$.

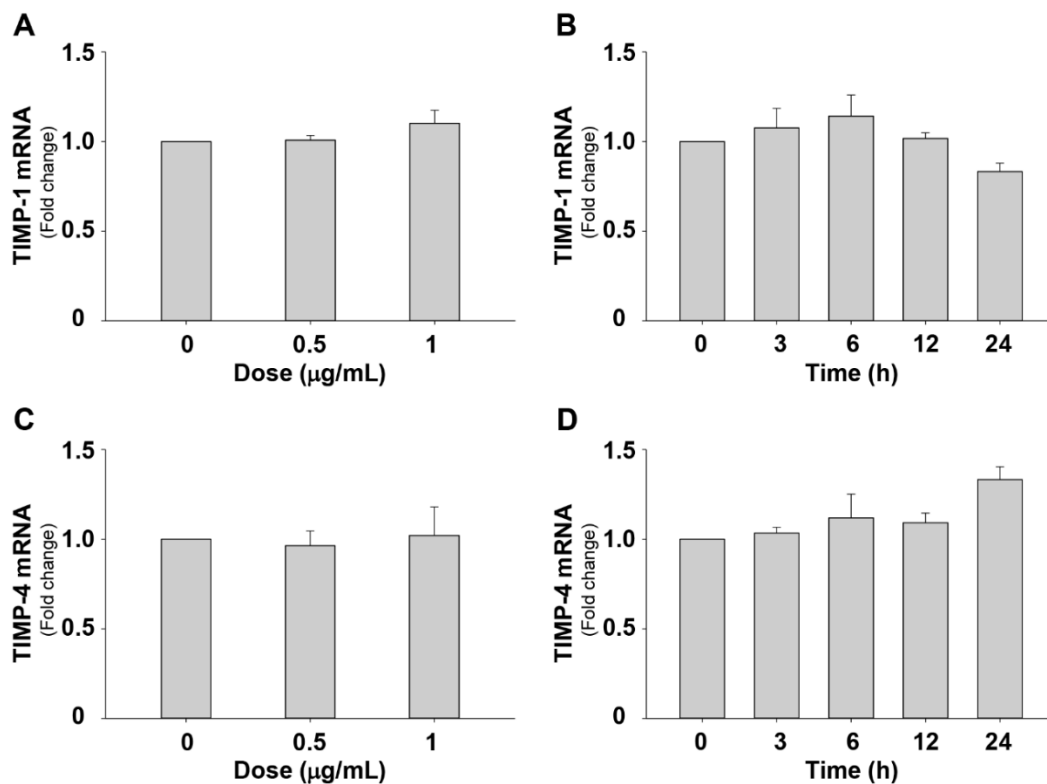


Figure 7. Dose- and time- dependent studies of TIMP-1 and TIMP-4 mRNA expression in BEAS-2B cells exposed to Nano-CuO.

For dose-response study, BEAS-2B cells were exposed to 0, 0.5 or 1 µg/mL of Nano-CuO for 6 h (**A, C**). For time-course study, BEAS-2B cells were exposed to 1 µg/mL of Nano-CuO for 0, 3, 6, 12 and 24 h (**B, D**). Cells without treatment were used as control. TIMP-1 and TIMP-4 mRNA expressions were determined by RT-qPCR. Data represent mean \pm SE (n=3).

2.3.5 Effects of Nano-CuO-induced ROS and MAPKs activation on MMP-3 expression

To explore whether Nano-CuO-induced ROS generation could trigger the upregulation of MMP-3, ROS inhibitors or scavengers, catalase (2000 U), NAC (20 mM), and Trolox (100 μ M), were used to pre-treat BEAS-2B cells for 2 h prior to exposure to Nano-CuO. The results showed that pretreatment of cells with catalase, NAC or Trolox significantly abolished Nano-CuO-induced increased MMP-3 mRNA expression (Figure 8A), and secreted MMP-3 protein level and activity (Figure 8C, E). Nano-CuO exposure caused significant lower MMP-3 expression and activity in BEAS-2B ρ^0 cells as compared to that in their parental cells (Figure 8B, D, F). These results suggest that ROS generation in BEAS-2B cells exposed to Nano-CuO is involved in Nano-CuO-induced increased expression and activity of MMP-3.

The results have shown that exposure to Nano-CuO caused activation of MAPKs through Nano-CuO-induced ROS generation. In order to investigate whether MAPKs activation were involved in Nano-CuO-induced MMP-3 upregulation, MAPKs inhibitors, including p38 inhibitor SB203580 (10 μ M), Erk1/2 inhibitor PD98059 (10 μ M), and JNK inhibitor SP600125 (10 μ M), were used to pre-treat BEAS-2B cells for 2 h prior to Nano-CuO treatment for another 6 h. The RT-qPCR results showed that Nano-CuO-induced MMP-3 upregulation was significantly abolished by SB203580, PD98059, or SP600125 pretreatment (Figure 9A). In addition, the secreted MMP-3 protein level in conditioned medium was significantly decreased by pre-treatment of the cells with p38, Erk1/2 and JNK

inhibitors (Figure 9B). β -casein zymography also demonstrated that Nano-CuO-induced increased MMP-3 activity was ameliorated by pre-treatment of the cells with MAPKs inhibitors (Figure 9C). These results indicated that increased MMP-3 expression and activity caused by Nano-CuO exposure was through Nano-CuO-caused oxidative stress and activation of MAPKs pathway.

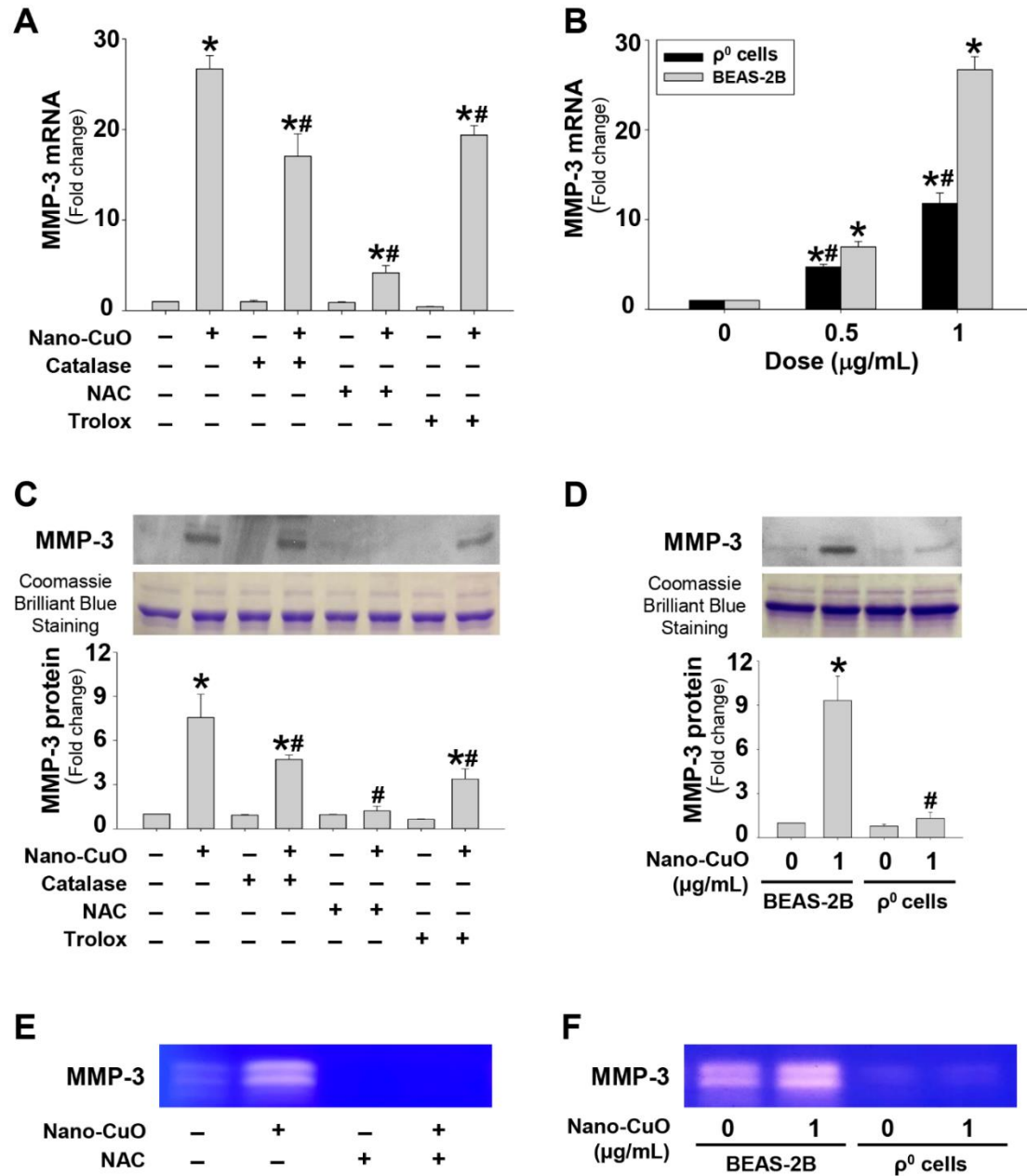


Figure 8. Effects of ROS scavengers or inhibitors, and mitochondrial DNA depletion on Nano-CuO-induced MMP-3 expression.

BEAS-2B cells were pre-treated with ROS scavengers or inhibitors (CAT 2000 U, NAC 20 mM, and Trolox 100 µM) for 2 h prior to exposure to 1 µg/mL of Nano-CuO for 6 h (A). BEAS-2B ρ⁰ cells were exposed to 0.5 and 1 µg/mL of Nano-

CuO for 6 h (**B**). Cells without treatment were used as control. (**C, D**) Conditioned media were collected for determination of MMP-3 by Western blot after BEAS-2B and BEAS-2B p⁰ cells were exposed to 1 µg/mL of Nano-CuO for 12 h with/without pre-treatment of NAC, CAT, or Trolox for 2 h. Equal protein loading was verified by Coomassie Brilliant Blue staining. (**E, F**) MMP-3 activity was measured by β-casein zymography. Data represent mean ± SE (n=3). * Significant difference as compared to the control group, $p < 0.05$; # Significant difference as compared to the Nano-CuO-treated alone group, $p < 0.05$.

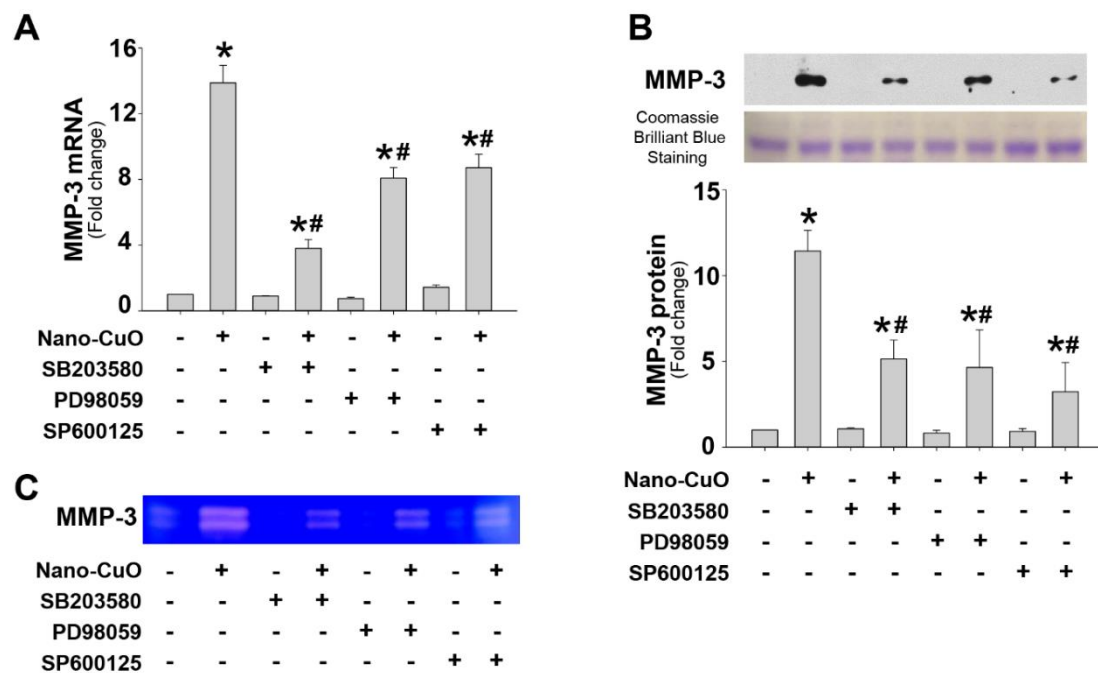


Figure 9. Effects of MAPKs inhibitors on Nano-CuO-induced MMP-3 upregulation in BEAS-2B cells.

BEAS-2B cells were pre-treated with p38 inhibitor SB203580 (10 μ M), Erk inhibitor PD98059 (10 μ M), or JNK inhibitor SP600125 (10 μ M) for 2 h prior to exposure to 1 μ g/mL of Nano-CuO. After 6 h treatment, total RNA was isolated for measurement of MMP-3 mRNA by real-time PCR (A). After 12 h treatment, conditioned media were collected for measurement of MMP-3 expression by Western blot (B), or for MMP-3 activity by β -casein zymography (C). Cells without treatment were used as control. Data represent mean \pm SE (n=3). * Significant difference as compared to the control, $p < 0.05$; # Significant difference as compared to the Nano-CuO-treated alone group, $p < 0.05$.

2.3.6 Nano-CuO exposure caused downregulation of tight and adherens junction-associated proteins in lung epithelial BEAS-2B cells

To determine whether exposure to metal nanoparticles could cause alteration expression of tight junction-associated proteins (ZO-1, occludin, and claudin-1) and adherens junction-associated protein E-cadherin, BEAS-2B cells were exposed with 0, 0.5 and 1 $\mu\text{g}/\text{mL}$ of Nano-CuO or Nano-TiO₂ for 48 h and the proteins were extracted for Western blot. The results showed that Nano-CuO exposure caused a significant decrease in the expression of ZO-1, occludin, claudin-1, and E-cadherin with a dose-dependent manner (Figure 10A, B, and Figure 11 A, B). The time-course study revealed that Nano-CuO exposure induced decreased expression of E-cadherin as early as 12 h after treatment, and reduced expression of ZO-1, occludin, claudin-1 after 24 h or 48 h of exposure (Figure 10C, D, and Figure 11C, D). The expression of ZO-1 and E-cadherin were also examined by dual immunofluorescent staining. The results demonstrated that exposure to 1 $\mu\text{g}/\text{mL}$ Nano-CuO for 48 h caused a significant decrease in the expression of ZO-1 and E-cadherin (Figure 10E and Figure 11E).

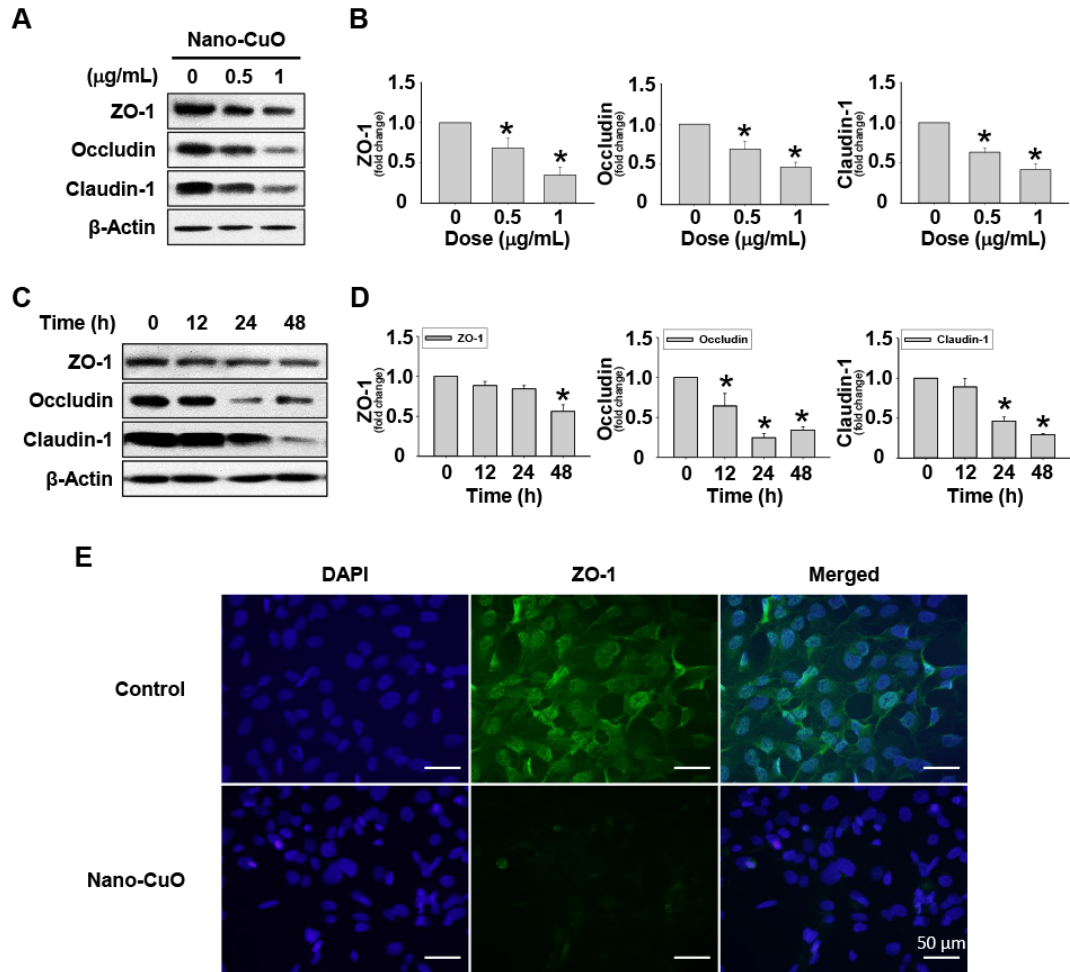


Figure 10. Dose- and time-dependent effects of Nano-CuO exposure on tight junction-associated proteins in BEAS-2B cells.

BEAS-2B cells were treated with 0, 0.5 and 1 μg/mL of Nano-CuO for 48 h (**A**, **B**) or 1 μg/mL of Nano-CuO for 0, 12, 24 and 48 h (**C**, **D**). The protein was isolated to detect the expression of tight junction-associated proteins. (**A**, **C**) were the results of a single Western blot experiment, while (**B**, **D**) were the average expression level of ZO-1, occludin, and claudin-1 normalized to β-actin from three independent experiments. Data represent mean ± SE (n=3). * Significant difference as compared to the control group. $p < 0.05$. (**E**) For immunofluorescent staining, cells

were treated with Nano-CuO for 48 h. Immunofluorescent staining of ZO-1 (green) was shown. DAPI (blue) stains the whole nuclei of cells. Scale bar represents 50 μm for all panels.

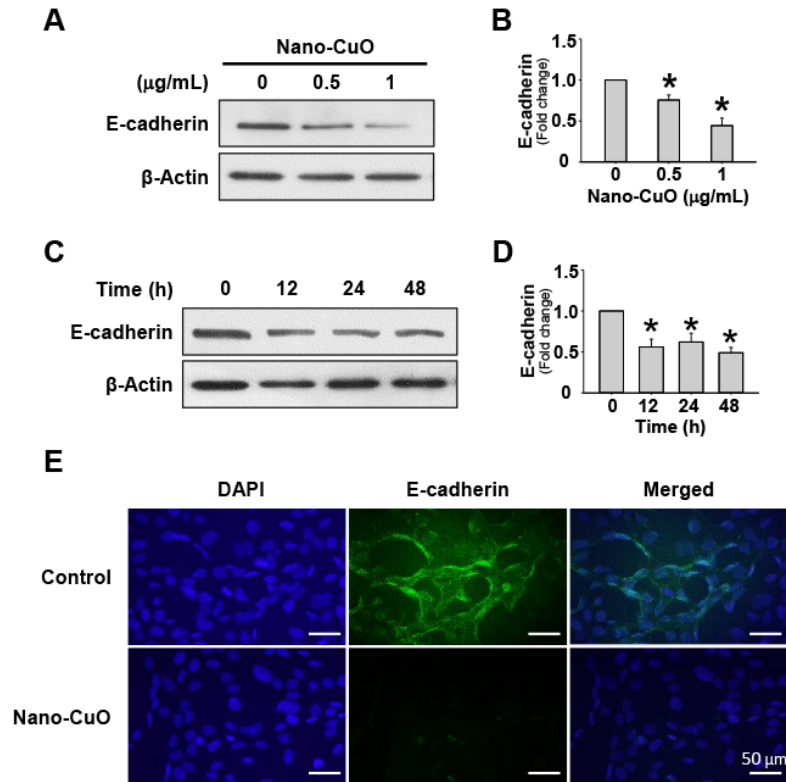


Figure 11. Dose- and time- dependent effects of Nano-CuO exposure on adherens junction-associated protein E-cadherin in BEAS-2B cells.

BEAS-2B cells were treated with 0, 0.5 and 1 µg/mL of Nano-CuO for 48 h (**A, B**) or 1 µg/mL of Nano-CuO for 0, 12, 24 and 48 h (**C, D**). The protein was isolated to detect the expression of adherens junction-associated protein E-cadherin. (**A, C**) were the results of a single Western blot experiment, while (**B, D**) were the average expression level of E-cadherin normalized to β-actin from three independent experiments. Data represent mean ± SE (n=3). * Significant difference as compared to the control group. $p < 0.05$. (**E**) For immunofluorescent staining, cells were treated with Nano-CuO for 48 h. Immunofluorescent staining of E-cadherin

(green) was shown. DAPI (blue) stains the whole nuclei of cells. Scale bar represents 50 μm for all panels.

2.3.7 The role of MMP-3 in Nano-CuO-induced downregulation of tight and adherens junction-associated proteins

To investigate the role of MMP-3 in Nano-CuO-induced downregulation of tight junction-associated proteins and adherens junction-associated protein, BEAS-2B cells were transfected with 30 nM of MMP-3 siRNA for 6 h and then exposed to 1 µg/mL of Nano-CuO for another 48 h. Negative Control No. 2 siRNA was used as a negative control. The efficiency of MMP-3 siRNA transfection was confirmed by Western blot. Nano-CuO-induced upregulation of MMP-3 was significantly blocked by MMP-3 siRNA, but not by control siRNA transfection (Figure 12A). In order to observe whether MMP-3 knock-down by siRNA will affect other MMPs, MMP-2 and MMP-9 activities were determined by gelatin zymography assay. The results showed that MMP-2 and MMP-9 were not affected (Figure 12B). MMP-3 siRNA transfection significantly restored the reduced expression of ZO-1, occludin, claudin-1, and E-cadherin caused by Nano-CuO (Figure 13A, B, and Figure 14A, B). The immunofluorescent staining results further confirmed that Nano-CuO-caused decrease of tight junction-associated proteins and adherens junction-associated protein were attenuated by MMP-3 siRNA (Figures 13C and 14C).

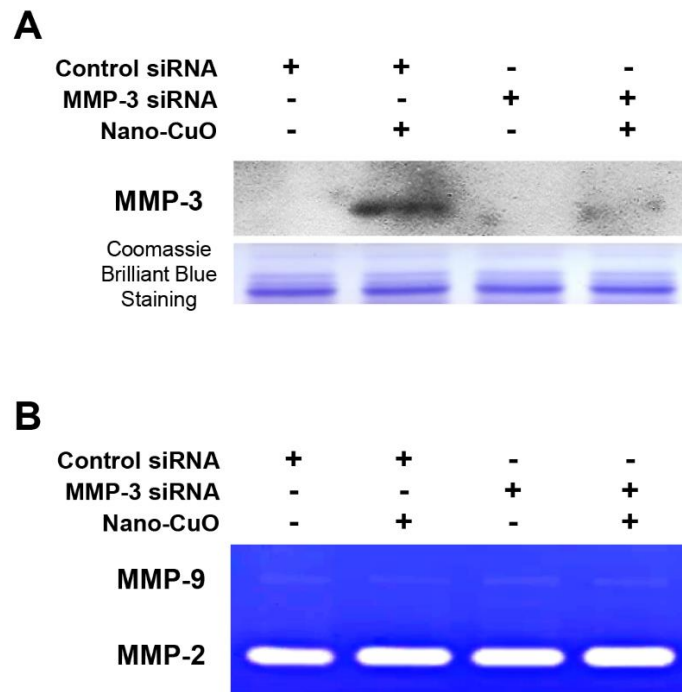


Figure 12. The efficiency of MMP-3 siRNA transfection and the effects of MMP-3 siRNA on MMP-2 and MMP-9 activities in BEAS-2B cells.

BEAS-2B cells were transfected with MMP-3 siRNA or Negative Control No. 2 siRNA. After 6 h transfection, the cells were exposed to 1 $\mu\text{g}/\text{mL}$ of Nano-CuO for another 12 h. Conditioned media were collected to detect the expression of MMP-3 by Western blot (**A**) and the activities of MMP-2 and MMP-9 by gelatin zymography assay (**B**). Equal protein loading was verified by Coomassie Brilliant Blue staining.

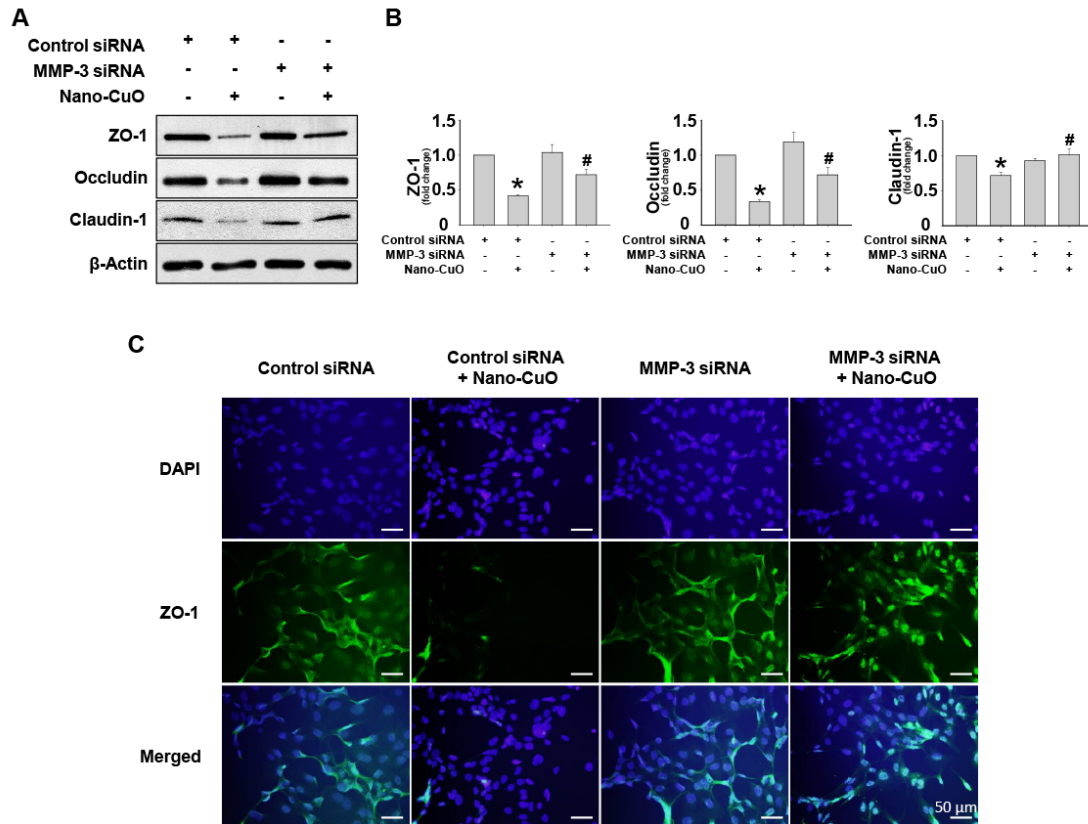


Figure 13. The role of MMP-3 on Nano-CuO-induced downregulation of tight junction-associated proteins in BEAS-2B cells.

BEAS-2B cells were transfected with MMP-3 siRNA or Negative Control No. 2 siRNA. After 6 h transfection, the cells were exposed to 1 $\mu\text{g}/\text{mL}$ of Nano-CuO for another 48 h. The protein was isolated from the cells to detect the expression of tight junction-associated proteins by Western blot (**A**, **B**), or the cells were used for immunofluorescent staining (**C**). Scale bar in (**C**) represents 50 μm for all panels. Data represent mean \pm SE (n=3). * Significant difference as compared to the control group, $p < 0.05$; # Significant difference as compared to the Nano-CuO-treated group transfected with Negative Control No. 2 siRNA, $p < 0.05$.

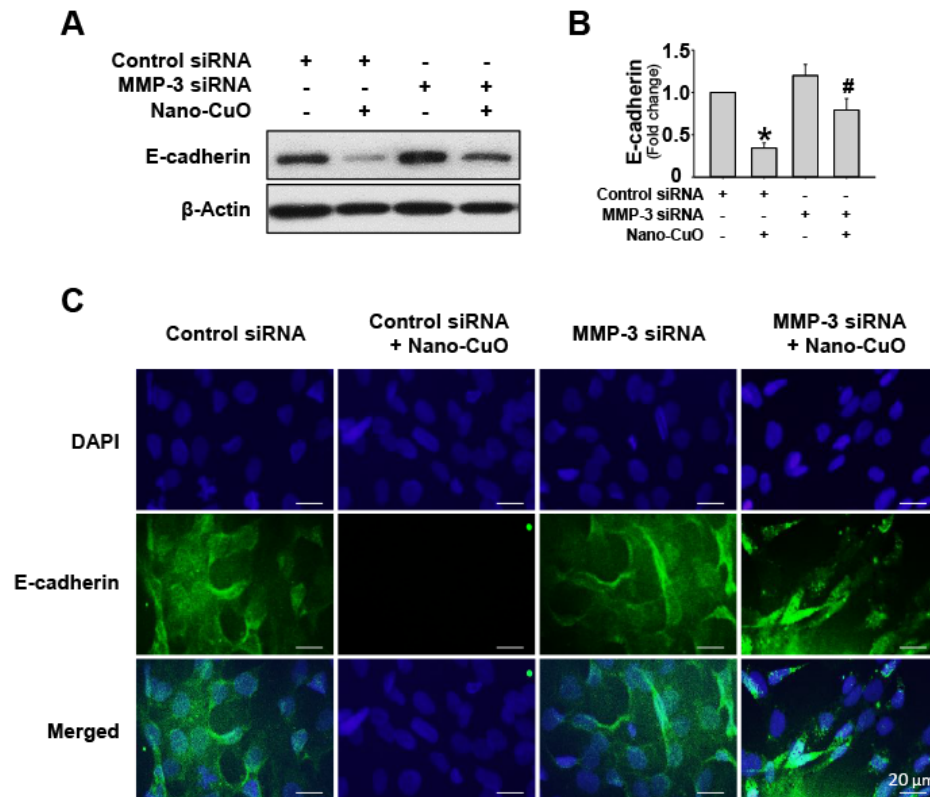


Figure 14. The role of MMP-3 on Nano-CuO-induced downregulation of adherens junction-associated protein E-cadherin in BEAS-2B cells.

BEAS-2B cells were transfected with MMP-3 siRNA or Negative Control No. 2 siRNA. After 6 h transfection, the cells were exposed to 1 $\mu\text{g}/\text{mL}$ of Nano-CuO for another 48 h. The protein was isolated from the cells to detect the expression of adherens junction-associated protein E-cadherin by Western blot (**A**, **B**), or the cells were used for immunofluorescent staining (**C**). Scale bar in (**C**) represents 20 μm for all panels. Data represent mean \pm SE (n=3). * Significant difference as compared to the control group, $p < 0.05$; # Significant difference as compared to the Nano-CuO-treated group transfected with Negative Control No. 2 siRNA, $p < 0.05$.

2.4 Discussion

Nano-CuO is widely used in various medical and industrial fields, such as wood-protection, antimicrobial productions, and nano-pigments (Evans et al. 2008; Ren et al. 2009; Semenzin et al. 2019; Tal Ben-Moshe 2009). With the increasing use of Nano-CuO, the potential health effects of Nano-CuO on human and environment are urgently needed to be investigated. Lungs are constantly in contact with ambient environment, thus they are one of major routes for various exogenous stimuli, such as microbes, environmental pollutants, nanoparticles, etc., to enter the body. Therefore, cells in first defend line of lung tissues against exogenous materials, such as epithelial cells, would be firstly exposed to nanoparticles after inhalation. BEAS-2B cells, non-tumorigenic epithelial cells that were derived from human lung tissues, have been widely used to evaluate the adverse effects of metal nanoparticles, such as lung inflammation, fibrosis, DNA damage, and cell transformation (Mo et al. 2021; Naz et al. 2020; Park et al. 2015; Strauch et al. 2017). Therefore, BEAS-2B cells were chosen in this study.

Our results demonstrated that exposure of BEAS-2B cells to Nano-CuO, but not Nano-TiO₂, caused severe cytotoxicity in a dose-dependent manner. Even at the very low concentrations of Nano-CuO, such as 1.5 µg/mL, it still reduced about 20% of cell viability. Non-cytotoxic doses of Nano-CuO were chosen in the present study because exposure to a dose that is lower than a cytotoxic dose can help identify potential health effects of Nano-CuO rather than those due to cytotoxicity. In addition, NIOSH recommended the exposure limits of copper fume of 0.1 mg/m³ (TWA). Assuming an adult worker works over 1000 days (8 h per

day) at 0.1 mg/m^3 of copper fume with 20 L/min ventilation rate, the total copper fume deposited in the lungs would be 384 mg (assuming no clearance and 40% deposition rate) ($0.1 \text{ mg/m}^3 \times 20 \text{ L/min} \times 60 \text{ min/h} \times 8 \text{ h/day} \times 1000 \text{ days} \times 40\% = 384 \text{ mg}$). The surface area of human lung is about 100 m^2 , so the exposure concentration of copper fume would be about $0.384 \text{ }\mu\text{g/cm}^2$. Previous study recommended a factor $\times 10$ for uneven deposition (Akerlund et al. 2019), then the copper fume exposure concentration would be $3.84 \text{ }\mu\text{g/cm}^2$, which is about 19-fold higher than the dose we used in this study. Therefore, $1 \text{ }\mu\text{g/mL}$ ($0.2 \text{ }\mu\text{g/cm}^2$) of Nano-CuO as the exposure dose we have chosen in the present study is reasonable.

Oxidative stress is a central hypothetical mechanism that accounts for the adverse effects induced by various metal nanoparticles (Akhtar et al. 2016; Horie et al. 2018; Lai et al. 2018; Naz et al. 2020; Wu et al. 2020). Oxidative stress occurs when production of ROS disturbs the balance of antioxidant ability and oxidative pressure. Nanoparticles, including Co, CuO, ZnO, and CeO₂, can cause excessive ROS production which may overwhelm antioxidant defenses and induce oxidative stress in different cell lines (Karlsson et al. 2008; Manke et al. 2013; Mo et al. 2009a; Wan et al. 2008; Wan et al. 2012; Zhang et al. 1998). In the present study, our results demonstrated that Nano-CuO exposure caused a dose- and a time-response increase in ROS generation in the BEAS-2B cells, and the increased ROS appeared as early as 3 h post-exposure. Nano-CuO-induced ROS generation was blocked by pre-treatment of BEAS-2B cells with ROS scavengers or inhibitors, such as catalase, NAC and Trolox. Mitochondria and NADPH oxidase are the

potential sources of ROS generation caused by nanoparticles (Karlsson et al. 2009; Mo et al. 2009a). To explore the potential sources of Nano-CuO-induced ROS, mitochondria-specific superoxide scavenger Mito-TEMPO or NADPH oxidase inhibitor diphenyleneiodonium (DPI) was used to pre-treat cells prior to exposure to Nano-CuO. The results demonstrated that Mito-TEMPO significantly suppressed Nano-CuO-induced ROS, while DPI did not change ROS generation, suggesting that Nano-CuO-caused ROS production was originated from mitochondria rather than from activation of NADPH oxidase. These results were further confirmed by using BEAS-2B ρ^0 cells; exposure of BEAS-2B ρ^0 cells to Nano-CuO caused significantly lower ROS generation as compared to that in the parental cells.

In addition, nanoparticle-caused ROS generation also contributes to the activation of cell signaling pathways, inflammatory cytokine and chemokine expression, and transcription factors (Manke et al. 2013). Although the components that mediate these effects differ among the different nanoparticles, there is commonality through their ability to cause oxidative stress. MAPKs are a kind of protein kinases that are sensitive to ROS stimulation and act important roles in responding to oxidative stress. A previous study indicated that Nano-CuO-induced oxidative stress was involved in Nano-CuO-induced DNA damage and cell death via activation of p38 MAPK pathway in human vascular endothelial cells (HUVEC) (He et al. 2020). Nano-CuO-induced ROS also caused increased phosphorylation of Erk MAPK and p53, leading to cytotoxicity in human keratinocytes HaCaT and mouse embryonic fibroblasts MEF (Luo et al. 2014). Our

previous study also showed that Nano-CuO-caused upregulation of PAI-1 in endothelial cells which was mediated by p38 phosphorylation was due to oxidative stress (Yu et al. 2010). In the present study, Nano-CuO exposure caused increased phosphorylation of p38, Erk and JNK at as early as 3 h after Nano-CuO exposure, corresponding with Nano-CuO-induced ROS generation which was also occurred at 3 h post-exposure. And pre-treatment of the cells with ROS inhibitors or scavengers, such as CAT, NAC and Trolox, could significantly inhibit MAPKs activation induced by Nano-CuO. Meanwhile, the expression of MMP-3 caused by Nano-CuO was also abolished by ROS scavengers or inhibitors at both mRNA and protein levels. To further explore the role of MAPKs activation in the upregulation of MMP-3, inhibitors of MAPKs, such as p38 specific inhibitor, SB203580, Erk specific inhibitor, PD98059, and JNK specific inhibitor, SP600125, were used to pretreat BEAS-2B cells prior to exposure to Nano-CuO. The results manifested that these three specific MAPKs inhibitors significantly inhibited Nano-CuO-induced upregulation of MMP-3. Our results suggest that Nano-CuO-induced MMP-3 upregulation may be through MAPKs activation via Nano-CuO-induced ROS generation.

MMPs belong to a superfamily of enzymes that are able to degrade various kinds of extracellular matrix proteins, playing important roles in the process of tissue remodeling and repair (Nagase and Woessner 1999; Nagase and Brew 2002; Sternlicht and Werb 2001; Visse and Nagase 2003). In normal physiological conditions, the expression and activity of MMPs are precisely regulated by transcriptional factors and cytokines and are balanced by endogenous inhibitors

which are tissue inhibitors of metalloproteinases (TIMPs) (Balkowiec et al. 2018; Cui et al. 2017). However, under pathologic conditions, overexpression of MMPs may lead to disruption of intercellular junction proteins and dysfunction of epithelial barrier, which may further contribute to the development of various lung diseases, such as inflammation, chronic obstructive pulmonary disease, asthma, and fibrosis (Carlier et al. 2021; Ohta et al. 2012; Zou et al. 2020). For example, MMP-9 has been reported to be involved in the disruption of tight junction-associated protein occludin in human lung epithelial BEAS-2B cells, and BB94, a MMP inhibitor, significantly alleviated the downregulation of occludin induced by silica nanoparticles (Liu et al. 2020). In addition, overexpression of MMP-2 and MMP-9 could decrease tight junction-associated protein ZO-1 and increase blood-brain barrier (BBB) permeability, which were inhibited by pre-treatment of MMP-2/9 inhibitor SB-3CT *in vivo* and *in vitro* (Zhang et al. 2018). In our previous study, MMP-2 and MMP-9 were also involved in the Nano-Ni-induced downregulation of tight junction-associated proteins, including ZO-1, occludin, and claudin-1, in human keratinocytes (Yuan et al. 2021). However, few studies focused on the effects of MMP-3, another member of MMPs family, on intercellular junction proteins in lungs.

Lungs are constantly challenged by external environmental agents, such as various particles, microbes, etc. Therefore, the integrity of the epithelial barrier is essential to provide effective protection for the lungs (Bhat et al. 2018; Buckley and Turner 2018; Zihni et al. 2016). Tight junction, adherens junction, and other cell junctions together lock the epithelial cells into a stable layer and function as

the barrier. The dysregulation of cell junction-associated proteins may lead to impaired epithelial barrier function and further result in tissue damage (Lappi-Blanco et al. 2013; Ohta et al. 2012; Zou et al. 2020). Nanoparticles-induced disruption of cell junction-associated proteins has been reported (Chen et al. 2020; Chen et al. 2016; Liu et al. 2020; Xu et al. 2015; Yuan et al. 2021). For example, a study revealed that exposure to zinc oxide nanoparticles disrupted the endothelial tight and adherens junctions and further led to inflammatory cell infiltration in mouse lungs (Chen et al. 2020). Another study revealed that exposure to silica nanoparticles decreased the expression of tight junction-associated proteins, such as ZO-1, occludin, and claudin-1 (Liu et al. 2020). In the present study, our results demonstrated that exposure of BEAS-2B cells to Nano-CuO for 48 h resulted in the disruption of tight and adherens junctions, reflected by decreased expression of ZO-1, occludin, claudin-1, and E-cadherin. Meantime, our results demonstrated that exposure to Nano-CuO caused significantly increased MMP-3 expression in both transcriptional and translational levels in human lung epithelial cells, whereas the expression of TIMP1 and TIMP-4 was not altered. Our results also showed that exposure of BEAS-2B cells to Nano-CuO did not cause any changes in the expression of MMP-2 and only caused a slight, but not significant increase in the expression of MMP-9 (data not shown). This raises the intriguing possibility that Nano-CuO-induced MMP-3 upregulation may be involved in Nano-CuO-induced lung epithelial barrier dysfunction, which was confirmed by the MMP-3 siRNA transfection. Knocking down MMP-3 by MMP-3 siRNA

significantly restored Nano-CuO-caused reduction of ZO-1, occludin, claudin-1, and E-cadherin.

Previous studies have shown that MMP-3 is involved in the downregulation of cell junction-associated proteins (Yamashita et al. 2011). For example, in the lung tissues of patients with idiopathic pulmonary fibrosis (IPF), both MMP-3 mRNA and protein expression levels were increased (Yamashita et al. 2011), and the upregulated level of MMP-3 was correlated with an increased permeability index (McKeown et al. 2009). In mice, overexpression of MMP-3 caused the decrease of tight junction-associated proteins, such as ZO-1 and occludin in blood vessels and increased the blood-spinal cord barrier (BSCB) permeability after spinal cord injury, while these effects were attenuated in MMP-3 KO mice (Lee et al. 2014). MMP3 upregulation also reduced the barrier integrity in microvascular endothelial cells (BMVECs) and increased the blood-brain barrier (BBB) permeability in mice (Zhang et al. 2021a).

Taken together, our study demonstrated that exposure of human lung epithelial BEAS-2B cells to Nano-CuO caused MMP-3 upregulation, which further induced downregulation of tight and adherens junction-associated proteins. The results also revealed that Nano-CuO-induced upregulation of MMP-3 was mediated by phosphorylation of MAPKs due to Nano-CuO-induced oxidative stress. These results provide further understanding of pulmonary inflammation and fibrosis caused by metal nanoparticle exposure.

CHAPTER III: EXAMINE WHETHER NANO-CUO EXPOSURE WOULD ACTIVATE FIBROBLASTS AND THE ROLE OF MMP-3 AND OPN IN THIS PROCESS

3.1 Introduction

Nano-CuO has been shown to cause oxidative stress, inflammatory response, oxidative DNA lesions, immunotoxicity, and even cell death (Costa et al. 2018; Juganson et al. 2015; Karlsson et al. 2008; Naz et al. 2020). In chapter II, I have shown that Nano-CuO exposure caused upregulation of matrix metalloproteinase-3, and our previous study showed that MMP-3 was involved in the occurrence of epithelial-mesenchymal transition in human lung epithelial cells, which is a cellular process playing crucial roles in disease development such as cancer and fibrosis (Zhang et al. 2021b). Several *in vivo* studies also showed that Nano-CuO exposure induced epithelial cell injury, pulmonary inflammation, and finally lung fibrosis in mice (Ko et al. 2018; Lai et al. 2018). However, the mechanism underlying Nano-CuO-induced lung fibrosis is still unclear.

Activation of fibroblasts is considered the cellular drive that leads to the development of fibrosis (Darby and Hewitson 2007). Activated fibroblasts have a high capacity to produce extracellular matrix proteins and express α -SMA, which contribute to the form of fibrotic foci and contraction of fibrotic tissues (Darby and Hewitson 2007; Dong and Ma 2017). Nanoparticle-induced activation of fibroblasts

have been reported in previous studies (Bonner 2010; Dong and Ma 2015; Dong and Ma 2016; Hussain et al. 2014; Kabadi et al. 2019; Ryman-Rasmussen et al. 2009; Snyder-Talkington et al. 2013; Venter and Niesler 2018; Wang et al. 2013). For example, Previous study revealed that multi-walled carbon nanotubes (MWCNTs) exposure caused secretion of TGF- β 1 in alveolar macrophages and subsequently induced TGF- β 1-dependent fibrotic responses in both co-culture model and male spontaneously hypertensive rats (Wang et al. 2013). Another study demonstrated that MWCNTs induced NLRP3 inflammasome activation in airway epithelial cells, which further mediated non-TGF- β dependent pro-fibrotic responses in lung fibroblasts (Hussain et al. 2014). However, whether Nano-CuO could activate fibroblasts and the underlying mechanisms are still not fully elucidated.

Osteopontin (OPN), also named secreted phosphoprotein 1 (SPP1), is an important cytokine in body fluids and extracellular matrix. Human OPN has two well-known integrin-binding motifs: a typical RGD motif and an SVVYGLR integrin-binding site, through which it binds integrin family such as α v β 3, playing key roles in many physiological and pathological progress, including inflammation, cancer, COPD, asthma, and fibrosis (Mangum et al. 2004; Mori et al. 2008; O'Regan 2003; Ophascharoensuk et al. 1999; Pardo et al. 2005; Rangaswami et al. 2006; Samitas et al. 2011; Simoes et al. 2009; Takahashi et al. 2001; Wang and Denhardt 2008). Elevated expression of OPN has been observed in lung diseases, such as asthma and IPF, and the upregulated OPN level is associated with the severity of these lung diseases (Pardo et al. 2005; Samitas et al. 2011; Simoes et al. 2009).

Nanoparticle-induced overexpression of OPN has been reported *in vitro* and *in vivo*. For example, OPN was highly and persistently induced in mouse lungs responding to MWCNTs exposure in both acute and chronic phases, and knocking-out OPN had a protective effect against MWCNTs-induced fibrotic focus formation and fibroblast accumulation in mouse lungs (Dong and Ma 2017). Another study also showed that OPN was highly expressed in bleomycin-induced lung fibrosis, while RMV-7, an αv integrin monoclonal antibody, significantly suppressed the fibrotic responses caused by bleomycin in both *in vitro* and *in vivo* models (Takahashi et al. 2001). However, whether Nano-CuO exposure could cause upregulation of OPN and its role in the fibrotic responses caused by Nano-CuO are unclear. In addition, the bioactivity of OPN is modified by proteolytic cleavage through which OPN exposes its integrin-binding motifs that are masked in intact OPN, and cleaved-OPN exerts enhanced biological activity than the intact protein (Agnihotri et al. 2001; Denhardt et al. 2001; Senger et al. 1996; Senger and Perruzzi 1996; Takahashi et al. 1998). Previous study has reported that OPN is a substrate of MMP-3 and cleavage of OPN by MMP-3 potentiated the bioactivity of OPN (Agnihotri et al. 2001). Interestingly, MMP-3, a member of MMPs and an important mediator of pulmonary fibrosis, is always co-expressed with OPN in fibrotic responses (Agnihotri et al. 2001; Craig et al. 2015; Szalay et al. 2009). This raises the intriguing possibility that MMP-3-cleaved OPN may be involved in metal oxide nanoparticle-induced pulmonary fibrosis. Therefore, investigating the relationship between MMP-3-cleaved OPN and fibroblast activation after metal

nanoparticle exposure will contribute to our full understanding of the mechanisms underlying metal nanoparticle-induced pulmonary fibrosis.

In the present chapter, a triple co-culture model consisting of human lung epithelial cells, macrophages, and fibroblasts was established to explore the role of MMP-3 in the fibrotic responses *in vitro* after nanoparticle exposure. We hypothesized that exposure of human lung epithelial cells and macrophages to Nano-CuO would increase the expression and activity of MMP-3, which cleaved OPN to produce bioactive OPN fragment, contributing to the fibroblast activation and lung fibrosis finally.

3.2 Materials and methods

3.2.1 Nanoparticles and their characterization

See “Nanoparticles and their characterization” in Materials and methods in the section 2.2.1 of Chapter II.

3.2.2 Chemicals and reagents

CellTiter 96® AQueous Non-Radioactive Cell Proliferation Assay (MTS assay) was purchased from Promega (Madison, WI), and alamarBlue Cell Viability Reagent (alamarBlue assay) was from Invitrogen (Eugene, OR). Phorbol 12-myristate 13-acetate (PMA) was obtained from Promega Corporation (Madison, WI). MMP-3 substrate β -casein and GRGDSP peptides were from SIGMA (Saint Louis, MO).

Antibodies against β -actin (cat.# 58169), collagen type 1 (Col1A1, cat.# 84336), fibronectin (cat.# 26836), TGF- β (cat.# 3711), and horseradish peroxidase (HRP)-conjugated horse anti-mouse IgG (cat.# 7076) and goat anti-rabbit IgG (cat.# 7074) were obtained from Cell Signaling Technology (Beverly, MA). Anti-osteopontin (OPN) antibody (cat.# PIPA534579) was purchased from Invitrogen Corporation (Carlsbad CA). Anti-MMP-3 antibody (cat.# 53015 and 52915) was from abcam (Cambridge, MA), and anti- α -SMA (cat.# A5228) antibodies from SIGMA (Saint Louis, MO).

All other chemicals were purchased from Fisher Scientific (Fair Lawn, NJ) except when otherwise stated. All chemicals used were of analytical grade.

3.2.3 Cell culture

Human U937 monocytes (cat.# CRL-1593.2) and normal human bronchial epithelial cells BEAS-2B (cat.# CRL-9609) were purchased from American Type Culture Collection (ATCC, Manassas, VA) and maintained in RPMI 1640 medium with L-glutamine, supplemented with 10% Fetal Bovine Serum (FBS), 100 U/mL penicillin, and 100 µg/mL streptomycin (Corning, Manassas, VA) in a humidified atmosphere at 37 °C and 5% CO₂. Prior to use, U937 monocytes were differentiated into macrophages (U937*) with 100 nM PMA at 37 °C for 48 h.

Human fibroblasts MRC-5 cells were obtained from ATCC (cat.# CCL-171) and maintained in Eagle's Minimum Essential Medium (EMEM) supplemented with 10% FBS, 100 U/mL penicillin, and 100 µg/mL streptomycin (Corning, Manassas, VA) in a humidified atmosphere at 37 °C and 5% CO₂.

3.2.4 Collection of conditioned media

4 × 10⁵ BEAS-2B or U937* cells per well were seeded in 6-well plates in 2 mL complete EMEM. After overnight culture, the cells were exposed to Nano-CuO for 12 h. The cell culture media were collected and centrifugated. For co-culture of BEAS-2B and U937*, BEAS-2B cells were seeded in 6-well plates and incubated overnight. Then U937* macrophages were added at the ratio of 1:1 or 1:9 (U937*:BEAS-2B, total 4 × 10⁵ cells per well). BEAS-2B-U937* co-culture was cultured in 2 mL complete EMEM for 12 h in a humidified atmosphere at 37 °C and 5% CO₂. Then the co-culture was exposed to 0.5 or 1 µg/mL of Nano-CuO for another 12 h. The cell culture media were collected and centrifugated, and the

supernatant was used as conditioned media to culture MRC-5 cells for 0, 12, 24, 48 and 72 h. Supernatants from unexposed cells were used as negative control.

3.2.5 Triple co-culture model

The triple co-culture model was composed of three kinds of human cell lines: human lung bronchial epithelial cells (BEAS-2B), macrophages (differentiated U937), and fibroblasts (MRC-5), and was set according to the previous studies with a little modification (Akerlund et al. 2019; Barosova et al. 2020; Kabadi et al. 2019; Rothen-Rutishauser et al. 2005). Briefly, BEAS-2B cells were seeded at first in the inserts of Corning Transwell®-Clear unit (24 mm diameter insert, 0.4 µm pore size, polyester membrane, Corning, NY) in 2 mL complete EMEM. 1.5 mL complete medium was added in the lower chamber. After overnight incubation, the medium was aspirated, and 2 mL U937* macrophage suspension was added on top of the BEAS-2B epithelial monolayer at the ratio of 1:1 or 1:9 (U937*:BEAS-2B). The total BEAS-2B and U937* cells were 2×10^5 cells per insert. U937* macrophages were allowed to attachment for 12 h and the medium was changed. The cells were incubated for another 24 h at 37 °C and 5% CO₂.

MRC-5 cells were seeded in 6-well plates at a density of 1×10^5 cells/mL in a volume of 2 mL/well and incubated for 48 h. Then, the inserts above were placed in the well with MRC-5 cells, and 1 mL of complete EMEM was added in the insert and 1.5 mL in the lower chamber. The triple co-culture model was incubated for 12 h in a humidified atmosphere at 37 °C and 5% CO₂. Then BEAS-2B and U937*

cells in the inserts were exposed to 1 µg/mL of Nano-CuO for 12 h. After exposure, the inserts were taken out and MRC-5 cells in the lower chamber were incubated for another 36 h.

3.2.6 Cytotoxicity assays

The cytotoxicity of Nano-CuO in BEAS-2B, U937, and MRC-5 cells were determined by both alamarBlue assay and MTS assay as described in our previous studies (Mo et al. 2009b). Briefly, cells were seeded in 96-well plates. After 12 h incubation, cells were treated with different doses of Nano-CuO in a total volume of 200 µL per well. Cells without treatment were used as control. After treatment, the cytotoxicity was determined by recording the colorimetric absorbance at 490 nm for MTS assay and fluorescence at ex530/em590 for alamarBlue assay. The cell viability was presented as the percentage as compared to the control.

3.2.7 Wound healing assay

Fibroblast migration ability was evaluated by *in vitro* wound healing assay. Briefly, MRC-5 fibroblasts were seeded in 12-well plates and incubated in EMEM media until ~70-80% confluency. The wound was carefully made by scratching a straight line in the monolayer using a pipette tip. A second scratch was made perpendicular to the first one and the wells were washed twice with 1 x PBS to remove any detached cells. After treatment with conditioned media for 48 h, the cell image was captured by a microscopy (Nikon, Japan) and the wound closure

area was calculated by using NIH ImageJ software (<https://imagej.nih.gov/ij/>), which was used to determine the migration ability of fibroblasts.

3.2.8 β -casein zymography assay

See “ β -casein zymography assay” in Materials and methods in the section 2.2.8 of Chapter II.

3.2.9 Protein extraction and Western blot

See “Protein extraction and Western blot” in Materials and methods in the section 2.2.9 of Chapter II.

To determine the level of cleaved-OPN, the media were collected and concentrated by Amicon® Ultra centrifugal filter units (with Ultracel-10K membrane) for 10 times before electrophoresis. The gel stained with 0.1% Coomassie Brilliant Blue R-250 was used as loading reference.

3.2.10 Transfection of BEAS-2B and U937* cells with MMP-3 siRNA

Transfection was performed as described in the section 2.2.10 of chapter II with modifications. Briefly, BEAS-2B cells were seeded in the inserts and incubated for 24 h, then U937* cells were seeded at a ratio of 1:1 or 1:9 (U937*:BEAS-2B) onto the BEAS-2B cell layer in antibiotic-free RPMI1640 supplemented with 10% FBS and allowed to attach. Cells were then transfected with a mixture of 6 μ L of TurboFectin 8.0 Transfection Reagent (Origene, Rockville, MD) and 30 nM of MMP-3 siRNA (Ambion, Carlsbad, CA) in a total volume of 1

mL antibiotic-free and FBS-free RPMI 1640 medium for 6 h. Afterwards, 1 mL of RPMI 1640 medium containing 2 times FBS and antibiotics was added, and the cells were incubated for another 12 h. Silencer™ Select Negative Control No. 2 siRNA (Ambion, Carlsbad, CA) was used as a negative control. After exposure to Nano-CuO for 12 h, the conditioned media were collected and the roles of MMP-3 in cleavage of OPN and activation of fibroblasts were determined.

3.2.11 Statistical analysis

Results were expressed as the mean \pm standard error (SE). The differences among groups with one independent variable were evaluated by one-way analysis of variance (ANOVA) with Bonferroni post-hoc test. The differences among groups with two independent variables were evaluated by two-way analysis of variance (ANOVA) with Holm-Sidak test. All analyses were carried out using SigmaPlot 13.0 software (Systat Software, San Jose, CA). In all statistical analyses, a *p*-value < 0.05 was deemed statistically significant.

3.3 Results

3.3.1 Cytotoxic effects of Nano-CuO on MRC-5, U937*, and BEAS-2B cells

To find a non-cytotoxic dose for the mechanism study, the cytotoxicity of Nano-CuO on MRC-5, U937*, and BEAS-2B cells were at first determined by alamarBlue assay. MRC-5 cells were exposed to various concentrations of Nano-CuO for 48 h, U937* and BEAS-2B cells were exposed to different doses of Nano-CuO for 24h. After exposure, cell viability was measured by alamarBlue assay. The results showed that exposure of MRC-5 (Figure 15A), U937* (Figure 15B), and BEAS-2B cells (Figure 1B) to 1 $\mu\text{g}/\text{mL}$ or lower concentrations of Nano-CuO did not cause significant decreases in cell viability. These results were further confirmed by using MTS assay (data not shown). Therefore, non-cytotoxic doses ($\leq 1 \mu\text{g}/\text{mL}$) were chosen for the following *in vitro* experiments.

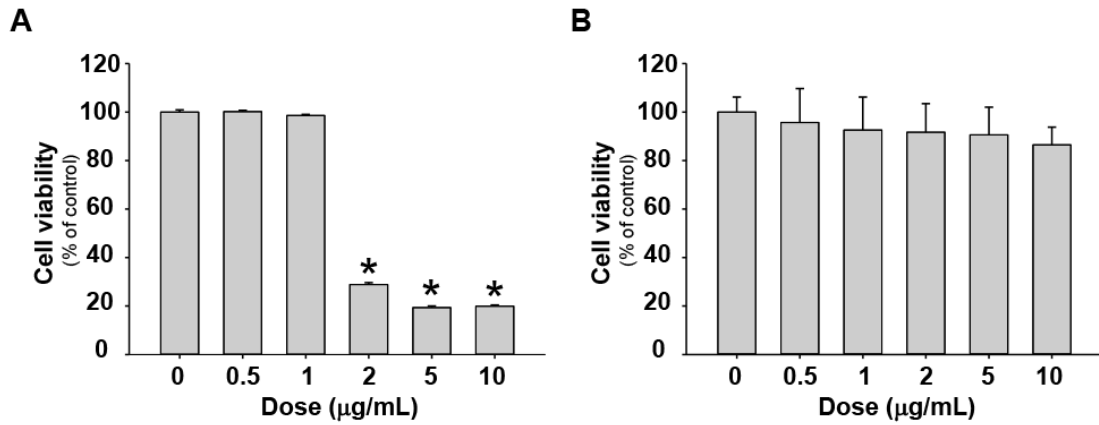


Figure 15. Cytotoxicity of Nano-CuO on human MRC-5 fibroblasts and U937-derived macrophages.

MRC-5 fibroblasts (**A**) and U937* macrophages (**B**) were seeded into 96-well plates and treated with different doses of Nano-CuO for 48 (**A**) and 24 h (**B**), respectively. The cytotoxicity was determined by alamarBlue assay. Cells without treatment were used as control. Data represent mean \pm SE (n=6). * Significant difference as compared to the control group, $p < 0.05$.

3.3.2 Exposure to Nano-CuO increased the expression and activity of MMP-3 in BEAS-2B and U937* cells, but not in MRC-5 cells

The effects of Nano-CuO on MMP-3 expression and activity in BEAS-2B, U937*, and MRC-5 cells were detected by Western blot and β -casein zymography assay, respectively. In chapter II, I have shown that exposure to Nano-CuO caused a dose-dependent increase in the expression and activity of MMP-3 in BEAS-2B cells, and the peak occurred at 12 h after Nano-CuO exposure. Therefore, in this chapter, BEAS-2B, U937*, and MRC-5 cells were exposed to 0, 0.5 and 1 $\mu\text{g/mL}$ of Nano-CuO for 12 h, and the expression and activity of MMP-3 were measured after exposure. The results demonstrated that exposure to Nano-CuO caused a dose-dependent increase in the expression of MMP-3 in both BEAS-2B and U937* cells (Figure 16A, C, E, G). The MMP-3 activity detected by β -casein zymography was consistent with its protein expression results (Figure 16B, D, F, H). Exposure of BEAS-2B cells to 1 $\mu\text{g/mL}$ of Nano-CuO caused a 3~4-fold increase in MMP-3 activity. Similarly, a 3~4-fold increment of MMP-3 activity was also observed in U937* macrophages after Nano-CuO exposure. However, in MRC-5 cells, Nano-CuO exposure did not cause any change in the expression and activity of MMP-3 (data not shown).

To further explore the effects of Nano-CuO exposure on the activity of MMP-3 in the co-culture system, BEAS-2B and U937* cells were co-cultured at the rate of 1:1 and 9:1 (BEAS-2B:U937*) and then exposed to 1 $\mu\text{g/mL}$ of Nano-CuO for 12 h. After Nano-CuO exposure, the MMP-3 activity in the media was measured by using β -casein zymography. The results demonstrated that Nano-CuO induced

a 3~4-fold increase in the MMP-3 activity in both 1:1 and 9:1 co-culture models (Figure 17), which are similar to those in mono-culture models.

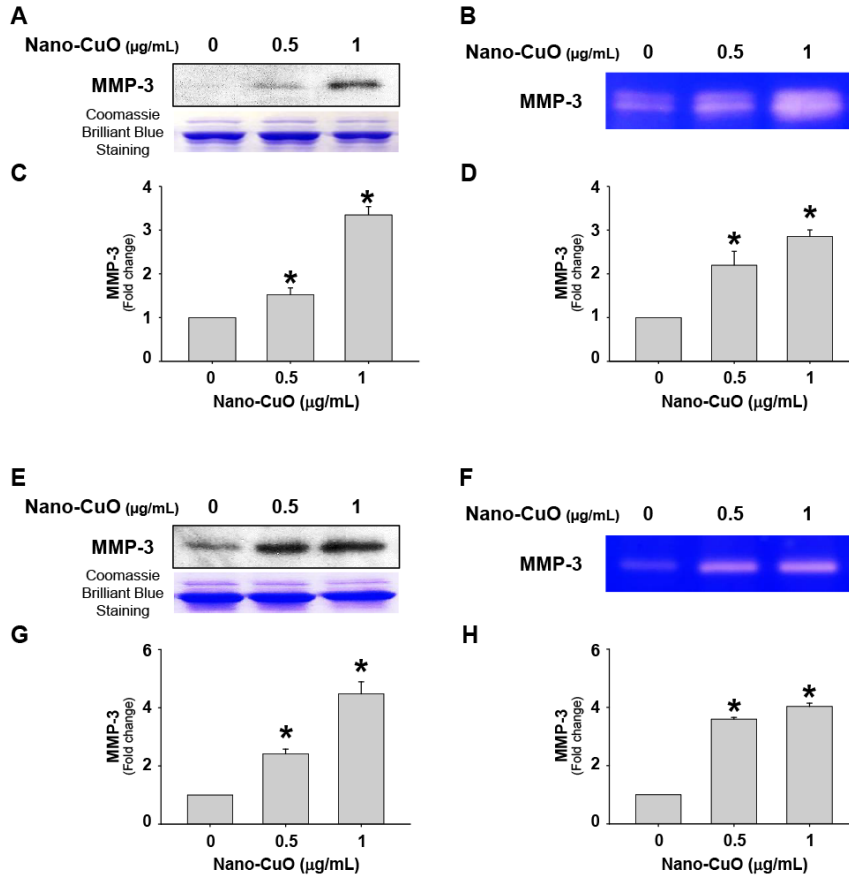


Figure 16. Increased secretion of MMP-3 in BEAS-2B cells and U937* macrophages exposed to Nano-CuO.

BEAS-2B cells (**A-D**) and U937* macrophages (**E-H**) were exposed to 0, 0.5 and 1 μg/mL of Nano-CuO for 12 h. After treatment, the conditioned media were collected. MMP-3 protein level in the conditioned media was detected by Western blot (**A, E**). Equal protein loading was verified by Coomassie Brilliant Blue staining. MMP-3 activity in the conditioned media was detected by β-casein zymography (**B, F**). **A, B, E** and **F** were the results of a single experiment, while **C, D, G** and **H** were normalized band densitometry readings averaged from three independent experiments. Data represent mean ± SE (n=3). * Significant difference as compared to the control group, $p < 0.05$.

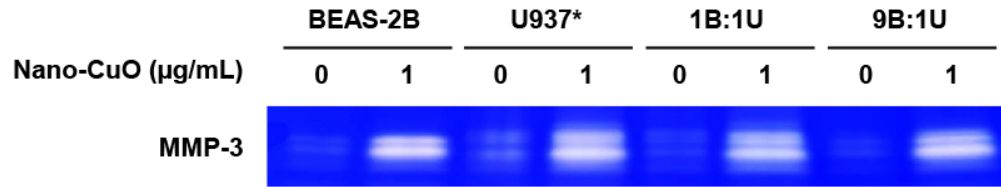


Figure 17. Increased MMP-3 activity in BEAS-2B and U937* cells exposed to Nano-CuO.

BEAS-2B cells, U937* macrophages, or co-culture of BEAS-2B and U937* cells at the ratio of 1:1 or 9:1 (BEAS-2B:U937*) were exposed to 1 $\mu\text{g/mL}$ of Nano-CuO for 12 h. After treatment, the conditioned media were collected. MMP-3 activity in the conditioned media was detected by β -casein zymography. For the electrophoresis, equal volume of conditioned media was loaded.

3.3.3 Exposure to Nano-CuO caused upregulation of OPN in BEAS-2B and U937* cells, but not in MRC-5 cells

To study whether exposure to Nano-CuO could cause upregulation of OPN, BEAS-2B, U937*, and MRC-5 cells were treated with 0, 0.5 and 1 $\mu\text{g}/\text{mL}$ of Nano-CuO for 12 h, the expression of full-length OPN in cells and cleaved-OPN in media were determined by Western blot. The results showed that Nano-CuO exposure induced a dose-dependent increase in the full-length OPN in BEAS-2B and U937* cells cleaved-OPN in the conditioned media from BEAS-2B and U937* cells (Figure 18A, B, C, D). However, in MRC-5 cells, Nano-CuO exposure did not induce a significant increase in either full-length or cleaved-OPN (data not shown).

In the co-culture system, Nano-CuO-induced OPN production in both cells and in media were detected by Western blot. BEAS-2B and U937* cells were seeded at a ratio of 1:1 or 9:1 (BEAS-2B:U937*) and exposed to 0.5 or 1 $\mu\text{g}/\text{mL}$ of Nano-CuO for 12 h, respectively. Nano-CuO exposure caused, in both ratio of 1:1 and 9:1 co-culture system, a dose-dependent increase in the expression of full-length OPN in cells and cleaved-OPN in the media (Figure 18A, B, C, D). The expression of cleaved-OPN in the conditioned media from co-culture systems were also compared with that from monoculture. The results showed that exposure to 1 $\mu\text{g}/\text{mL}$ of Nano-CuO caused a similar fold increase in cleaved-OPN in both monoculture and co-culture systems (Figures 18D and 19).

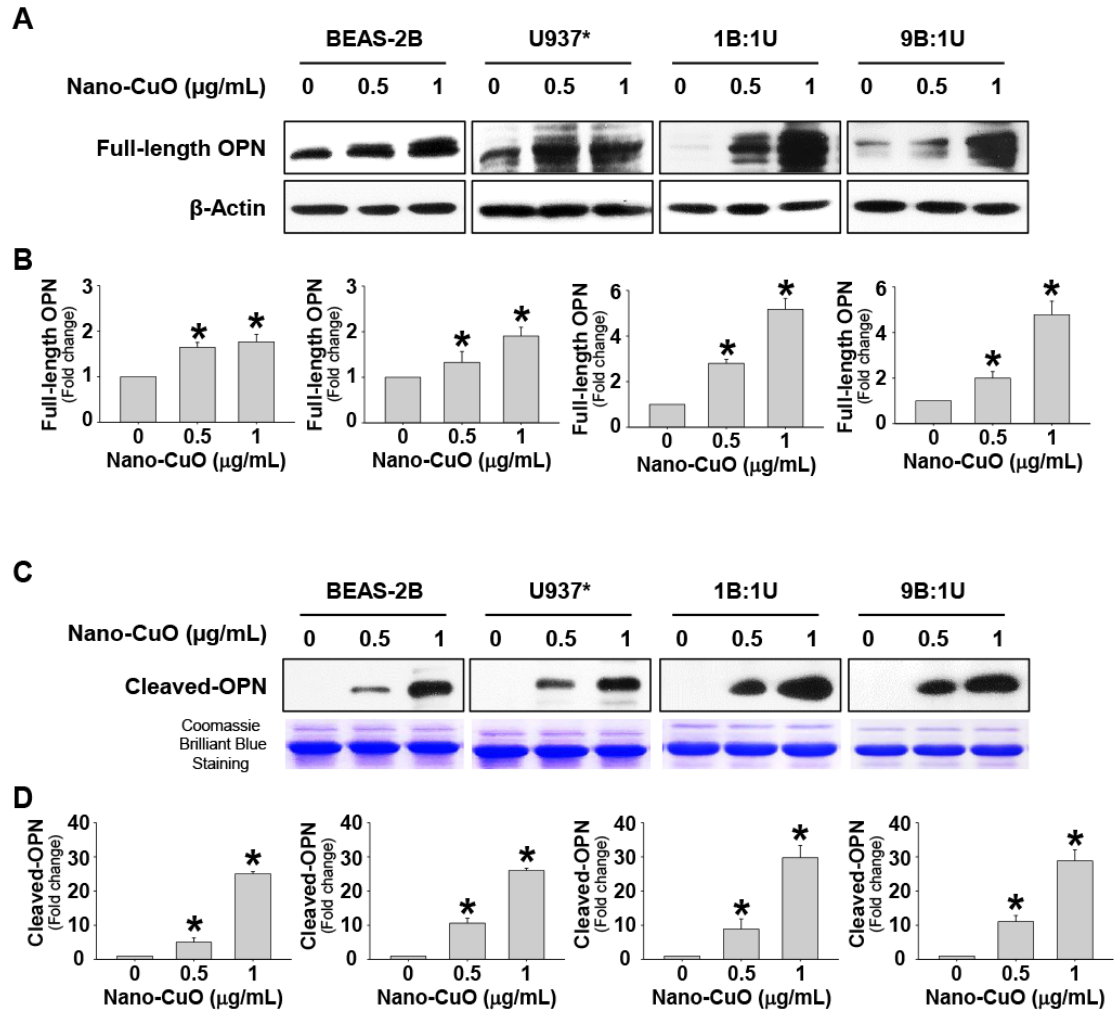


Figure 18. Increased expression of OPN in BEAS-2B cells and U937* macrophages exposed to Nano-CuO.

BEAS-2B cells, U937* macrophages, or co-culture of BEAS-2B and U937* macrophages at the ratio of 1:1 or 9:1 (BEAS-2B:U937*) were exposed to 0, 0.5 and 1 $\mu\text{g/mL}$ of Nano-CuO for 12 h. After treatment, the cells and conditioned media were collected. Full-length OPN in the cells and cleaved OPN in the conditioned media were detected by Western blot (**A**, **C**). **A** and **C** were the results of a single experiment. **B** was the average expression level of full-length OPN normalized to β -actin from three independent experiments. In **C**, equal protein

loading was verified by Coomassie Brilliant Blue staining. **D** was normalized band densitometry readings averaged from three independent experiments. Data represent mean \pm SE (n=3). * Significant difference as compared to the control group, $p < 0.05$.

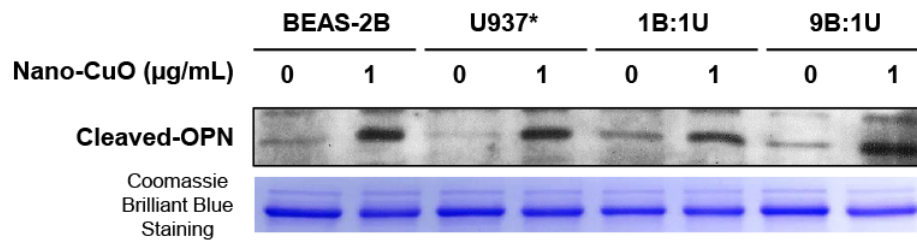


Figure 19 Increased production of cleaved-OPN in BEAS-2B cells and U937* macrophages exposed to Nano-CuO.

To compare the production of cleaved-OPN in monoculture and co-culture systems, BEAS-2B cells, U937* macrophages, or co-culture of BEAS-2B and U937* macrophages at the ratio of 1:1 or 9:1 (BEAS-2B:U937*) were exposed to 1 $\mu\text{g/mL}$ of Nano-CuO for 12 h. After treatment, the conditioned media were collected. Cleaved-OPN in the media were detected by Western blot. Equal protein loading was verified by Coomassie Brilliant Blue staining.

3.3.4 The role of MMP-3 in Nano-CuO-induced production of cleaved-OPN

To determine the role of MMP-3 in Nano-CuO-induced production of cleaved-OPN, BEAS-2B or U937* cells were transfected with 30 nM of MMP-3 siRNA for 6 h and then exposed to 1 µg/mL of Nano-CuO for another 12 h. Media were collected for the detection of cleaved-OPN. Negative Control No. 2 siRNA was used as a negative control. The results showed that MMP-3 siRNA transfection significantly abolished the production of cleaved-OPN caused by Nano-CuO exposure in both BEAS-2B and U937* culture media (Figure 20A, B, C, D). However, the expression of Nano-CuO-induced full-length OPN in cells was not affected by MMP-3 siRNA transfection (Data not shown).

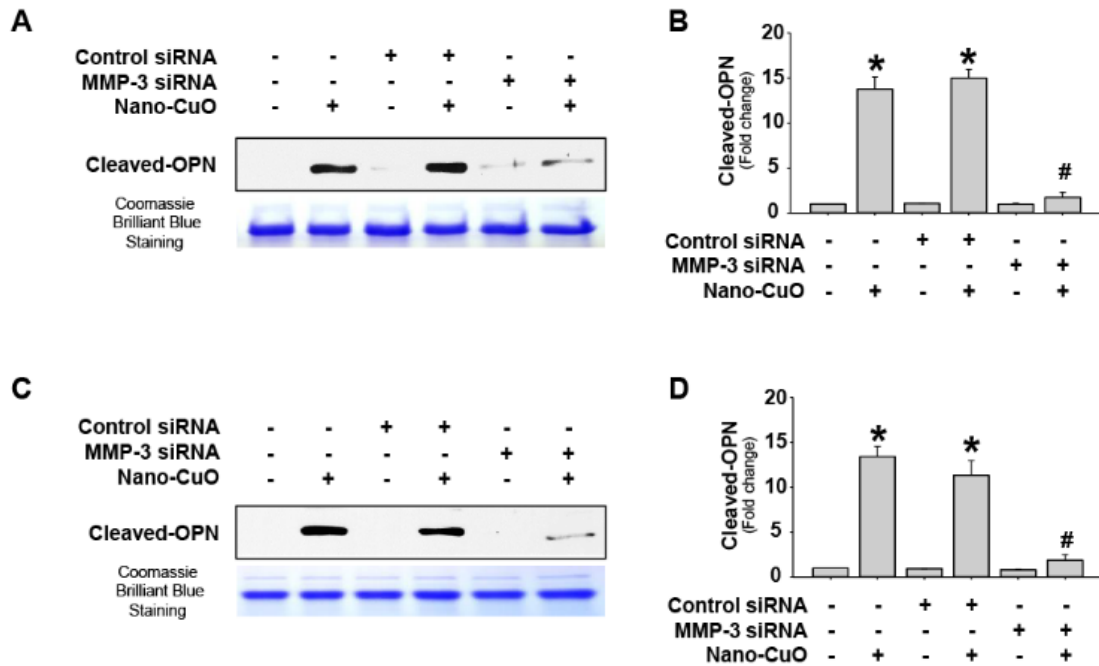


Figure 20. The role of MMP-3 on Nano-CuO-induced production of cleaved-OPN in BEAS-2B cells and U937* macrophages.

BEAS-2B cells (**A**) and U937* macrophages (**C**) were transfected with 30 nM of MMP-3 siRNA or Negative Control No. 2 siRNA for 6 h. After transfection, the cells were exposed to 1 $\mu\text{g}/\text{mL}$ of Nano-CuO for 12 h. The conditioned media were collected to detect the level of cleaved-OPN protein by Western blot. Equal protein loading was verified by Coomassie Brilliant Blue staining. **A** and **C** were the results of a single experiment. **B** and **D** were normalized band densitometry readings averaged from three independent experiments. Data represent mean \pm SE ($n=3$).

* Significant difference as compared to the control group, $p<0.05$. # Significant difference as compared to the Nano-CuO-treated group transfected with Negative Control No. 2 siRNA, $p<0.05$.

3.3.5 Direct Nano-CuO exposure did not activate MRC-5 cells

To explore whether exposure to Nano-CuO would cause activation of fibroblasts, MRC-5 cells were treated with 0, 0.5, and 1 $\mu\text{g/mL}$ of Nano-CuO for 48 h, and the expression of $\alpha\text{-SMA}$, Col1A1, and fibronectin were measured by Western blot. The results showed that direct exposure to Nano-CuO for 48 h did not cause significant alterations in the expression of $\alpha\text{-SMA}$, Col1A1, and fibronectin (Figure 21A, B). For the time-response study, MRC-5 cells were exposed to 1 $\mu\text{g/mL}$ of Nano-CuO for 0, 12, 24, 48, and 72 h. The results demonstrated that Nano-CuO did not cause activation of MRC-5 cells at all the time points after Nano-CuO treatment (Figure 21C, D).

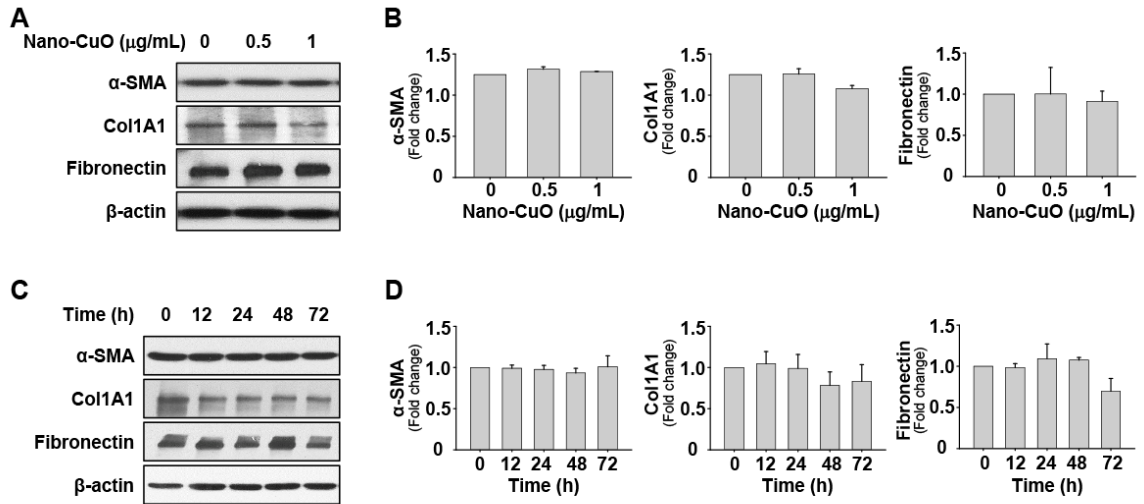


Figure 21. Direct Nano-CuO exposure had no effects on activation of MRC-5 fibroblasts.

For dose-response study, MRC-5 cells were treated with 0, 0.5 and 1 $\mu\text{g/mL}$ of Nano-CuO for 48 h (**A**, **B**). For time-course study, MRC-5 cells were treated with 1 $\mu\text{g/mL}$ of Nano-CuO for 0, 12, 24, 48 and 72 h (**C**, **D**). After exposure, proteins were isolated to detect the expression of α -SMA, Col1A1, and fibronectin. **A** and **C** were the results of a single Western blot experiment. **B** and **D** were the average expression level of α -SMA, Col1A1, and fibronectin normalized to β -actin from three independent experiments. Data represent mean \pm SE ($n=3$). * Significant difference as compared to the control group, $p<0.05$.

3.3.6 Conditioned media from Nano-CuO-exposed BEAS-2B or U937* cells caused activation of unexposed MRC-5 fibroblasts

To investigate whether some mediators, such as MMP-3 and cleaved-OPN, released from Nano-CuO-exposed BEAS-2B or U937* could cause activation of MRC-5 cells, BEAS-2B or U937* cells were treated with 0, 0.5 and 1 $\mu\text{g}/\text{mL}$ of Nano-CuO for 12 h and the conditioned media were collected. MRC-5 fibroblasts were then cultured in the conditioned media for 48 h. The conditioned media from cells without Nano-CuO exposure were used as control. The results demonstrated that conditioned media from Nano-CuO-exposed BEAS-2B cells or U937* macrophages caused significant activation of MRC-5 cells after 48 h exposure, reflected by dose-dependent increases in α -SMA, Col1A1, and fibronectin proteins (Figure 22A, B, E, F). For the time-course studies, BEAS-2B or U937* cells were treated with 1 $\mu\text{g}/\text{mL}$ of Nano-CuO for 12 h and the conditioned media were collected. MRC-5 fibroblasts were then exposed to the conditioned media for 0, 12, 24, 48 and 72 h. Conditioned media from Nano-CuO-exposed BEAS-2B cells or U937* macrophages induced a time-dependent increase in α -SMA protein in MRC-5 fibroblasts, which peaked at 72 h after adding conditioned media. And the conditioned media caused significant increases in the expression of Col1A1 and fibronectin, which reached peak at 48 h after adding conditioned media (Figure 22C, D, G, H). Migration of MRC-5 fibroblasts was evaluated by wound healing assay. The results showed that conditioned media from Nano-CuO-exposed BEAS-2B cells or U937* macrophages significantly promoted the migration of MRC-5 fibroblasts (Figure 23A, B, C, D).

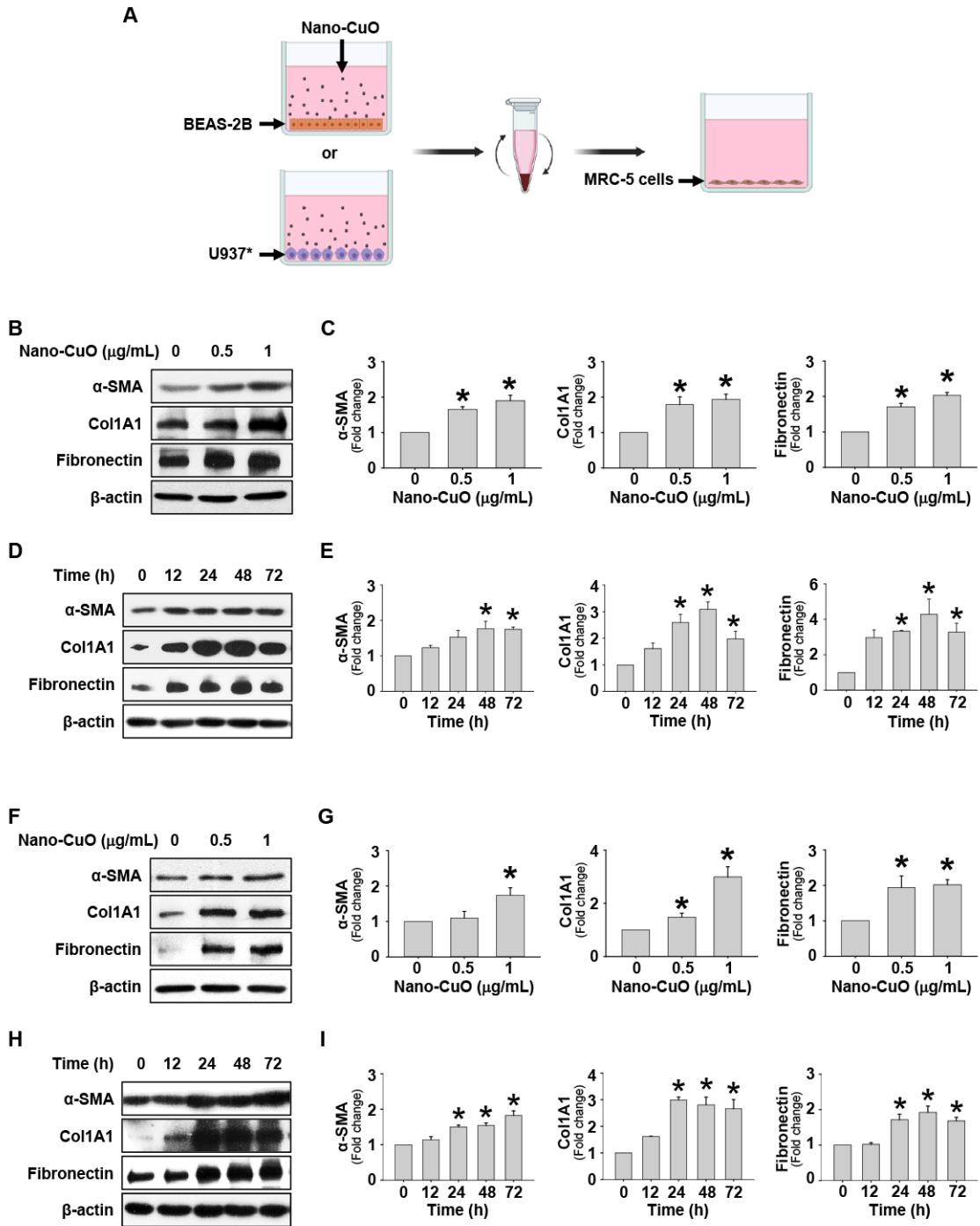


Figure 22. Conditioned media from Nano-CuO-exposed BEAS-2B or U937* cells caused activation of unexposed MRC-5 fibroblasts.

(A) is the experimental protocol. For dose-response study, BEAS-2B or U937* cells were treated with 0, 0.5 and 1 $\mu\text{g/mL}$ of Nano-CuO for 12 h and the

conditioned media were collected. MRC-5 fibroblasts were then exposed to the conditioned media from exposed BEAS-2B cells (**B**, **C**) or U937* macrophages (**F**, **G**) for 48 h. For time-course study, BEAS-2B or U937* cells were treated with 1 $\mu\text{g}/\text{mL}$ of Nano-CuO for 12 h and the conditioned media were collected. MRC-5 fibroblasts were then exposed to the conditioned media from exposed BEAS-2B cells (**D**, **E**) or U937* macrophages (**H**, **I**) for 0, 12, 24, 48 and 72 h. After exposure, proteins from MRC-5 cells were isolated to detect the expression of α -SMA, Col1A1, and fibronectin. **B**, **D**, **F** and **H** were the results of a single Western blot experiment. **C**, **E**, **G**, and **I** were the average expression level of α -SMA, Col1A1, and fibronectin normalized to β -actin from three independent experiments. Data represent mean \pm SE (n=3). * Significant difference as compared to the control group, $p < 0.05$.

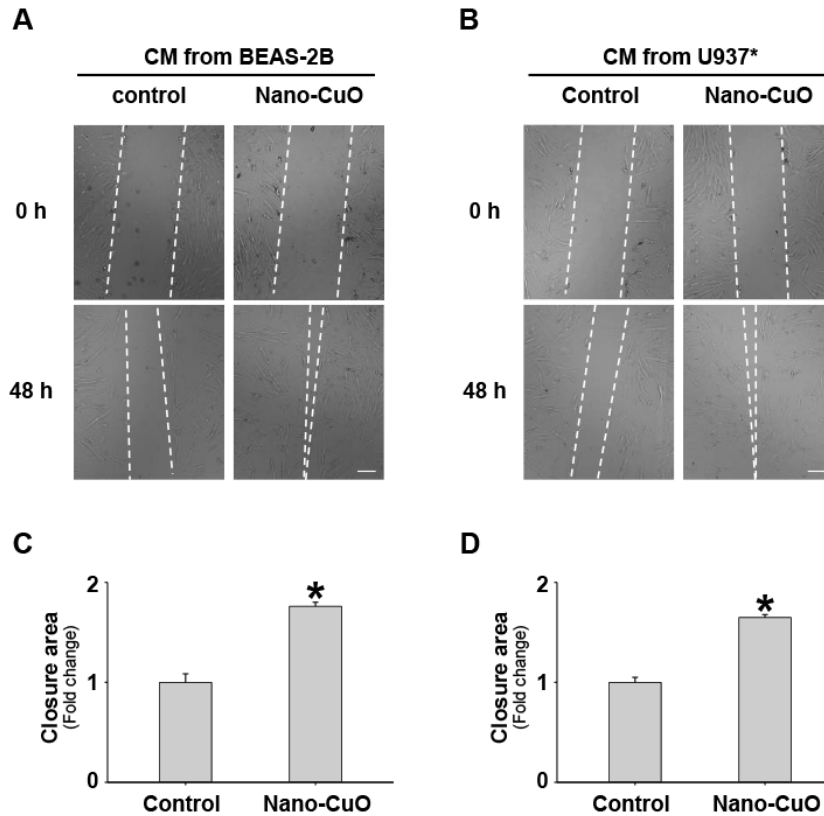


Figure 23. Conditioned media from Nano-CuO-exposed BEAS-2B or U937* cells enhanced migration of unexposed MRC-5 fibroblasts.

BEAS-2B or U937* cells were treated with 0 or 1 $\mu\text{g}/\text{mL}$ of Nano-CuO for 12 h and the conditioned media were collected. MRC-5 fibroblasts were then exposed to the conditioned media from exposed BEAS-2B cells (**A**, **C**) or U937* macrophages (**B**, **D**) for 48h. Migration of MRC-5 cells was detected by wound healing assay. **A** and **B** were the results of a single representative image. **C** and **D** were the average closure area from three independent experiments. Scale bar represents 200 μm . Data represent mean \pm SE (n=3). * Significant difference as compared to the control group, $p < 0.05$.

3.3.7 Conditioned media from Nano-CuO-exposed co-culture of BEAS-2B and U937* cells caused activation of unexposed MRC-5 fibroblasts

To further investigate whether conditioned media from Nano-CuO-exposed co-culture of BEAS-2B and U937* cells could cause activation of unexposed MRC-5 cells, BEAS-2B and U937* cells were seeded at the ratio of 1:1 or 9:1 (BEAS-2B:U937*). For the dose-response study, co-culture systems were exposed to 0, 0.5 and 1 $\mu\text{g/mL}$ of Nano-CuO for 12 h and the conditioned media were collected. MRC-5 fibroblasts were then exposed to the conditioned media for 48 h. The results showed that both conditioned media caused significant activation of MRC-5 cells, reflected by dose-dependent increases in α -SMA, Col1A1, and fibronectin proteins (Figure 24A, B, E, F). For the time-course study, co-culture of BEAS-2B and U937* cells with ratio of 1:1 or 9:1 was treated with 1 $\mu\text{g/mL}$ of Nano-CuO for 12 h and the conditioned media were collected. MRC-5 fibroblasts were then exposed to the conditioned media for 0, 12, 24, 48 and 72 h. The results demonstrated that both conditioned media induced time-dependent increases of α -SMA, Col1A1, and fibronectin, which reached peak at 48 or 72 h after adding conditioned media (Figure 24C, D, G, H).

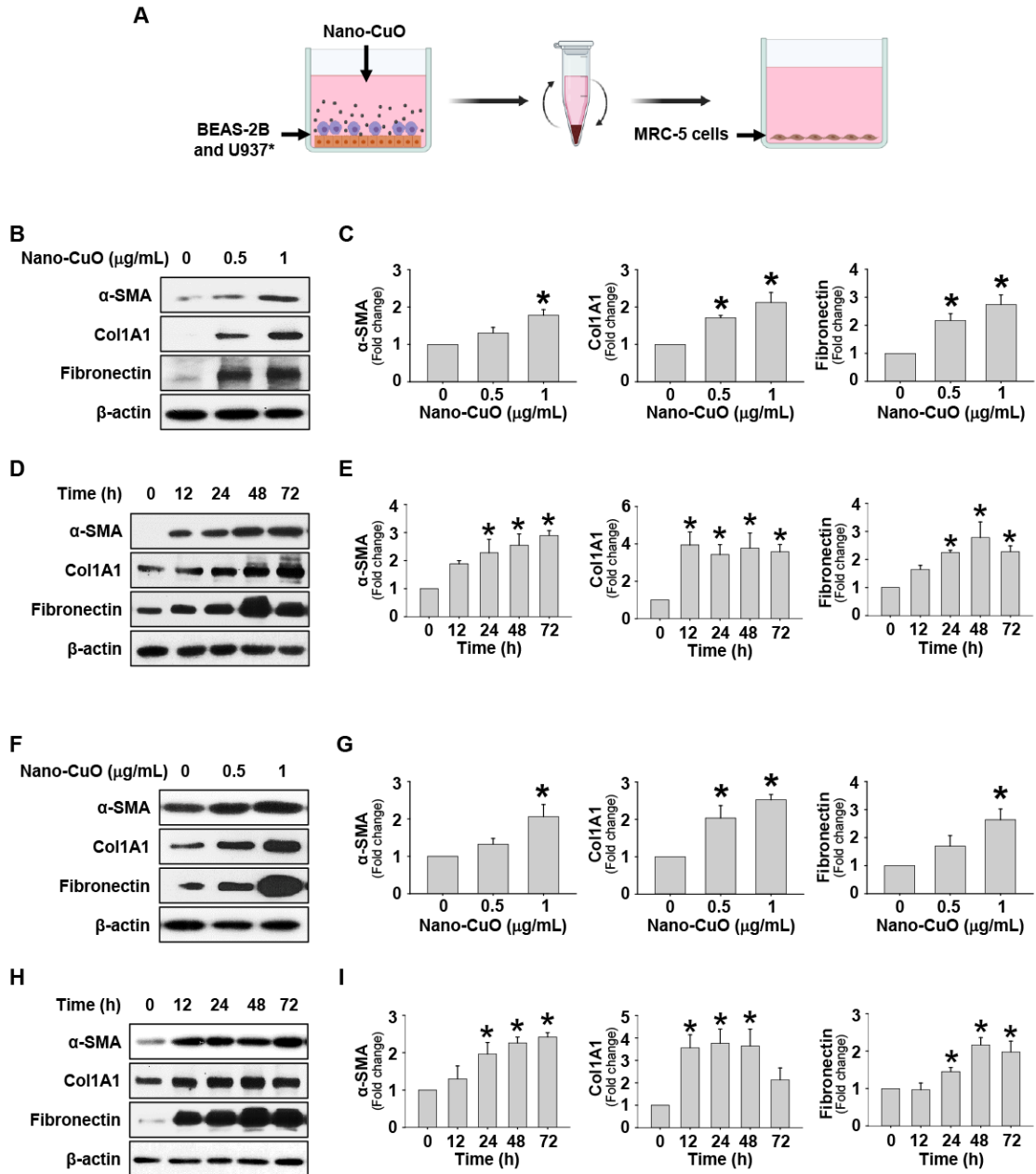


Figure 24. Conditioned media from Nano-CuO-exposed co-culture of BEAS-2B and U937* cells caused activation of unexposed MRC-5 fibroblasts.

(A) Experimental protocol of the co-culture experiments. For dose-response study, co-culture of BEAS-2B and U937* cells with the ratio of 1:1 (B) or 9:1 (F) was treated with 0, 0.5 and 1 $\mu\text{g/mL}$ of Nano-CuO for 12 h and the conditioned media were collected. MRC-5 fibroblasts were then exposed to the conditioned media for

48 h. For time-course study, co-culture of BEAS-2B and U937* cells with ratio of 1:1 (**D**) or 9:1 (**H**) was treated with 1 $\mu\text{g/mL}$ of Nano-CuO for 12 h and the conditioned media were collected. MRC-5 fibroblasts were then exposed to the conditioned media for 0, 12, 24, 48 and 72 h. After exposure, proteins from MRC-5 cells were isolated to detect the expression of α -SMA, Col1A1, and fibronectin. **B, D, F** and **H** were the results of a single Western blot experiment. **C, E, G,** and **I** were the average expression level of α -SMA, Col1A1, and fibronectin normalized to β -actin from three independent experiments. Data represent mean \pm SE (n=3).

* Significant difference as compared to the control group, $p < 0.05$.

3.3.8 Exposure of BEAS-2B and U937* cells to Nano-CuO caused activation of unexposed MRC-5 fibroblasts in a triple co-culture system

Then we explored whether BEAS-2B and U937* cells exposed to Nano-CuO could activate unexposed MRC-5 cells in a triple co-culture system. BEAS-2B cells and U937* cells were seeded at the ratio of 9:1 or 1:1 (BEAS-2B:U937*) in the insert of transwell unit and MRC-5 cells were seeded in the lower chamber of the unit. After the establishment of the triple co-culture system, BEAS-2B and U937* cells were exposed to 0, 0.5 and 1 $\mu\text{g/mL}$ of Nano-CuO for 12 h and then the inserts were taken out. MRC-5 cells in the lower chamber were incubated for another 36 h. After incubation, proteins from MRC-5 cells were isolated for Western blot to detect the expression of α -SMA, Col1A1, and fibronectin. The results demonstrated that in both models, exposure of BEAS-2B and U937* cells to Nano-CuO led to a significant activation of unexposed MRC-5 cells in the lower chamber of the transwell unit, which was reflected by the dose-dependent increases of α -SMA, Col1A1, and fibronectin expression (Figure 25A, B, C, D).

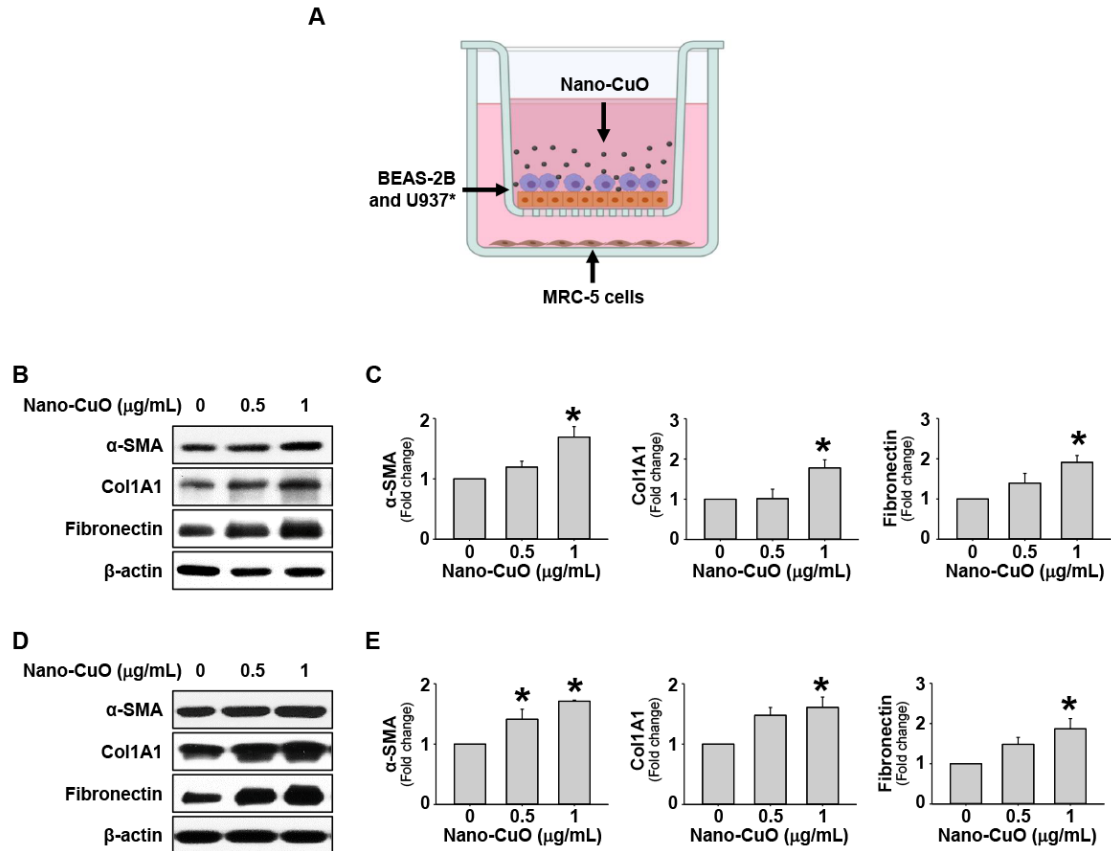


Figure 25. Exposure of BEAS-2B and U937* cells to Nano-CuO caused activation of unexposed MRC-5 fibroblasts in a triple co-culture system.

(A) Experimental protocol for the triple co-culture experiments. BEAS-2B cells and U937* cells were seeded at the ratio of 1:1 (B) or 9:1 (D) (BEAS-2B:U937*) in the inserts of transwell unit and MRC-5 cells were seeded in the lower chamber of the unit. After establishment of the triple co-culture system, BEAS-2B and U937* cells were exposed to 0, 0.5 and 1 $\mu\text{g/mL}$ of Nano-CuO for 12 h, then the inserts were taken out. MRC-5 cells in the lower chamber were incubated for another 36 h and proteins were isolated to detect the expression of α -SMA, Col1A1, and fibronectin. B and D were the results of a single Western blot experiment. C and E were the average expression level of α -SMA, Col1A1, and fibronectin normalized to β -actin

from three independent experiments. Data represent mean \pm SE (n=3). *
Significant difference as compared to the control group, $p < 0.05$.

3.3.9 The role of MMP-3 in Nano-CuO-induced activation of MRC-5 cells in the triple co-culture system

To investigate the role of MMP-3 in MRC-5 cell activation in the triple co-culture model, BEAS-2B and U937* cells were transfected with 30 nM of MMP-3 siRNA for 6 h and then exposed to 1 $\mu\text{g}/\text{mL}$ of Nano-CuO for 12 h. After exposure, the inserts were taken out and the MRC-5 fibroblasts seeded in the lower chamber were incubated for another 36 h. The proteins isolated from MRC-5 fibroblasts were used to detect the expression of α -SMA, Col1A1, and fibronectin by Western blot. Negative control No. 2 siRNA was used as a negative control. The results showed that MMP-3 siRNA transfection significantly suppressed the activation of MRC-5 cells, which was reflected by inhibited expression of α -SMA, Col1A1, and fibronectin in the triple co-culture system (Figure 26A, B, C, D). Furthermore, migration of MRC-5 fibroblasts caused by Nano-CuO was significantly attenuated by MMP-3 siRNA transfection (Figure 27A, B, C, D).

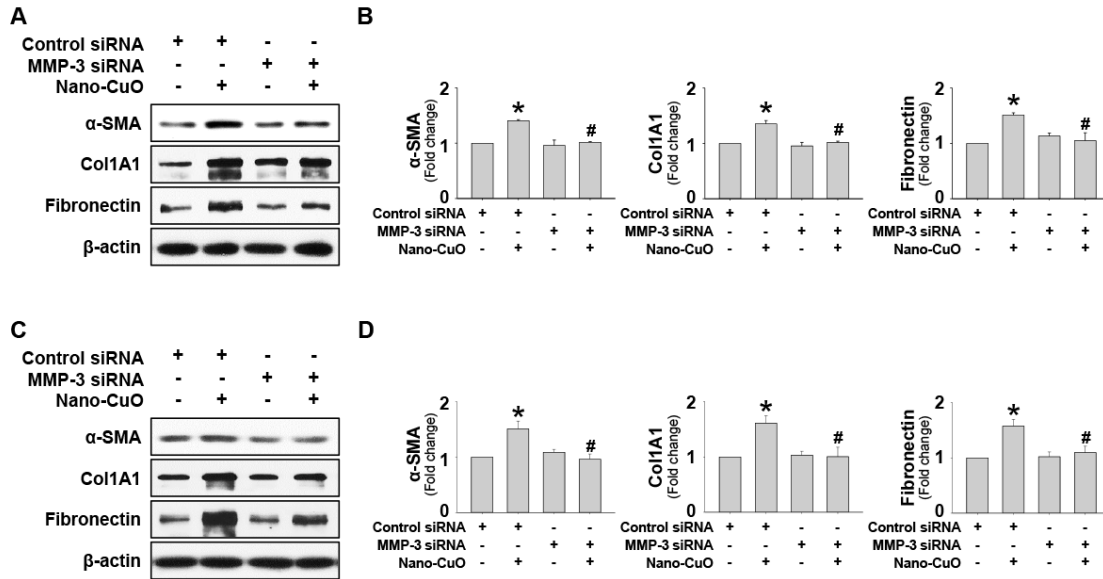


Figure 26. The role of MMP-3 on Nano-CuO-induced activation of MRC-5 fibroblasts in the triple co-culture system.

BEAS-2B and U937* cells were seeded at the ratio of 1:1 (**A**) or 9:1 (**C**) (BEAS-2B:U937*) in the inserts of transwell unit and transfected with 30 nM of MMP-3 siRNA or Negative Control No. 2 siRNA for 6 h. After transfection, the cells were exposed to 1 $\mu\text{g}/\text{mL}$ of Nano-CuO for 12 h. After exposure, the inserts were taken out and the MRC-5 fibroblasts seeded in the lower chamber were incubated for another 36 h. The proteins isolated from MRC-5 fibroblasts were used to detect the expression of α -SMA, Col1A1, and fibronectin by Western blot. **A** and **C** were the results of a single Western blot experiment. **B** and **D** were the average expression level of α -SMA, Col1A1, and fibronectin normalized to β -actin from three independent experiments. Data represent mean \pm SE (n=3). * Significant difference as compared to the control group, $p < 0.05$; # Significant difference as compared to the Nano-CuO-treated group transfected with Negative Control No. 2 siRNA, $p < 0.05$.

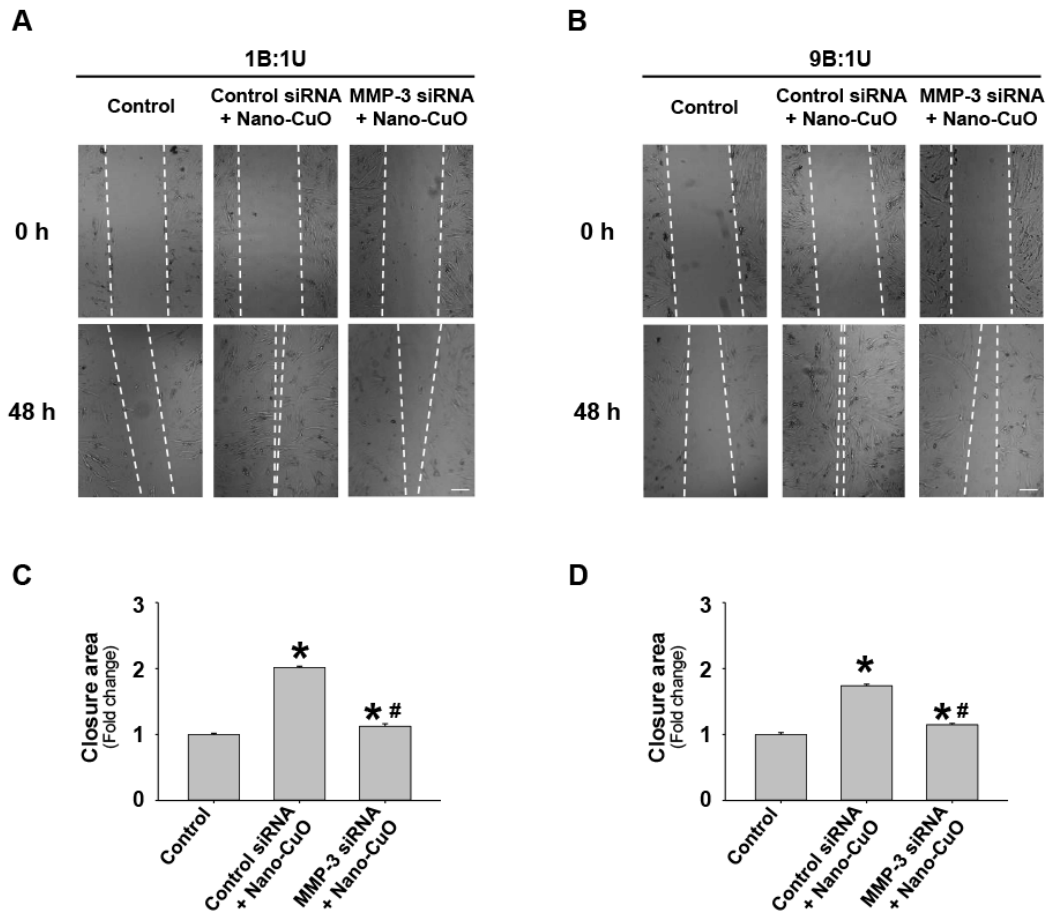


Figure 27 MMP-3 siRNA transfection attenuated Nano-CuO-induced migration of MRC-5 fibroblasts in the triple co-culture system.

BEAS-2B and U937* cells were seeded at a ratio of 1:1 (**A, C**) or 9:1 (**B, D**) (BEAS-2B:U937*) in the inserts of transwell unit and transfected with 30 nM of MMP-3 siRNA or Negative Control No. 2 siRNA for 6 h. After transfection, the cells were exposed to 1 $\mu\text{g}/\text{mL}$ of Nano-CuO for 12 h. After exposure, the inserts were taken out and the MRC-5 fibroblasts seeded in the lower chamber were incubated for another 36 h. Migration of MRC-5 cells was detected by wound healing assay. Cells without any treatments were used as the control. **A** and **B** were the results of a single representative image. **C** and **D** were the average closure area from

three independent experiments. Data represent mean \pm SE (n=3). * Significant difference as compared to the control group, $p < 0.05$; # Significant difference as compared to the Nano-CuO-treated group with control siRNA transfection, $p < 0.05$.

3.3.10 The role of MMP-3-cleaved OPN in activation of unexposed MRC-5 cells in triple co-culture system

In the sections 3.3.2, 3.3.3, and 3.3.4, I have shown that Nano-CuO exposure induced upregulation of MMP-3 and production of MMP-3-cleaved OPN in BEAS-2B and U937* cells, and MMP-3 siRNA transfection significantly inhibited the production of MMP-3-cleaved OPN and activation of MRC-5 fibroblasts. To further explore whether MMP-3-cleaved OPN was involved in the activation of MRC-5 fibroblasts in the triple co-culture system, MRC-5 fibroblasts were pretreated with GRGDSP peptides (200 µg/mL), which could interrupt the binding of cleaved-OPN to cell surface integrins, and then BEAS-2B and U937* cells in the triple co-culture model were exposed to 1 µg/mL of Nano-CuO for 12 h. After exposure, the inserts were taken out and the MRC-5 fibroblasts seeded in the lower chamber were incubated for another 36 h. The proteins isolated from MRC-5 fibroblasts were used to detect the expression of α -SMA, Col1A1, and fibronectin by Western blot. The results revealed that GRGDSP treatment significantly attenuated the activation of MRC-5 fibroblasts in the triple co-culture system (Figure 28A, B, C, D), suggesting that MMP-3-cleaved OPN fragment played key roles in MRC-5 fibroblast activation. In addition, GRGDSP treatment also inhibited the migration of MRC-5 fibroblasts caused by Nano-CuO exposure in the triple co-culture system (Figure 29A, B, C, D).

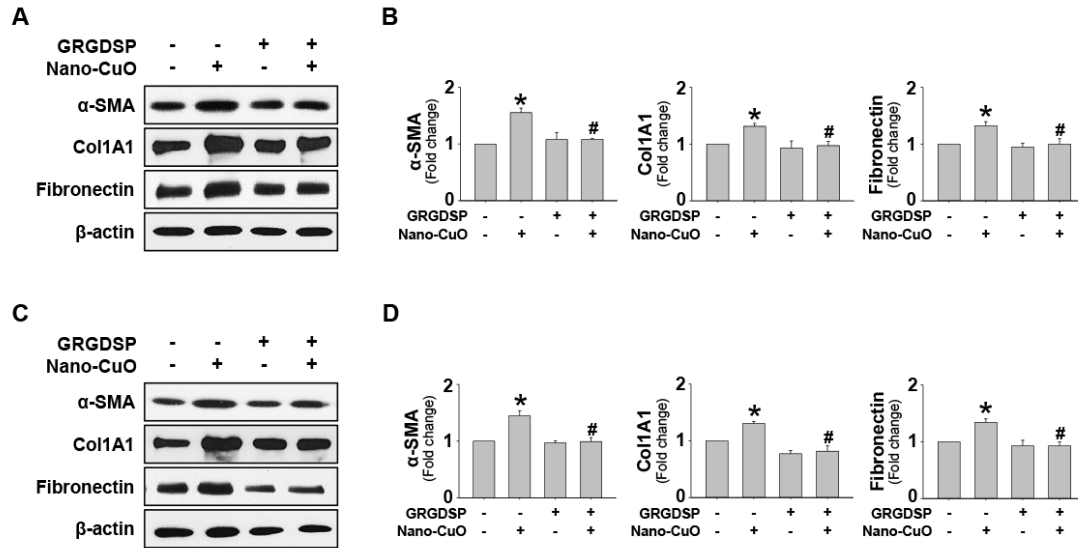


Figure 28. The role of MMP-3-cleaved OPN in Nano-CuO-induced activation of MRC-5 fibroblasts in the triple co-culture system.

BEAS-2B and U937* cells were seeded at the ratio of 1:1 (**A**) or 9:1 (**C**) (BEAS-2B:U937*) in the inserts, and MRC-5 fibroblasts were seeded in the lower chambers of transwell units. MRC-5 fibroblasts were pretreated with 200 μ g/mL of GRGDSP peptides, then BEAS-2B and U937* cells were exposed to 1 μ g/mL of Nano-CuO for 12 h. After exposure, the inserts were taken out and the MRC-5 fibroblasts seeded in the lower chamber were incubated for another 36 h. The proteins from MRC-5 fibroblasts were isolated to determine the activation of MRC-5 fibroblasts by Western blot. **A** and **C** were the results of a single Western blot experiment. **B** and **D** were the average expression level of α -SMA, Col1A1, and fibronectin normalized to β -actin from three independent experiments. Data represent mean \pm SE (n=3). * Significant difference as compared to the control group, $p < 0.05$; # Significant difference as compared to the Nano-CuO-treated alone group, $p < 0.05$.

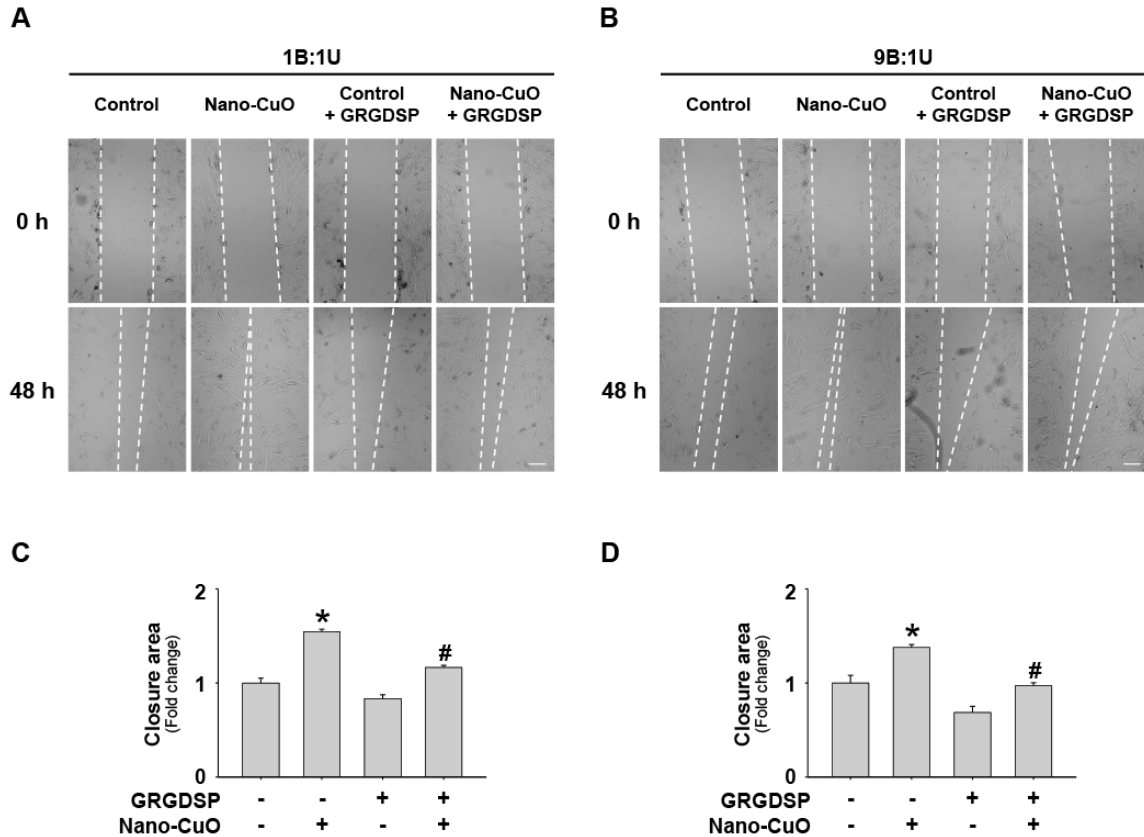


Figure 29. Pretreatment of GRGDSP peptides inhibited Nano-CuO-induced migration of MRC-5 fibroblasts in the triple co-culture system.

BEAS-2B and U937* cells were seeded at the ratio of 1:1 (**A**) or 9:1 (**B**) (BEAS-2B:U937*) in the inserts and MRC-5 fibroblasts were seeded in the lower chambers of transwell units. MRC-5 fibroblasts were pretreated with 200 μ M GRGDSP peptides, then BEAS-2B and U937* cells were exposed to 1 μ g/mL of Nano-CuO for 12 h. After exposure, the inserts were taken out and the MRC-5 fibroblasts seeded in the lower chamber were incubated for another 36 h. Migration of MRC-5 cells was detected by wound healing assay. **A** and **B** were the results of a single representative image. **C** and **D** were the average closure area from three independent experiments. Data represent mean \pm SE (n=3). * Significant

difference as compared to the control group, $p < 0.05$; # Significant difference as compared to the Nano-CuO-treated alone group, $p < 0.05$.

3.4 Discussion

In present study, we established a triple co-culture model, consisting of human lung epithelial cells, macrophages, and fibroblasts, to investigate the role of MMP-3 in lung fibrotic responses *in vitro* after exposure to Nano-CuO. Human lung epithelial BEAS-2B cells were selected because they have been widely used to evaluate pulmonary toxicity after nanoparticle exposure (Kabadi et al. 2019; Xia et al. 2013; Zhang et al. 2021b). Human U937 monocytes were selected because they have a higher passage number with stability and consistency, and they can differentiate into mature macrophages upon PMA-treatment (Verhoeckx et al. 2015). To mimic physiological condition in normal human lungs, BEAS-2B cells and U937* macrophages were seeded in a ratio of either 1:1 or 9:1 in the co-culture system. The ratios were selected based on the cell composition in normal human lung alveolar region. The 1:1 ratio corresponds to the total cell volume of alveolar epithelial cells (2653 μm^3) and macrophages (2492 μm^3). The 9:1 ratio corresponds to the highest ratio of the number of pneumocytes to macrophages reported in normal human lungs (Cappellini et al. 2020; Crapo et al. 1982; Garcia-de-Alba et al. 2010; Gomez et al. 1997; Jantzen et al. 2012; Loret et al. 2016; Michael J. Derelanko 2001). Comparing to monoculture, co-culture model provides more realistic micro-environmental conditions to mimic *in vivo* conditions, and it is a good *in vitro* method to study the role of cell-cell interactions or communications in nanoparticle-induced pulmonary toxicity (Kabadi et al. 2019; Klein et al. 2011; Muller et al. 2010; Rothen-Rutishauser et al. 2008; Wottrich et al. 2004). Jennifer et al. presented evidence that *in vitro* co-culture model is more sensitive as

compared to the conventional monoculture in evaluating the inflammatory responses in the lower respiratory tract after nanoparticle exposure (Kasper et al. 2011). Previous studies also reported that more concordant inflammatory and fibrotic genes were expressed in co-culture system than in monoculture when comparing gene expression in mouse lungs after nanoparticle exposure (Snyder-Talkington et al. 2013; Snyder-Talkington et al. 2015). In this study, our results demonstrated that in the triple co-culture model, mediators released from Nano-CuO-exposed BEAS-2B and U937* cells caused the activation of MRC-5 fibroblasts, whereas directly exposure to Nano-CuO did not induce the activation of MRC-5 cells, suggesting that co-culture models are more sensitive and suitable for evaluating nanoparticle-induced pulmonary toxicity *in vitro*.

During pulmonary inflammation, macrophages constantly communicate with epithelial cells, the underlying mesenchymal cells, such as fibroblasts, and extracellular matrix, which form a structure called epithelial-mesenchymal cell trophic unit (EMTU), to regulate lung homeostasis and immunity against inhaled particles and other pathogens (Hu and Christman 2019). These cell-cell communications are hypothesized to be crucial in leading to pulmonary injury and fibrotic responses after exposure to respirable inhaled nanomaterials (Bonner 2010; Dong and Ma 2016; Hussain et al. 2014; Kabadi et al. 2019; Snyder-Talkington et al. 2013; Venter and Niesler 2018; Wang et al. 2013). The roles of these cell-cell communications in fibrotic responses have been modelled in co-culture system or by using conditioned media, such as co-culture of epithelial cells and macrophages, or using conditioned media from either epithelial cells or

macrophages to culture fibroblasts in transwell or other 3D culture systems (Barosova et al. 2020; Hussain et al. 2014; Kabadi et al. 2019). For example, Salik and colleagues used conditioned media to explore the effects of MWCNTs-exposed normal human bronchial epithelial cells on MRC-5 cells, and their results showed the conditioned media from MWCNTs-treated HBE cells induced remarkable expression of pro-fibrotic markers in MRC-5 cells, such as tenascin-c and osteopontin (Hussain et al. 2014). Pranita's study also demonstrated that MWCNTs exposure caused inflammatory and fibrotic responses in a lung microtissues consisting of human macrophages, lung epithelial cells, and fibroblasts, reflected by increased expression of the genes, such as platelet-derived growth factor (PDGF) and COL3A1 (Kabadi et al. 2019). In the present study, we first employed a conditioned media approach to explore the effects of cell-cell communications of human epithelial cells and macrophages on fibroblast activation. Conditioned media from exposed human lung epithelial BEAS-2B cells, U937 differentiated macrophages (U937*), or co-culture of BEAS-2B and U937* macrophages at a ratio of 9:1 or 1:1 (BEAS-2B:U937*) were collected and used to culture human fibroblasts MRC-5. Our results showed that conditioned media from Nano-CuO-exposed BEAS-2B or U937* caused dose-dependent activation of MRC-5 cells, reflected by increased expression of α -SMA, Col1A1, and fibronectin proteins. Conditioned media from co-culture of BEAS-2B and U937* induced similar dose-dependent activation of MRC-5 cells in both 9:1 and 1:1 model. The four types of conditioned media caused significant increase in α -SMA, Col1A1 and fibronectin in MRC-5 cells, with α -SMA expression peaked at 72 h and Col1A1 and

fibronectin peaked at 48 h after adding conditioned media. Then we established a triple co-culture model, consisting of BEAS-2B, U937*, and MRC-5 cells, to study the role of cell-cell communications in fibrotic responses after Nano-CuO exposure. Our results revealed that in the triple co-culture system, both 9:1 and 1:1 ratio of exposed BEAS-2B and U937* cells led to dose-dependent activation of MRC-5 cells. However, directly exposure of MRC-5 cells to Nano-CuO did not result in its activation, suggesting that the cell-cell communications play important roles in Nano-CuO-induced fibrotic responses.

To further identify the roles of cell-cell communications in metal nanoparticle-induced pulmonary fibrotic responses, we focused on the effects of two matrix factors, MMP-3 and OPN, released from BEAS-2B and U937* after exposed to Nano-CuO, on activation of MRC-5 fibroblasts. OPN is a multifunctional protein that acts as a cytokine as well as extracellular matrix, playing key roles in the formation of lung injury and fibrosis (Mori et al. 2008; Ophascharoensuk et al. 1999; Pardo et al. 2005). OPN is secreted by many kinds of cells, such as macrophages, epithelial cells, endothelial cells, and fibroblasts (Mori et al. 2008; O'Regan 2003; Pardo et al. 2005; Takahashi et al. 2001). It is reported that OPN is highly expressed in nanomaterials-induced fibrosis in animal models, as well as in human fibrotic diseases such as IPF (Fujita et al. 2015; Khaliullin et al. 2017; Mangum et al. 2004; Pardo et al. 2005; Samitas et al. 2011; Simoes et al. 2009; Thompson et al. 2014). Knockout or blocking of OPN showed protect effects against nanomaterial- or bleomycin-induced fibroblast activation and fibrosis in both *in vivo* and *in vitro* studies (Dong and Ma 2017; Khaliullin et al. 2017;

Takahashi et al. 2001). For example, Dong's study revealed that OPN was highly induced after MWCNTs exposure in mouse lungs, and OPN knockout reduced the formation of fibrotic focus and accumulation of myofibroblasts in mouse lungs. In cellular level, OPN stimulated differentiation of fibroblasts and production of collagen and fibronectin, which was blocked by OPN neutralizing antibodies (Dong and Ma 2017). Decreased formation of granuloma and less deposition of collagen were also observed in lungs of OPN KO mice comparing to those in wild-type mice after MWCNTs administration (Khaliullin et al. 2017). In the current study, Nano-CuO exposure caused significant upregulation of OPN in BEAS-2B cells and U937* macrophages and induced activation of fibroblasts in the triple co-culture system. Treatment with H-Gly-Arg-Gly-Asp-Ser-Pro-OH - Calbiochem, a GRGDSP peptide interrupts binding of OPN to cell surface receptors, significantly inhibited the migration and activation of MRC-5 cells in the triple co-culture model, suggesting that Nano-CuO-induced OPN in BEAS-2B and U937* macrophages acted an important paracrine signaler to activate MRC-5 fibroblasts.

OPN displays multiple biological activities through its binding motifs, such as RGD motif or SVVYGLR integrin-binding site, to interact with a variety of cellular receptor molecules. Previous studies reported that proteolytic cleavage of OPN may either enhance or reduce the integrin-binding ability of OPN, suggesting that different cleavage sites may affect the biological activities of OPN-derived fragments or peptides (Agnihotri et al. 2001; Christensen and Sorensen 2014; Kon et al. 2014; Leitner et al. 2015; Lindsey et al. 2015; Tan et al. 2013). Matrix metalloproteinases are a large family of proteases that can degrade all kinds of

extracellular matrix proteins and cleave biomolecules, such as OPN (Apte and Parks 2015). MMPs have been demonstrated to be able to cleave OPN and unmask its receptor-binding sites, which modulates the biological function of OPN by altering its integrin-binding ability (Agnihotri et al. 2001; Kon et al. 2014; Leitner et al. 2015; Lindsey et al. 2015; Tan et al. 2013). For example, a study showed that MMP-9 can cleave murine OPN at several different sites, and the OPN-p151 peptide, which is cleaved at Gly-Leu bond (Gly¹⁵¹-Leu¹⁵²) of OPN sequence, showed an increased wound healing effects on fibroblasts (Lindsey et al. 2015). MMP-3, another member of the MMPs family, was revealed to cleave human OPN at Gly-Leu bond (Gly¹⁶⁶-Leu¹⁶⁷), which is 5 amino acids downstream of the RGD binding motif that enhances the binding ability of OPN to its receptors. And this MMP-3-cleaved OPN (~40 kDa) showed a significantly enhanced ability of adhesion and migration stimulus *in vitro* comparing with full-length OPN (Agnihotri et al. 2001). In this study, exposure of BEAS-2B and U937* cells to Nano-CuO caused remarkable increased expression of MMP-3 and production of MMP-3-cleaved OPN (~40 kDa), these raised our interests to explore whether MMP-3-cleaved OPN was involved in the activation of fibroblasts in the triple co-culture system, which was confirmed by transfection of MMP-3 siRNA in BEAS-2B and U937* cells. MMP-3 siRNA transfection significantly blocked the generation of MMP-3-cleaved OPN fragment (~40 kDa) and inhibited the activation of MRC-5 cells in the triple co-culture system, suggesting that MMP-3-cleaved OPN plays an important role in Nano-CuO-induced fibrotic responses.

Activation and differentiation of fibroblasts into myofibroblasts is a critical step in the development of pulmonary fibrosis. A variety of growth factors and cytokines can activate and stimulate fibroblast differentiation (Bonner 2010; Dong and Ma 2016; Thompson et al. 2014). For example, Li' study supported that silica nanoparticles induced secretion of pro-fibrotic cytokines, such as TGF- β 1, a well-documented fibrogenic cytokine, in macrophages, which further promoted the proliferation and differentiation of human lung fibroblasts MRC-5, reflected by increased expression of α -SMA and collagen I (Li et al. 2021). Our previous study revealed that exposure to Nano-Ni caused activation of TGF- β 1/Smad signaling pathway and further led to pulmonary fibrosis in mouse lungs (Mo et al. 2020b). In addition to TGF- β 1, OPN was showed to induce proliferation, migration, and activation of fibroblasts in mouse lungs (Dong and Ma 2017; Khaliullin et al. 2017; Takahashi et al. 2001). In OPN KO mice, marked decrease of collagen deposition and reduced inflammation in the lungs were observed after SWCNT exposure comparing to those in wild-type mice (Khaliullin et al. 2017). In another study, treatment of mice with RMV-7, an α v antibody interrupts the binding of OPN to integrins, significantly suppressed the formation of bleomycin-induced lung fibrosis, and *in vitro*, RMV-7 significantly repressed recombinant OPN-enhanced migration, adhesion, and proliferation of NIH3T3 murine fibroblasts (Takahashi et al. 2001). Similarly, in this study, Nano-CuO exposure caused production of MMP-3-cleaved OPN and further resulted in activation of fibroblasts, whereas no significant upregulation of TGF- β was observed (Figure 30). Additionally, PDGF and several other pro-inflammatory cytokines may also contribute to the

progression of lung fibrosis (Bonner 2010; Mangum et al. 2006; Thompson et al. 2014). For example, Salik's study showed that conditioned media from MWCNTs-treated HBE cells caused NLRP3 inflammasome-dependent but not TGF- β -dependent fibrotic responses in fibroblasts (Hussain et al. 2014).

Although OPN-induced activation of fibroblasts was confirmed in current study and other studies (Dong and Ma 2017; Khaliullin et al. 2017; Takahashi et al. 2001), the detail of OPN-induced fibroblasts activation and fibrosis still needs to be explored. Indeed, OPN is a multifunctional factor and has been showed to interact with other factors in fibrotic responses. Previous studies demonstrated that TGF- β 1 was significantly induced in wild-type mouse lungs at day 7 after SWCNT administration, while the TGF- β 1 level was unaltered in OPN KO mice, suggesting that OPN may act upstream of TGF- β 1 responding to nanomaterials exposure (Khaliullin et al. 2017). At the molecular level, it was shown that OPN could promote the production and activation of TGF- β 1, which further contribute to myofibroblast differentiation and fibrous matrix protein production in both *in vivo* and *in vitro* after exposure to MWCNTs (Dong and Ma 2017). Another study reported that recombinant OPN enhanced platelet-derived growth factor (PDGF)-mediated cell proliferation and DNA synthesis in murine fibroblasts, which was not affected by mOPN-GST alone (Takahashi et al. 2001). In addition, OPN may promote occurrence of epithelial-mesenchymal transition, which is a cellular process playing important roles in organ development, as well as disease formation, such as fibrosis (Hatipoglu et al. 2021). *In vivo*, OPN-siRNA treatment restored BLM-induced decrease of E-cadherin and reduced the expression of

vimentin. And *in vitro*, OPN knockdown inhibited the expression of Col1A1, fibronectin, and vimentin mRNA in TGF- β 1-treated A549 cells (Hatipoglu et al. 2021). However, further study is needed to explore the OPN-mediated activation of fibroblasts.

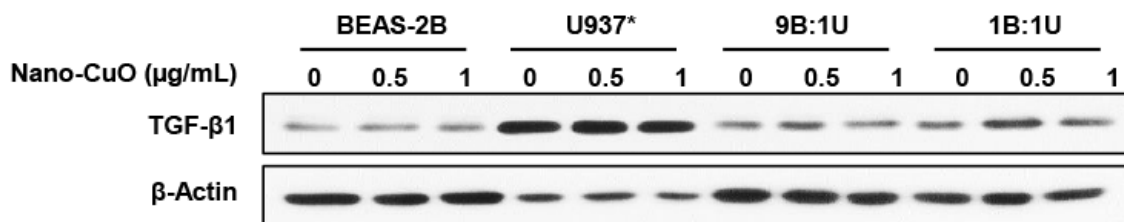


Figure 30. Exposure to Nano-CuO did not cause upregulation of TGF- β 1 in BEAS-2B cells and U937* macrophages.

BEAS-2B cells, U937* macrophages, or co-culture of BEAS-2B and U937* macrophages at the ratio of 1:1 or 9:1 (BEAS-2B:U937*) were exposed to 0, 0.5 and 1 $\mu\text{g/mL}$ of Nano-CuO for 12 h. After treatment, the cells were collected. TGF- β 1 in the cells were detected by Western blot.

CHAPTER IV: INVESTIGATE THE ROLE OF MMP-3 IN NANO-CUO-INDUCED LUNG INFLAMMATION, INJURY, AND FIBROSIS *IN VIVO*

4.1 Introduction

Matrix metalloproteinases (MMPs) are a big family of calcium-dependent zinc-containing endopeptidases, which are capable of breaking down all extracellular matrix and membrane proteins (Yuan et al. 2021), playing essential roles in tissue remodeling related processes, such as morphogenesis, angiogenesis, tissue repair, cancer, fibrosis, etc. Our previous studies demonstrated that metal nanoparticles caused upregulation of MMPs, such as MMP-2 and MMP-9, which were further involved in metal nanoparticle-induced lung inflammation, injury, and fibrosis (Mo et al. 2019; Mo et al. 2020a; Mo et al. 2020b; Wan et al. 2017). In chapter II and chapter III of this study, I have shown that Nano-CuO exposure caused increased expression and activity of MMP-3 in BEAS-2B cells and macrophages, which further dysregulated the expression of cell junction-associated proteins and activated fibroblasts, playing important roles in the development of pulmonary inflammation and fibrosis. In this chapter, we explored whether Nano-CuO exposure would cause expression of MMP-3 in mouse lungs, a member of MMPs family and a mediator of pulmonary fibrosis, and

explored the role of MMP-3 in Nano-CuO-induced lung inflammation, injury, and fibrosis in mice.

We hypothesized that Nano-CuO exposure would cause elevated expression of MMP-3, which further contributed to the disruption of the epithelial barrier, lung injury, inflammation, and fibrosis. And knocking down of MMP-3 might significantly alleviate these effects caused by Nano-CuO.

4.2 Materials and methods

4.2.1 Nanoparticles and their characterization

See “Nanoparticles and their characterization” in Materials and methods in the section 2.2.1 of Chapter II. In this chapter, Nano-CuO were dispersed in normal saline to make 0.5, 1, and 2 mg/mL work solutions and ultrasonicated by an ultrasonic cleaner FS30 (Fisher Scientific, Pittsburg, PA) for at least 10 min prior to the experiments.

4.2.2 Animals

C57BL/6J mice (male, 8-week-old, about 20-28 g) were purchased from The Jackson Laboratory (Bar Harbor, ME, USA) and housed in the animal research facility (at 20 ± 2 °C with $60 \pm 10\%$ humidity) with a 12 h light/dark cycle environment. Mice were allowed to get unrestricted access to food and water and have an acclimation period for 1-2 weeks before nanoparticle instillation. The general health of mice was monitored daily. Animal use was reviewed and

approved by the University of Louisville Institutional Animal Care and Use Committee.

4.2.3 Exposure of mice to Nano-CuO

Mice were exposed to Nano-CuO by intratracheal instillation as previously described (Mo et al. 2019; Mo et al. 2020b; Wan et al. 2017; Zhang et al. 1998; Zhang et al. 2003). C57BL/6J mice were randomly divided into control or Nano-CuO-treated group. The neck skin of the mouse was opened after general anesthesia, and the trachea was exposed for Nano-CuO instillation. For the dose-response study, mice were intratracheally instilled with 50 μ L per mouse of physiological saline containing 0, 25, 50, or 100 μ g Nano-CuO and sacrificed at day 3 after exposure. For the time-course study, mice were intratracheally instilled with 50 μ g per mouse of Nano-CuO and sacrificed at days 1, 3, 7, 14, 28, and 42 after exposure. The mice exposed to physiological saline were used as the control. After instillation, the wound was sutured immediately.

4.2.4 MMP-3 siRNA delivery in mice

Mouse Ambion® *In vivo* Pre-designed MMP-3 siRNA was acquired from Thermo Fisher Scientific (Waltham, MA). MMP-3 siRNA was dissolved in purified nuclease-free sterile water to be 250 μ M, which were further diluted with physiological saline (0.9% NaCl) to a 50 μ M working solution. For short-term exposure, mice were instilled intratracheally with MMP-3 siRNA (1 nmol per mouse) and 50 μ g per mouse of Nano-CuO at day 0 and sacrificed at day 3 after

exposure. For long-term exposure, mice were at first intratracheally instilled with MMP-3 siRNA (1 nmol per mouse) and 50 ug per mouse of Nano-CuO at day 0, and repeatedly administrated with MMP-3 siRNA (1 nmol per mouse each time) at day 7, 14 and 21 through oropharyngeal aspiration and sacrificed at day 28 after initial exposure. Oropharyngeal aspiration was operated as stated before (Lakatos et al. 2006; Nielsen et al. 2018). Ambion™ *In Vivo* Negative Control #1 siRNA was chosen as a negative control. All siRNAs used were annealed and HPLC-purified.

4.2.5 Preparation of bronchoalveolar lavage fluid (BALF)

BALF was harvested from mice to evaluate lung injury after Nano-CuO exposure as mentioned before with some adjustments (Mo et al. 2019; Mo et al. 2020b; Wan et al. 2017). After anesthesia by an overdose of tribromoethanol, mouse trachea and lungs were exposed and bilaterally lavaged by 6 x 0.5 mL of cold 1 x phosphate-buffered saline with 0.4 mM EDTA, with 2~3 times instillation and withdrawal in every lavage. The supernatant from first two lavage samples was immediately collected after centrifugation (200 g, 5 min, 4°C) and stored at -70°C for further analysis. Cells in all lavage fluid were collected, and the total number of cells was determined using a hemocytometer under a microscope. The counts for differential cells, such as neutrophils, macrophages, and lymphocytes, were performed on cytopsin slides after stained by Giemsa and May-Grünwald stains (Sigma-Aldrich, St. Louis, MO).

4.2.6 Biochemical analysis of BALF

LDH Cytotoxicity Detection Kits (TaKaRa Bio Inc., Shiga, Japan) were purchased to determine lactate dehydrogenase activity in BALF. Mouse CXCL1/KC QuantiKine[®] ELISA Kit (R&D Systems, Inc., Minneapolis, MN, USA) was used to determine the level of keratinocyte chemoattractant (KC) in BALF. Bio-Rad Protein Assay (Hercules, CA, USA) was chosen to measure the concentration of total protein in BALF via Bradford method.

4.2.7 Lung histology and trichrome staining

Mouse lungs were fixed with 10% neutral buffered formalin, dehydrated, degreased, and embedded in paraffin. The paraffin blocks were cut into 5 μ m sections by using a microtome (Thermo Scientific, Rockford, IL).

H&E staining was used to detect the histological alterations of mouse lungs induced by Nano-CuO exposure, which was described in detail in our previous studies (Mo et al. 2019; Mo et al. 2020b). Briefly, lung tissue sections were stained in Harris Hematoxylin for 3 min after deparaffinization and rehydration. Then the lung sections were rinsed briefly in acid water and mordanted in bluing reagent for 30 seconds each. After brief rinse with water and alcohol, sections were counterstained in Eosin Y solution for 2 min. After dehydration and clear, lung sections were mounted.

Masson's Trichrome staining was performed to confirm Nano-CuO-caused lung fibrosis as mentioned in our previous studies with modifications (Mo et al. 2019; Mo et al. 2020b; Wan et al. 2017). Briefly, after deparaffinization and

rehydration, lung sections were mordanted in Bouin's fixative for 12 h for the final coloration intensification, stained in Weigert's Iron Hematoxylin working solution for 15 min, and briefly rinsed with water and then stained in Biebrich Scarlet-Acid Fuchsin for another 3 min. Following rinse with water, sections were incubated in Phosphomolybdic Acid/Phosphotungstic Acid for 15 min, and then stained in Aniline Blue solution for another 20 min. After differentiation in 1% acetic acid, lung sections were dehydrated, cleared, and mounted.

4.2.8 Hydroxyproline assay

To determine the amount of collagen in lungs after Nano-CuO exposure, the content of hydroxyproline in mouse left lungs were measured with similar methods used in our published studies (Mo et al. 2019; Mo et al. 2020b; Wan et al. 2017). Briefly, mouse left lung tissues were dried at 65 °C for 24 h, weighed, and hydrolyzed in HCl (1 mL, 6 N) at 100°C overnight. After cooling down, 6 N NaOH was used to neutralize the hydrolysate to nearly pH 6.0. Then, 3% chloramine-T solution (pH 6.0) (Sigma-Aldrich, St. Louis, MO), which contains 50% isopropanol and 500 mM sodium acetate, was added to oxidize the free hydroxyproline to pyrrole intermediates. Perchloric acid was added next to stop the oxidation (Sigma-Aldrich, St. Louis, MO). Finally, Ehrlich's reagent (5% of 4-dimethylaminobenzaldehyde in methanol) was used to convert the oxidation products to formation of brightly colored chromophore which can be easily measured at OD 560 nm. Hydroxyproline (Sigma-Aldrich, St. Louis, MO) was used

to generate a standard curve to determine the hydroxyproline content in mouse lungs.

4.2.9 Total RNA extraction and real-time PCR

Total RNA in the lung tissues was extracted by mirVana miRNA Isolation Kit (Abcam, Cambridge, MA) according to the manufacturer's instructions. Briefly, lung tissues were homogenized by a motorized homogenizer in 10 times of lysis buffer, and 1/10 volume of miRNA Homogenate Additive was added to the tissue lysate. The mixture was incubated on ice for at least 10 min. A volume of Acid-Phenol:Chloroform that is equal to the lysate volume before addition of the miRNA Homogenate Additive was added in the tissue lysate and mixed thoroughly. The mixture was centrifuged at speed of 10,000 g for 5 min at room temperature and the supernatant was extracted for RNA isolation by adding isopropanol. After washing with 75% ethanol, the concentration of total RNA was measured by a DU 730 Spectrophotometer (Beckman Coulter, Fullerton, CA).

To quantify the expression of proinflammatory cytokines and fibrosis-related genes, RT-qPCR was performed by using a Mastercycler (Eppendorf, Westbury, NY) and a Bio-Rad iQ5 iCycler as previously described in "Extraction of total RNA and real-time PCR" in the section 2.2.7 of Chapter II. The mouse primers used were:

MMP-3 forward 5'- GCTTTGAAGGTCTGGGAGGAGGTG-3';

MMP-3 reverse 5'- CAGCTATCTTCCTGGGAAATCCTG-3';

IL-1 β forward 5'- TCATGGGATGATGATGATAACCTGCT-3';

IL-1 β reverse 5'-CCCATACTTTAGGAAGACACGGATT-3';

IL-6 forward 5'-TTGGGACTGATGCTGGTGACA-3';

IL-6 reverse 5'-TTGGAAATTGGGGTAGGAAGGA-3';

COL1A1 forward 5'-GTGCTCCTGGTATTGCTGGT-3';

COL1A1 reverse 5'-GGCTCCTCGTTTTCTTCTT-3';

COL3A1 forward 5'-GGGTTTCCCTGGTCCTAAAG-3';

COL3A1 reverse 5'-CCTGGTTTCCCATTTTCTCC-3';

β -actin forward 5'-GGCATTGTTACCAACTGGGAC-3';

and β -actin reverse 5'-ACCAGAGGCATACAGGGACAG-3'. The expression of genes described above were recorded as threshold cycle numbers (Ct) and assessed by the $2^{-\Delta\Delta Ct}$ method (Livak and Schmittgen 2001) that normalize against corresponding β -actin mRNA level.

4.2.10 Protein isolation and Western blot

Mouse lung tissue homogenization were performed in 20-time volume of ice-cold RIPA lysis buffer supplemented with PMSF, protease inhibitor cocktail, and sodium orthovanadate (Santa Cruz Biotechnology, Santa Cruz, CA) using a motorized homogenizer. The homogenates were placed on ice for 45 min. After centrifugation at 11,000 g at 4°C for 15 min, supernatant that containing total proteins was transfered to a new tube and the total protein concentration was determined by Bradford method by using a DU730 Spectrophotometer. Then protein samples were prepared for Western blot as described in "Western blot" in the section 2.2.9 of Chapter II. The primary antibodies for β -actin (cat.# 4970) and

Col1A1 (cat.# 72026) were purchased from Cell Signaling Technology (Beverly, MA), antibody for α -SMA (cat.# A5228) from Sigma- Aldrich (Saint Louis, MO), anti-fibronectin (cat.# sc-8422) from Santa Cruz (Dallas, TX), and anti-MMP-3 (cat.# 53015) from abcam (Cambridge, MA). HRP-conjugated goat anti-rabbit IgG was bought from CHEMICON (Temecula, CA), while HRP-conjugated horse anti-mouse IgG was from Cell Signaling Technology (Beverly, MA). After incubation with primary and secondary antibodies, the protein bands were detected by using SuperSignal™ West Pico PLUS Chemiluminescent Substrate (Thermo Scientific, Rockford, IL) followed by exposure to CL-XPosure™ film (Thermo Scientific). Bands on the film were quantified by NIH ImageJ software (<https://imagej.nih.gov/ij/>).

4.2.11 Statistical analysis

SigmaPlot 13.0 software (Systat Software, San Jose, CA) was chosen for statistical analyses. Data were showed as mean \pm standard error (SE). To analyze the differences among groups with one independent variable, one-way analysis of variance (ANOVA) was performed with Bonferroni post-hoc test. The differences among groups with two independent variables (such as siRNA and Nano-CuO) were analyzed by two-way ANOVA with Holm-Sidak test. p -value <0.05 was considered to be statistically significant.

4.3 Results

4.3.1 Dose- and time- response studies after Nano-CuO exposure

To obtain the appropriate dose and time for the study of pulmonary toxicity caused by Nano-CuO, dose- and time- response studies were performed in mice. In the dose-response study, mice were intratracheally instilled with 0, 25, 50, 100 μg per mouse of Nano-CuO. At day 3 after exposure, mice were sacrificed, and lung tissues were harvested. The results showed that Nano-CuO exposure led to a dose-dependent increase in the cellular and biochemical constituents in BALF (Figure 31A-G). Even the 25 μg per mouse of Nano-CuO exposure induced acute pulmonary inflammatory response, which were reflected by significantly increased total number of neutrophils, total protein levels, and LDH activity in BALF, but not CXCL1/KC level and total number of cells in BALF. Mice exposed to 50 μg and 100 μg per mouse of Nano-CuO caused significant increases in all the cellular and biochemical constituents described above. Cell differential in BALF from mouse after Nano-CuO instillation was also shown by cytopsin slides followed by staining with Giemsa and May-Grünwald stains (Figure 31G). Therefore, 50 μg per mouse of Nano-CuO was chosen as the exposure dose for the following *in vivo* experiments.

In the time-response study, mice were intratracheally instilled with 50 μg per mouse of Nano-CuO. At days 1, 3, 7, 14, 28 and 42 after exposure, the BALF were collected as described above. Nano-CuO instillation induced increases in total cells count and macrophages count in BALF from day 3 post-exposure, which peaked at day 14 post-exposure and then decreased. However, at days 28 and 42

after exposure, the total cells and macrophages counts were still higher than those in control group (Figure 32A, C). Nano-CuO exposure caused a remarkable increase in total number of neutrophils in BALF from day 1 after exposure, which reached its peak at day 3 and reduced from day 3 to day 7 post-exposure (Figure 32B). Lymphocytes were also observed at day 7 and 14 after exposure (Figure 32G), suggesting that Nano-CuO may also induce immune cell-mediated inflammatory responses. The total protein level and LDH activity in BALF were detected. Their levels increased at day 1, peaked at day 3 after exposure, and then went down but never reaching to the levels in control group (Figure 32D, E). The level of CXCL1/KC, a chemoattractant for neutrophils in mice, was significantly increased at day 1 after Nano-CuO instillation and declined at the following time points (Figure 32F). The results of cell differential caused by Nano-CuO were also shown by cytopsin slides (Figure 32G).

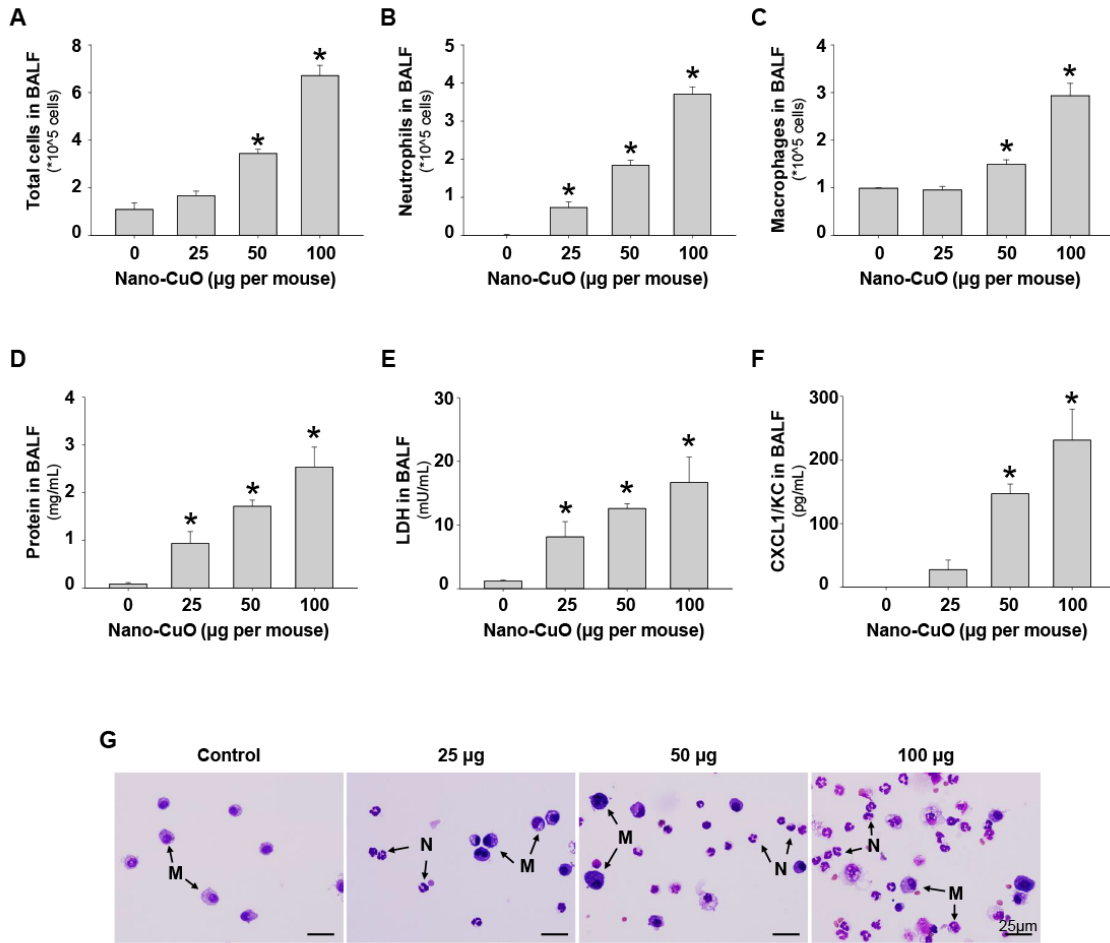


Figure 31. Dose-response results of cellular and biochemical constituents in BALF from mice after Nano-CuO exposure.

C57BL/6J mice were exposed to 0, 25, 50, 100 $\mu\text{g}/\text{mouse}$ of Nano-CuO intratracheally. At day 3 after exposure, mice were sacrificed and the BALF was harvested. The total cell count (**A**), neutrophil count (**B**), macrophage count (**C**), total protein level (**D**), LDH (**E**), and CXCL1/KC level (**F**) in BALF were measured. (**G**) were the cell differential smears of a single experiment. Scale bar represents 25 μm . Data represent mean \pm SE ($n=4\sim 6$). * $p<0.05$ vs. the control group.

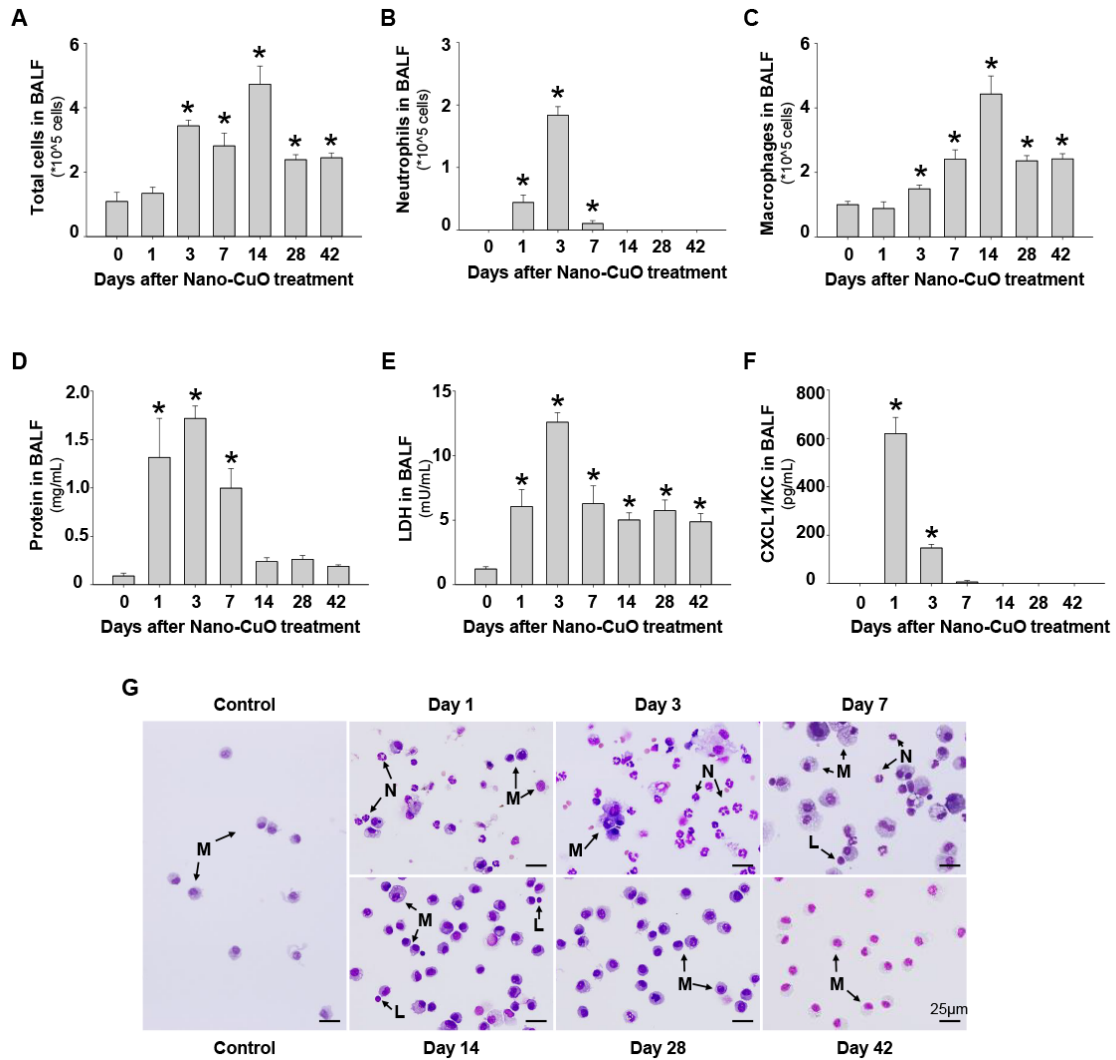


Figure 32. Time-response results of cellular and biochemical constituents in BALF from mice after Nano-CuO exposure.

C57BL/6J mice were intratracheally instilled with 50 μ g/mouse of Nano-CuO. Mice instilled with same volume of normal saline were used as control group. At days 1, 3, 7, 14, 28, and 42 after exposure, mice were sacrificed and BALF was harvested. The total cell count (**A**), neutrophil count (**B**), macrophage count (**C**), total protein level (**D**), LDH (**E**), and CXCL1/KC level (**F**) in BALF were measured. (**G**) were the

cell differential smears of a single experiment. Scale bar represents 25 μm . Data display mean \pm SE (n=4~6). * $p < 0.05$ vs. the control group.

4.3.2 Nano-CuO exposure upregulated MMP-3 in mouse lungs

In chapter II and chapter III, I have shown that exposure of human lung epithelial BEAS-2B cells and macrophages to Nano-CuO resulted in an increased expression of mRNA and protein of MMP-3, as well as an increased activity of MMP-3. To further explore whether Nano-CuO exposure caused those effects *in vivo*, we conducted a time-response study in mice. We found that exposure to 50 µg/mouse of Nano-CuO induced persistent increase in MMP-3 mRNA from day 1 to day 42 post-exposure in mouse lungs (Data not shown). The level of MMP-3 protein in BALF after Nano-CuO exposure was detected by Western blot. The Western blot results demonstrated that Nano-CuO instillation caused remarkable increases in MMP-3 protein in BALF (Figure 33A, B). These results suggested that Nano-CuO exposure could induce upregulation of MMP-3 in mouse lungs.

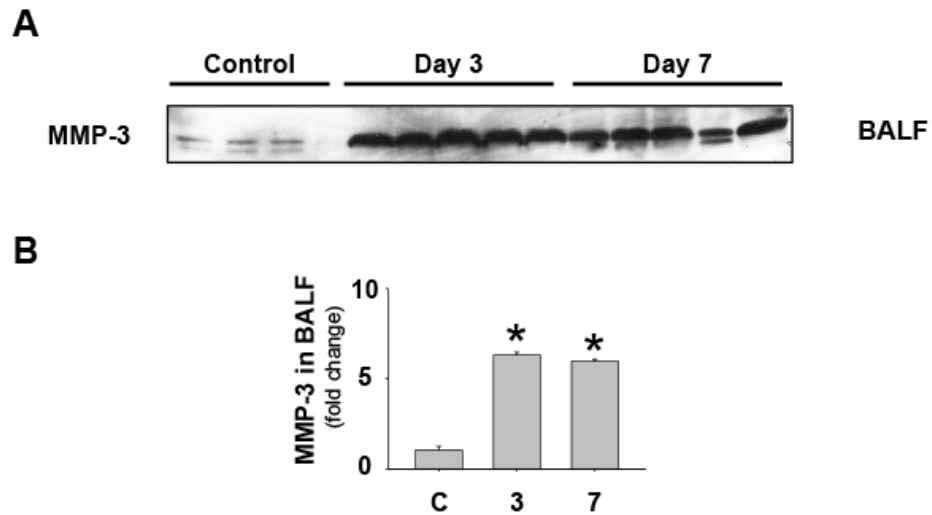


Figure 33. Increased MMP-3 protein level in BALF from mice after Nano-CuO exposure.

Mice were intratracheally exposed to 50 μ g per mouse of Nano-CuO. Mice instilled with same volume of normal saline were used as a control group. At day 3 and 7 after exposure, mouse lung BALF was collected. The level of MMP-3 protein in BALF was detected by Western blot. **A** was the results of Western blot experiment. **B** was the average normalized band densitometry readings of MMP-3 protein level in BALF. Data represent mean \pm SE (n=4~5). * $p < 0.05$ vs. the control group.

4.3.3 Nano-CuO exposure downregulated cell junction-associated proteins in mouse lungs

In section 2.3.6 of chapter II, the results illustrated that Nano-CuO exposure resulted in the disruption of cell junction-associated proteins *in vitro*. In this chapter, we investigated whether Nano-CuO exposure could also downregulate the expression of tight and adherens junction-associated proteins in mouse lungs. Mice were instilled with 50 µg per mouse of Nano-CuO intratracheally, and lung tissues were harvested at day 3 after exposure. The results demonstrated that Nano-CuO exposure significantly reduced the expression of tight junction-associated proteins, such as ZO-1 and occludin, and adherens protein E-cadherin in mouse lungs (Figure 34A, B).

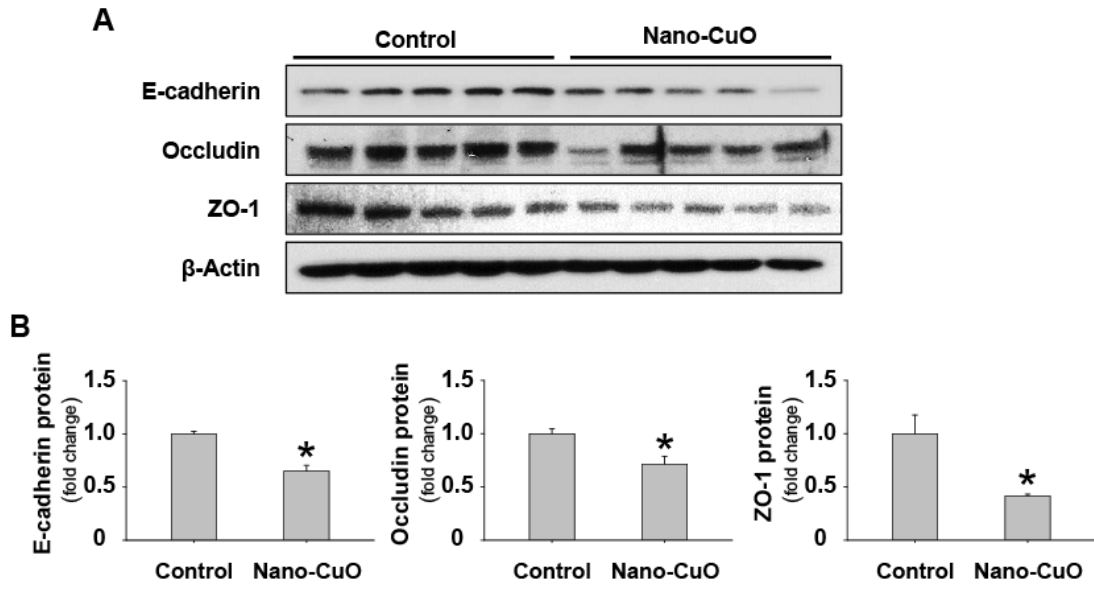


Figure 34. Nano-CuO exposure downregulated cell junction-associated proteins in mouse lungs.

Mice were instilled with 50 µg per mouse of Nano-CuO intratracheally. At day 3 after exposure, lung tissues were collected and prepared for Western blot. Adherens and tight junction-associated proteins were detected. **A** showed the results of representative Western blot experiment. **B** showed the average protein levels of E-cadherin, occludin, and ZO-1 normalized to β-actin. Data represent mean ± SE (n=5). * $p < 0.05$ vs. the control group.

4.3.4 Nano-CuO exposure induced overexpression of pro-inflammatory cytokines and fibrosis-related genes

To explore whether Nano-CuO exposure could induce upregulation of pro-inflammatory cytokines genes, such as IL-1 β and IL-6, and fibrosis-associated genes, such as Col1A1 and Col3A1, a time-response study was performed. Mice were intratracheally instilled with 50 μ g per mouse of Nano-CuO. At days 1, 3, 7, 14, 28, and 42 after exposure, lung tissues were harvested for total RNA extraction. Lung tissues from the control mice, which were instilled with equal volume of normal saline, were collected at day 1 post-exposure. The RT-qPCR results showed that Nano-CuO exposure led to elevated expression of IL-1 β mRNA as early as day 1 post-instillation, which retained at a significant higher level from day 1 to day 14 after Nano-CuO exposure (Figure 35A). Similarly, the mRNA level of IL-6 increased and peaked at day 1 post-exposure and went down from day 1 to day 7 (Figure 35B). Nano-CuO instillation also induced elevated expression of fibrosis-related genes Col1A1 and Col3A1 (Figure 35C, D). Expression of Col1A1 mRNA increased over time and reached peak at day 14 post-instillation, and went down to the levels of the control at day 28 (Figure 35C). Similarly, Col3A1 mRNA level peaked at day 3 and 7 post-exposure and then decreased to the levels of control at day 14 (Figure 35D). These results indicated that Nano-CuO exposure resulted in inflammation and fibrosis in mouse lungs.

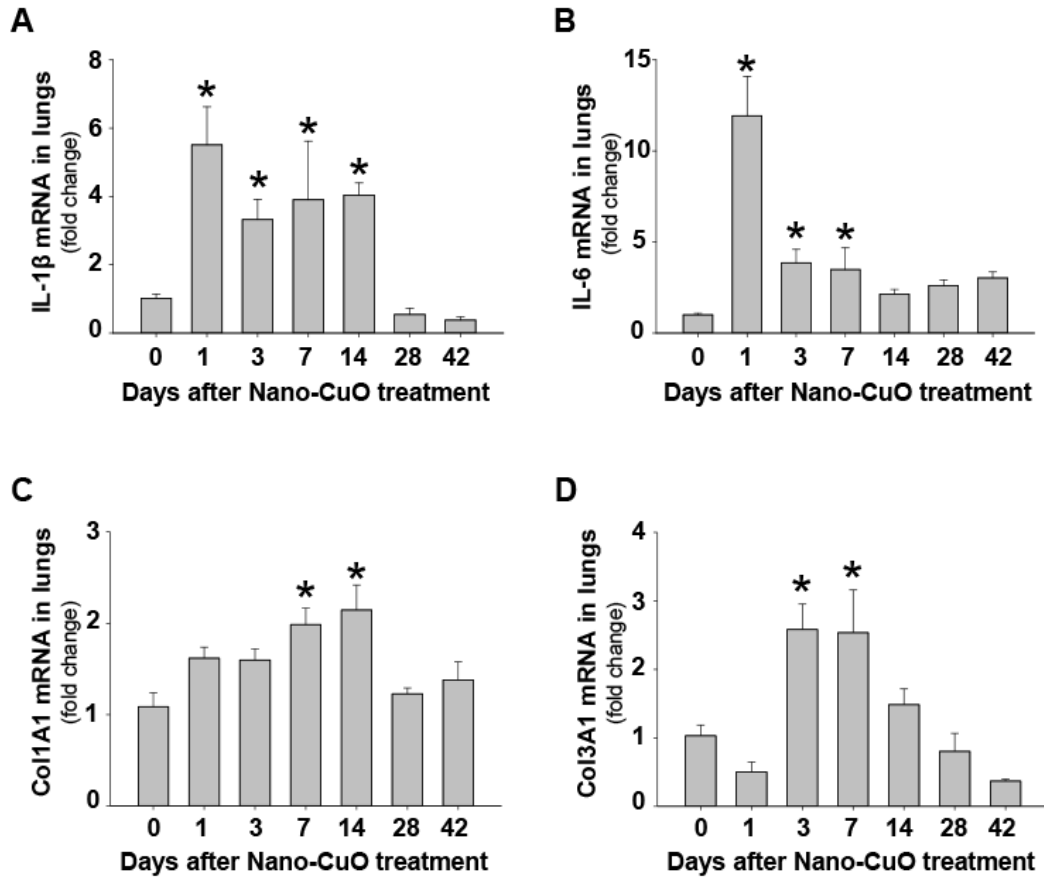


Figure 35. Upregulation of pro-inflammatory and fibrosis-related genes after Nano-CuO exposure.

Mice were intratracheally instilled with 50 μg per mouse of Nano-CuO. Mice instilled with same volume of normal saline were used as the control group. At days 1, 3, 7, 14, 28, and 42 after exposure, mouse lung tissues were collected. The expression of IL-1 β (A), IL-6 (B), Col1A1 (C), and Col3A1 (D) mRNA in lung tissues were detected by real-time PCR. Data represent mean \pm SE (n=4~5). * $p < 0.05$ vs. the control group.

4.3.5 Nano-CuO exposure induced lung inflammation and fibrosis in mice

To confirm that Nano-CuO exposure could induce pulmonary inflammation and fibrosis, mice were intratracheally instilled with 50 µg per mouse of Nano-CuO. At days 1, 3, 7, 14, 28, and 42 after exposure, mouse lung tissues were harvested and inflated with 10% formalin solution. Mouse lung tissues from the control group which were instilled with equal volume of normal saline were collected at day 1 post-exposure.

H&E staining was performed to observe the histopathological alterations of lungs caused by Nano-CuO. Normal lung tissue structure was shown in control mice (Figure 36A, E). In Nano-CuO-exposed mouse lungs, infiltration of large numbers of leukocytes, such as polymorphonuclear (PMN) cells and macrophages, were observed, suggesting that Nano-CuO exposure caused inflammatory responses in mouse lungs. It occurred as early as day 1 after Nano-CuO instillation. At day 1 after exposure, increased neutrophils were mainly observed in the peribronchial, peribronchiolar, and perivascular areas (Figure 36B). While on day 3 after exposure, a remarkable number of neutrophils were observed to infiltrate into alveolar spaces, alveolar septa, and peribronchiolar, which accounted for more than 50% of the total leukocytes in BALF (Figure 36C), suggesting that Nano-CuO exposure caused acute lung inflammation in mouse lungs. The number of Nano-CuO-induced macrophages significantly increased at day 3, peaked at day 14 after exposure. At days 28 and 42 after exposure, excessive macrophages were still observed in mouse lungs (Figure 32C & Figure 36D, F, G, H), indicating that Nano-CuO exposure induced chronic lung

inflammation in mice. At day 7 after exposure, aggregation of macrophages was found at peribronchial, peribronchiolar, and perivascular areas, and enlarged macrophages were observed in lung alveolar spaces (Figure 36D). Emphysema and thickened lung alveolar walls were also observed in the lung sections at days 14, 28 and 42 after Nano-CuO exposure (Figure 36F, G, H).

Trichrome staining was conducted to observe pulmonary fibrosis caused by Nano-CuO. No fibrosis was observed in the control mice and Nano-CuO-instilled mice at days 1, 3, and 7 after Nano-CuO exposure (Figure 36I, J, K, L). Nano-CuO-caused lung fibrosis was verified by trichrome staining from day 14 to day 42 post-exposure with an increasing tendency over time (Figure 36M, N, O). Thickening of alveolar septa was also observed from day 14 to day 42 after exposure. The amount of hydroxyproline in left lungs was also measured to confirm pulmonary fibrosis caused by Nano-CuO exposure. The results demonstrated that Nano-CuO exposure led to notable increases in the content of hydroxyproline in left lungs at days 14, 28, and 42 post-exposure (Figure 37A). Nano-CuO-induced lung fibrosis was further confirmed by determining the expression level of fibrosis-associated proteins, such as α -SMA, Col1A1, and fibronectin in mouse lungs. The results showed that Nano-CuO exposure induced remarkable increases in the levels of α -SMA, Col1A1, and fibronectin proteins (Figure 37B, C), suggesting that Nano-CuO exposure caused fibrosis in mouse lungs.

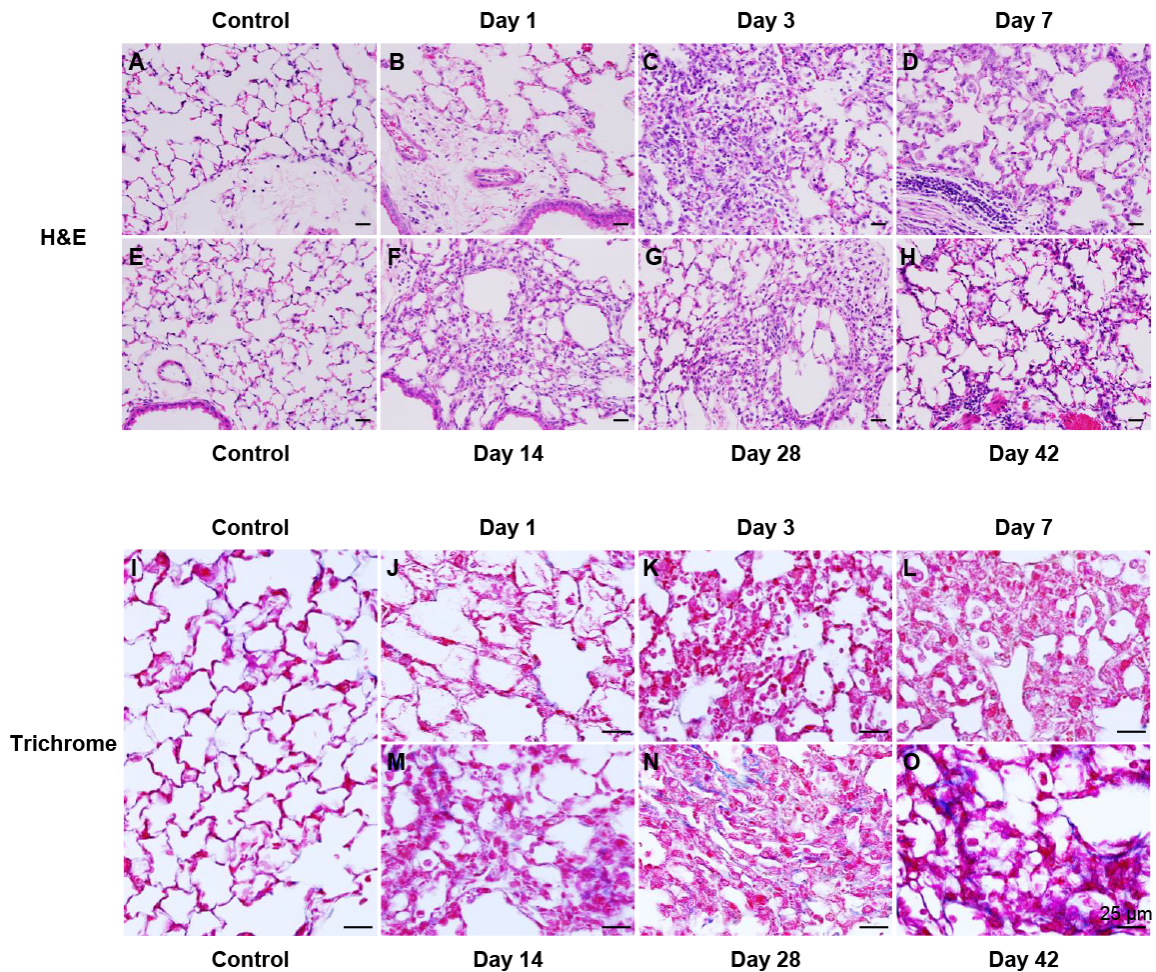


Figure 36. Histology of mouse lungs after Nano-CuO exposure.

Mice were intratracheally instilled with 50 μg per mouse of Nano-CuO. Mice instilled with same volume of normal saline were used as the control. At days 1, 3, 7, 14, 28, and 42 after exposure, mouse lungs were harvested and prepared for H&E staining (**A-H**) or trichrome staining (**I-O**). Normal lung parenchyma structure was shown in the control group (**A**, **E**, **I**). Nano-CuO-induced acute lung inflammation was evidenced by the infiltration of excessive neutrophils into lung parenchyma (**B**, **C**). **D**, **F**, **G** and **H** showed Nano-CuO-caused subacute and chronic lung inflammation and fibrosis, which were supported by infiltration of a large number of macrophages and thickened alveolar walls. Emphysema was also

observed in mouse lungs at day 14, 28, and 42 after exposure (**F, G, H**). Nano-CuO-induced lung fibrosis was shown by trichrome staining (**I-O**). No obvious fibrosis was observed at days 1, 3, and 7 after exposure (**I, J, K, L**). Gradually increased deposition of collagen was observed at days 14, 28, and 42 post-exposure (**M, N, O**), which showed development of fibrosis. Scale bar represents 25 μm in all panels.

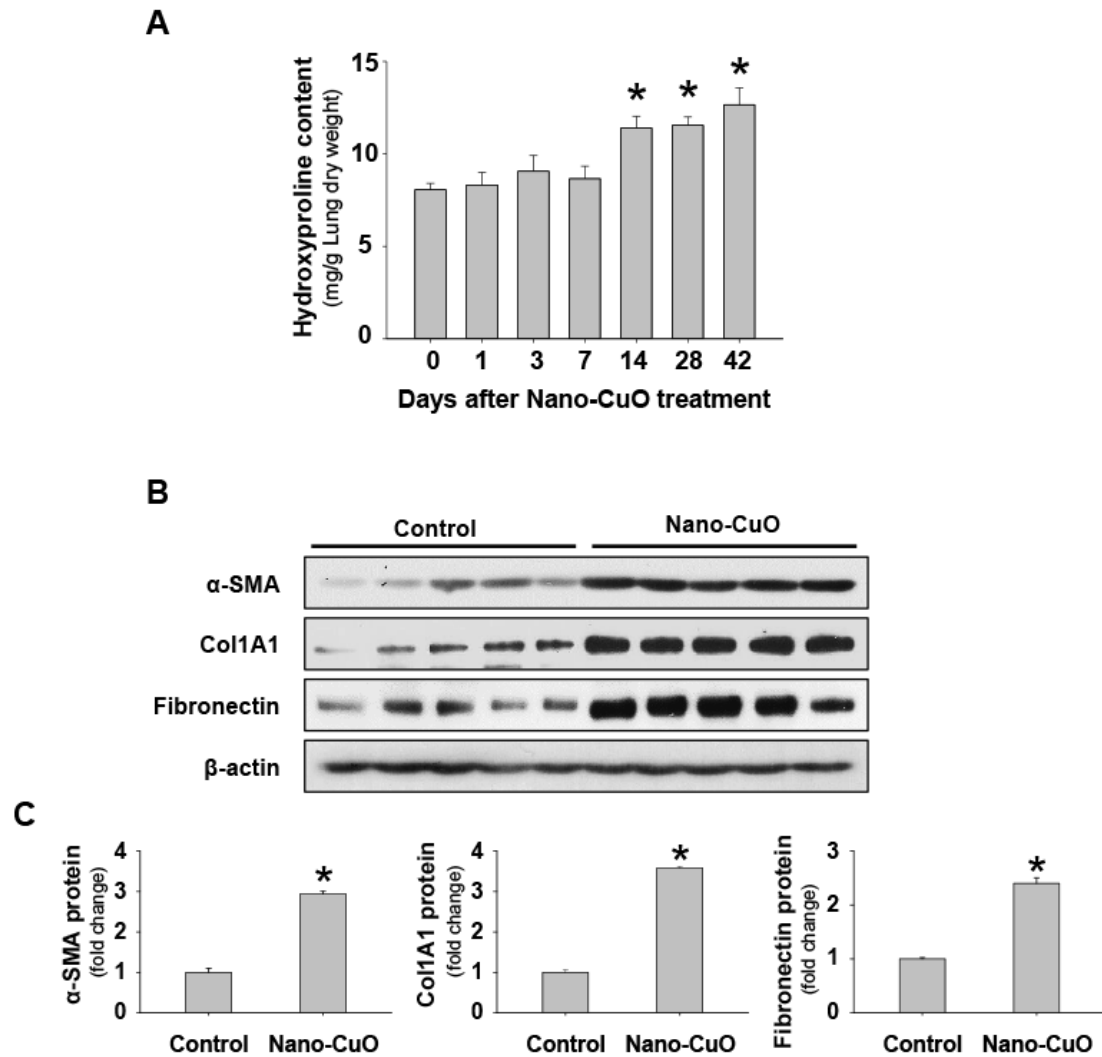


Figure 37. Nano-CuO exposure increased the hydroxyproline content and fibrosis-associated proteins in mouse lungs.

Mice were intratracheally exposed to 50 μ g per mouse of Nano-CuO. Mice instilled with same volume of normal saline were used as control group. At days 1, 3, 7, 14, 28, and 42 after exposure, lung tissues were harvested. **A** showed the hydroxyproline content in left lungs. Mouse lung tissues harvested at day 28 post-exposure were used to detect the levels of fibrosis-associated proteins caused by Nano-CuO. **B** were results of Western blot experiments. **C** were the average

protein levels of α -SMA, Col1A1, and fibronectin normalized to β -actin. Data represent mean \pm SE (n=5). * $p < 0.05$ vs. the control group.

4.3.6 Knocking-down MMP-3 ameliorated Nano-CuO-induced acute lung inflammation and injury in mice

To determine the role of MMP-3 in Nano-CuO-induced acute lung inflammation and injury, mice were instilled with Nano-CuO (50 µg/mouse) with 1 nmol per mouse of Ambion® *In Vivo* MMP-3 siRNA intratracheally and sacrificed at day 3 after exposure. Ambion™ *In Vivo* Negative Control #1 siRNA was chosen as the negative control. Effective MMP-3 knockdown in mouse lungs was verified by Western blot. Nano-CuO-caused overexpression of MMP-3 in mouse lungs and in BALF were significantly reduced by MMP-3 siRNA treatment, however, the MMP-3 expression was not affected in control siRNA treated mouse lungs (Figure 38A, B).

For the BALF constituents, the results demonstrated that MMP-3 siRNA treatment significantly decreased the cellular and biochemical constituents in BALF caused by Nano-CuO instillation (Figure 39A-G). The increased total number of cells, and neutrophils caused by Nano-CuO were significantly reduced after MMP-3 siRNA treatment, but not altered after control siRNA treatment (Figure 39A-C, G). Although the levels of biochemical constituents, such as the total protein, LDH activity, and CXCL1/KC, were still higher in MMP-3 siRNA-treated mice, the increased levels were significantly lower than those in control siRNA-treated mice (Figure 39D-F).

Lung sections were stained by H&E staining to observe the effects of MMP-3 siRNA treatment on histopathological changes caused by Nano-CuO. The results revealed that Nano-CuO exposure led to severe acute lung inflammation

at day 3 after exposure, which were evidenced by the infiltration of excessive leukocytes into alveolar space and septa, peribronchial, peribronchiolar, and perivascular areas (Figure 40B). Similar inflammatory responses were observed in Nano-CuO-exposed mice treated with control siRNA (Figure 40C). However, in MMP-3 siRNA-treated mice, the inflammatory responses caused by Nano-CuO were in a much less extent compared to those in control siRNA-treated mice (Figure 40D). The number of infiltrated leukocytes into lungs were much less than that observed in control siRNA-treated mice (Figure 40D). These results suggest that MMP-3 knockdown ameliorates Nano-CuO-induced acute pulmonary inflammation and injury in mouse lungs.

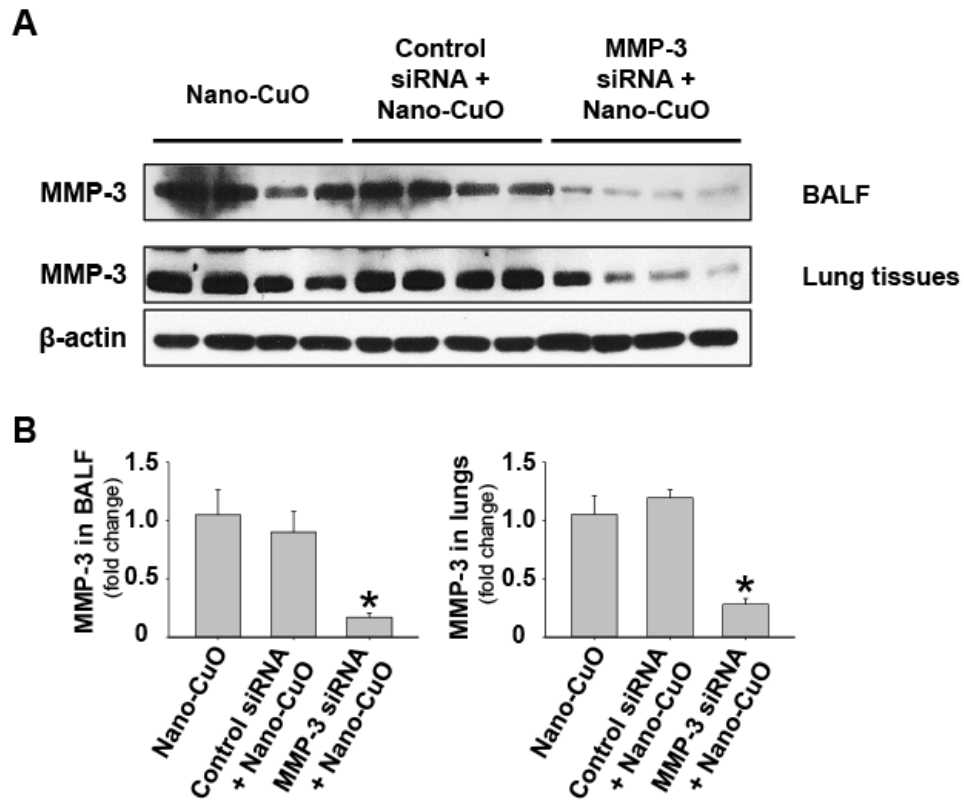


Figure 38. The efficiency of MMP-3 siRNA treatment in mouse lungs.

Mice were instilled with 50 μ g per mouse of Nano-CuO and 1 nmol per mouse of Ambion® *In Vivo* MMP-3 siRNA intratracheally and sacrificed at day 3 after exposure. The levels of MMP-3 protein in BALF and lung tissues were determined by Western blot. Ambion™ *In Vivo* Negative Control #1 siRNA was used as a negative control. **A** was results of Western blot experiments. In **B**, the average expression level of MMP-3 in lung tissues was normalized to β -actin; the average protein level of MMP-3 in BALF was band densitometry readings. Data represent mean \pm SE (n=4). * $p < 0.05$ vs. the Nano-CuO-exposed mice with control siRNA instillation.

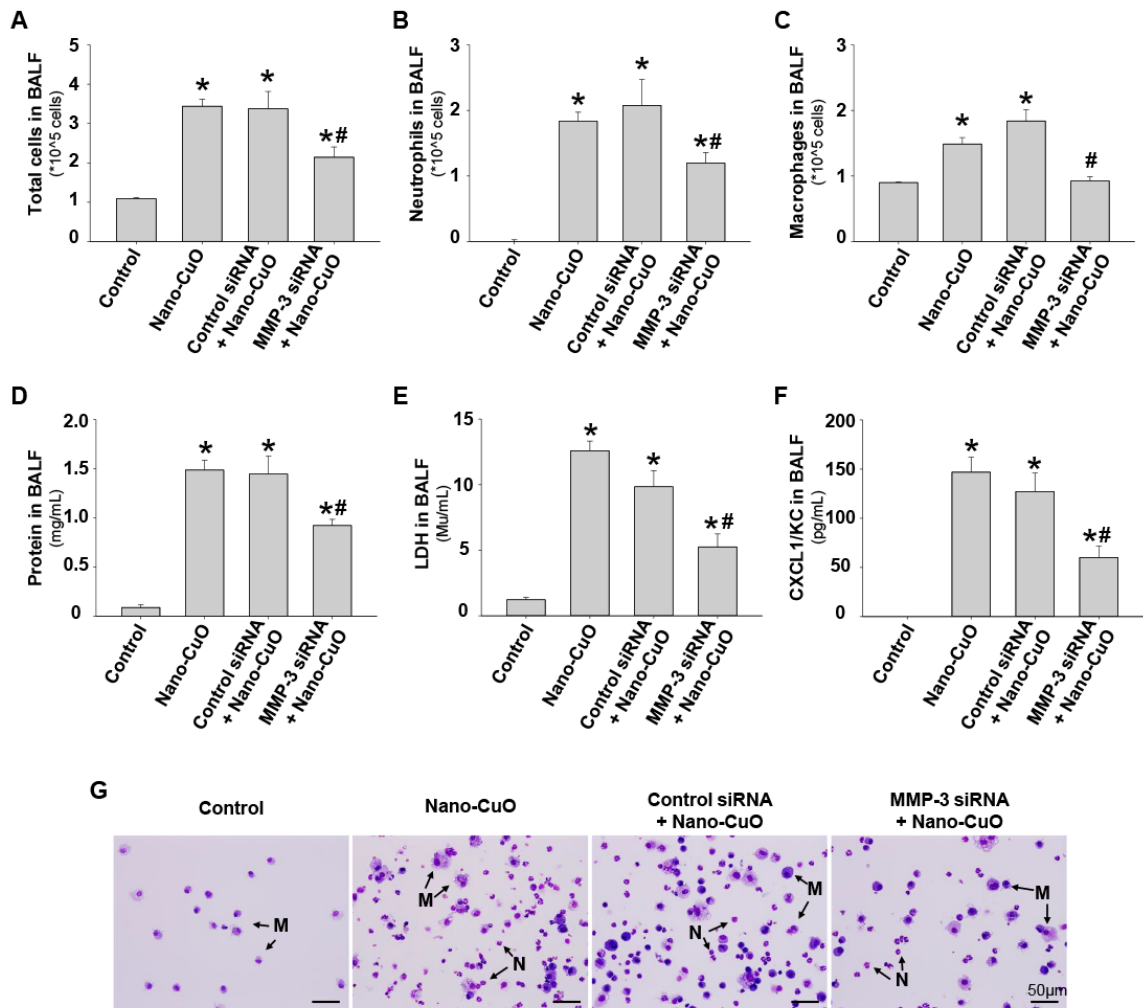


Figure 39. MMP-3 siRNA treatment significantly decreased the cellular and biochemical constituents in BALF caused by Nano-CuO exposure.

Mice were intratracheally exposed to Nano-CuO (50 μ g/mouse) with 1 nmol per mouse of Ambion[®] *In Vivo* MMP-3 siRNA. Mice were sacrificed at day 3 after exposure and BALF was harvested. Ambion[™] *In Vivo* Negative Control #1 siRNA was used as a negative control. Nano-CuO-caused increases in total cell count (A), neutrophil count (B), macrophage count (C), total protein level (D), LDH (E),

and CXCL1/KC level (**F**) in BALF were significantly inhibited by MMP-3 siRNA treatment. (**G**) were the cell differential smears of a single experiment. Data represent mean \pm SE (n=4~6). * $p < 0.05$ vs. the control group; # $p < 0.05$ vs. the Nano-CuO-treated group with Control siRNA treatment.

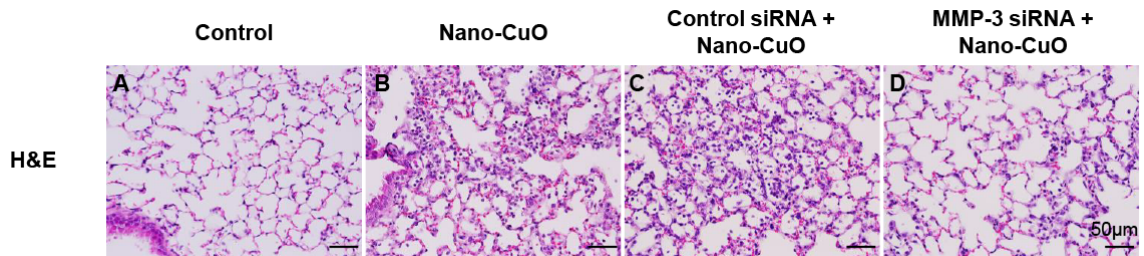


Figure 40. Knocking-down MMP-3 ameliorated Nano-CuO-caused acute lung injury and inflammation in mice.

Mice were intratracheally instilled with Nano-CuO (50 $\mu\text{g}/\text{mouse}$) and 1 nmol per mouse of Ambion[®] *In Vivo* MMP-3 siRNA and sacrificed at day 3 after exposure. Ambion[™] *In Vivo* Negative Control #1 siRNA was chosen as a negative control. Normal lung parenchyma was showed in control group (**A**). Nano-CuO-induced acute lung inflammation was evidenced by the infiltration of excessive neutrophils into lung parenchyma (**B**), similar inflammatory responses were observed in Nano-CuO-instilled mice treated with control siRNA (**C**). However, only a much lesser extent of lung inflammation was observed in Nano-CuO-instilled mice treated with MMP-3 siRNA (**D**). Scale bar represents 50 μm in all panels.

4.3.7 Knocking-down MMP-3 ameliorated Nano-CuO-induced downregulation of cell junction-associated proteins in mouse lungs

Dysfunction of epithelial barrier is considered a crucial factor to pulmonary inflammation and injury. Our results have shown that Nano-CuO exposure caused downregulation of cell junction-associated proteins. To explore the role of MMP-3 in Nano-CuO-caused downregulation of cell junction-associated proteins, mice were intratracheally instilled with Nano-CuO (50 µg/mouse) with 1 nmol per mouse of Ambion® *In Vivo* MMP-3 siRNA and sacrificed at day 3 after exposure. Ambion™ *In Vivo* Negative Control #1 siRNA was used as a negative control. The results showed that MMP-3 knockdown significantly restored the downregulation of occludin, ZO-1, and E-cadherin caused by Nano-CuO (Figure 41A, B).

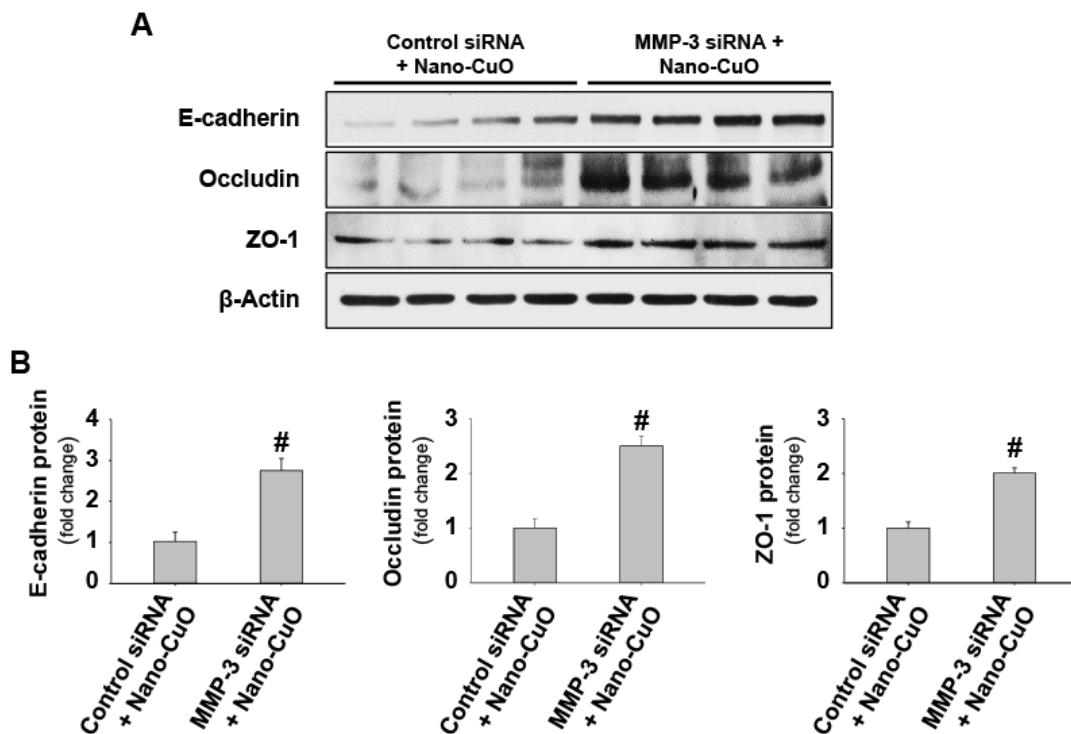


Figure 41. MMP-3 knockdown significantly restored the decreased expression of cell junction-associated proteins caused by Nano-CuO exposure in mouse lungs. Mice were exposed to 50 μg per mouse of Nano-CuO with 1 nmol per mouse of Ambion® *In Vivo* MMP-3 siRNA or Ambion™ *In Vivo* Negative Control #1 siRNA via intratracheal instillation and sacrificed at day 3 after exposure. The protein levels of E-cadherin, occludin, and ZO-1 in lung tissues were detected by Western blot. **A** showed the results of representative Western blot experiments. **B** was average protein levels of E-cadherin, occludin, and ZO-1 in lung tissues normalized to β -actin. Data represent mean \pm SE (n=4). # $p < 0.05$ vs. the Nano-CuO-exposed mice with control siRNA treatment.

4.3.8 Knocking-down MMP-3 alleviated Nano-CuO-caused chronic lung inflammation and fibrosis in mice

To explore whether MMP-3 played roles in Nano-CuO-induced chronic lung inflammation and fibrosis, mice were intratracheally instilled with Nano-CuO (50 µg/mouse) and 1 nmol per mouse of Ambion® *In Vivo* MMP-3 siRNA and were repeatedly administrated with MMP-3 siRNA at days 7, 14, and 21 through oral pharyngeal aspiration. Mice were sacrificed at day 28 after initiating exposure. Ambion™ *In Vivo* Negative Control #1 siRNA was chosen as a negative control.

After H&E staining, normal lung structure was shown in the control group (Figure 42A). Nano-CuO instillation caused extensive chronic lung inflammation. Aggregation of macrophages and large numbers of enlarged macrophages were observed in alveolar spaces (Figure 42B). Similar chronic inflammation caused by Nano-CuO was observed in mice treated with control siRNA (Figure 42C). However, in mice with MMP-3 siRNA treatment, Nano-CuO-induced inflammation was much milder (Figure 42D). The number of macrophages and inflamed lung fraction were much lesser than those in control siRNA-treated mice, suggesting that MMP-3 knockdown alleviates Nano-CuO-induced chronic lung inflammation in mice.

Nano-CuO-induced fibrosis was observed in lung sections at day 28 after exposure, which was evidenced by the increased deposition of collagen in alveolar septa, by which collagen was stained blue (Figure 42F). Similar extent of fibrosis caused by Nano-CuO was observed in mice with control siRNA treatment (Figure 42G). However, in mice treated with MMP-3 siRNA, the extent of Nano-CuO-

caused lung fibrosis was much less than those in mice with control siRNA treatment (Figure 42H). Hydroxyproline is an important component (~14% of total amino acid) of collagen and is found in few proteins other than collagen, therefore hydroxyproline content has been used as an indicator to quantify lung fibrosis (Mo et al. 2019; Mo et al. 2020b; Taylor et al. 2002). In the lungs of control siRNA-treated mice, Nano-CuO exposure induced a remarkable increase in the amount of hydroxyproline, which was similar to those in Nano-CuO-instilled mice without siRNA treatment (Figure 43A). However, in mice treated with MMP-3 siRNA, the hydroxyproline content caused by Nano-CuO exposure was significantly lower than those in control siRNA-treated mice (Figure 43A). To further verify the role of MMP-3 in Nano-CuO-caused lung fibrosis, the expression of fibrosis-related proteins, such as α -SMA, Col1A1, and fibronectin, were detected by Western blot. The results showed that Nano-CuO-induced expression of α -SMA, Col1A1, and fibronectin proteins in mouse lungs were significantly lower in MMP-3 siRNA-treated mice as compared to those in control siRNA-treated mice (Figure 43B, C). These results suggest that MMP-3 knockdown ameliorates Nano-CuO-induced pulmonary fibrosis in mouse lungs.

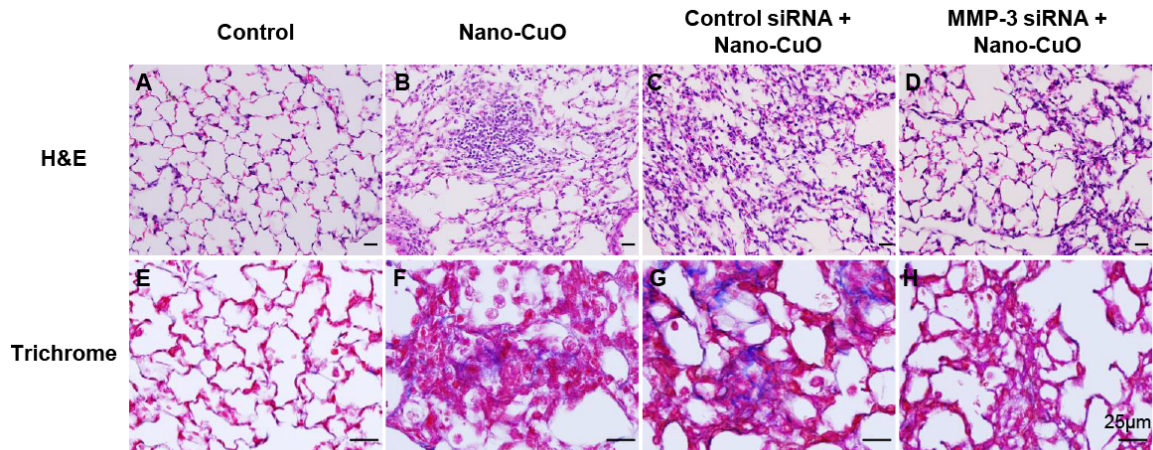


Figure 42. Knocking-down of MMP-3 ameliorated Nano-CuO-caused chronic lung inflammation and fibrosis in mice.

Mice were intratracheally instilled with 50 µg per mouse of Nano-CuO and 1 nmol per mouse of Ambion® *In Vivo* MMP-3 siRNA and were repeatedly administered with MMP-3 siRNA at days 7, 14, and 21 through oral pharyngeal aspiration. Mice were sacrificed at day 28 after initiating exposure. Ambion™ *In Vivo* Negative Control #1 siRNA was used as the negative control. Normal lung structure was observed in control mice stained by H&E stain (**A**) or by trichrome staining (**E**). Nano-CuO-induced chronic lung inflammation was evidenced by the infiltration of excessive macrophages into lung parenchyma (**B**, **C**). However, only a much lesser extent of lung chronic inflammation was observed in Nano-CuO-instilled mice treated with MMP-3 siRNA (**D**). Nano-CuO-induced fibrosis was visualized by trichrome staining (**F**, **G**, collagen stained blue), but no fibrosis or a much lesser extent of fibrosis was observed in Nano-CuO-instilled mice treated with MMP-3 siRNA (**H**). Scale bar represents 25 µm in all panels.

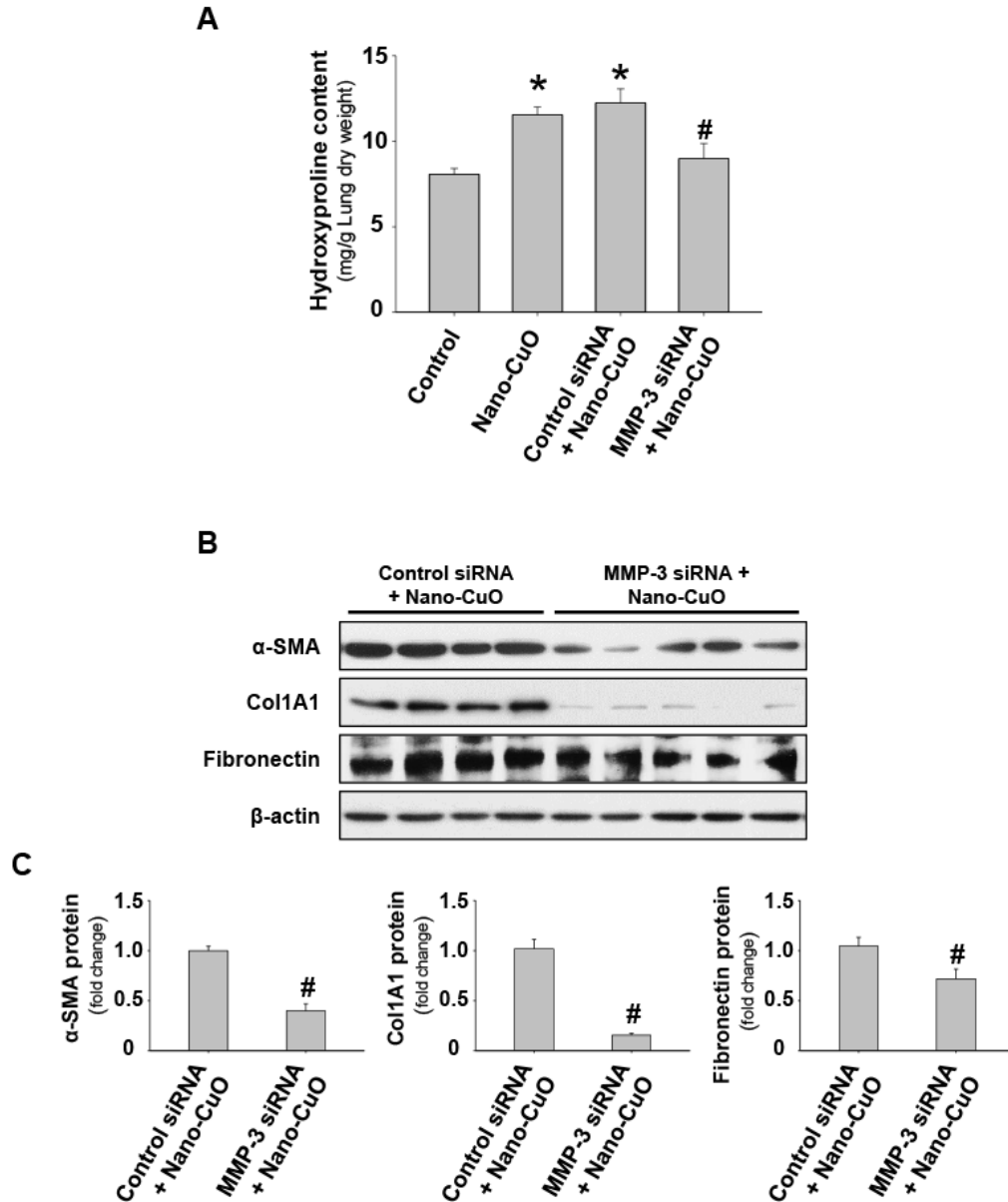


Figure 43. MMP-3 siRNA treatment reduced the increases of hydroxyproline content and fibrosis-related proteins caused by Nano-CuO in mouse lungs.

Mice were instilled with 50 μg per mouse of Nano-CuO and 1 nmol per mouse of Ambion® *In Vivo* MMP-3 siRNA intratracheally and were repeatedly administrated with MMP-3 siRNA at days 7, 14, and 21 through oral pharyngeal aspiration. Mice were sacrificed at day 28 after initiating exposure. Ambion™ *In Vivo* Negative

Control #1 siRNA was chosen as a negative control. **A** showed the amount of hydroxyproline in left lungs. **B** showed results of representative Western blot experiments. **C** was the average protein levels of α -SMA, Col1A1, and fibronectin normalized to β -actin. Data represent mean \pm SE (n=4~5). * $p < 0.05$ vs. the control group; # $p < 0.05$ vs. the Nano-CuO-instilled group with Control siRNA treatment.

4.4 Discussion

Nano-CuO with a diameter of less than 100 nm have some unique properties including high surface area, physiochemical stability, and high thermal and electrical conductivity (Msebawi et al. 2021; Xu et al. 2021), which may endow nanoparticles with more toxic effects. Our and other previous studies have shown that some metal (oxide) nanoparticles are more toxic than their bulk materials and may possess different mechanisms of toxicity (Juganson et al. 2015; Mo et al. 2020b; Wang et al. 2012a). With the widespread usage of Nano-CuO, the risk of exposure to Nano-CuO in workers and consumers has dramatically increased. Therefore, it is urgent to fully understand the toxic effects of Nano-CuO.

Metal nanoparticle-induced lung inflammation and injury have been reported before (Gosens et al. 2016; Mo et al. 2020b). In the present study, we explored the lung toxicity caused by Nano-CuO in mice. Bronchoalveolar lavage fluid (BALF) was harvested to evaluate Nano-CuO-induced lung inflammation and injury. The results demonstrated that Nano-CuO exposure (50 µg per mouse) led to severe acute lung injury and inflammation in mice, which was evidenced by excessive leukocytes and elevated cytokines, LDH, and total protein level in BALF. Neutrophil count, a sensitive parameter to detect particle-related lung injury, raised as early as day 1 after Nano-CuO exposure, peaked at day 3, and then declined. The number of Nano-CuO-induced macrophages increased at day 3 and reached the maximum at day 14 after exposure; even at days 28 and 42 after exposure, the macrophage count remained higher than that in the control group. The level of CXCL1/KC, a chemoattractant for neutrophils in mice, peaked at day 1 after

exposure, and declined from day 1 to day 7 after exposure. LDH and total protein have been used to define lung injury (Mo et al. 2019; Mo et al. 2020b). In the present study, Nano-CuO exposure significantly increased the activity of LDH and the level of total protein, which raised at day 1 after exposure, and reached the maximum levels at day 3. At days 28 and 42 post-exposure, their levels were still high than that in the control mice. These results suggest that Nano-CuO caused persistent inflammation following instillation of Nano-CuO.

Growing studies showed that MMPs, such as MMP-3, were engaged in inflammatory responses (Cobos-Correa et al. 2009; Gelzo et al. 2022; Nerusu et al. 2007; Schor et al. 2000; Sorokin 2010; Warner et al. 2001). For example, lipopolysaccharide-induced MMP-3 caused the increased infiltration of leukocytes into eye vitreous cavities in wild-type mouse, whereas the infiltration of leukocytes was significantly lower in MMP-3 KO mice (Van Hove et al. 2016). Similarly, in wild-type female mice, lipopolysaccharide induced severe mouse lung inflammation, reflected by increased neutrophil count, total protein level, and proinflammatory factors, such as TNF- α and IL-6; whereas the levels of these inflammatory parameters were significantly lower in MMP-3 KO female mice (Puntorieri et al. 2016). In the present study, Nano-CuO caused increased expression of MMP-3 in mouse lungs from day 1 to day 42 after exposure, thus, we further explored the role of MMP-3 in Nano-CuO-induced lung inflammation. Mice were intratracheally instilled with Nano-CuO (50 μ g/mouse) and 1 nmol per mouse of Ambion® *In Vivo* MMP-3 siRNA. At day 3 after exposure, the BALF was harvested. Our results showed that the inflammatory parameters described above

were significantly lower in MMP-3 siRNA-treated mice than those in the control mice, suggesting that MMP-3 played significant roles in Nano-CuO-induced lung inflammation and injury.

In lungs, the physical barrier constituted by airway epithelium provides an effective protection for lungs. The integrity of epithelial barrier depends on cell junctions, such as tight junctions and adherens junctions. Alteration of these junction-associated proteins would affect the integrity of epithelial barrier and further result in lung injury (Brune et al. 2015; Heijink et al. 2014; Ohta et al. 2012). Previous studies have reported that nanoparticle exposure could disrupt the expression of tight junction-associated proteins, such as ZO-1, claudin, and adherens protein E-cadherin in lung epithelial cells (Chen et al. 2020; Liu et al. 2020). In chapter II, my results have shown that Nano-CuO induced decreased expression of tight and adherens junction-associated proteins in human lung epithelial BEAS-2B cells. Therefore, in this chapter, we explored whether Nano-CuO exposure would cause the disruption of cell junction-associated proteins *in vivo*. The results showed that exposure to Nano-CuO resulted in the downregulation of tight junction-associated proteins ZO-1 and occludin, and adherens junction-associated protein E-cadherin in mouse lungs at day 3 after exposure. MMP-3 could degrade basement membrane and cleave extracellular cellular proteins, raising the possibility that MMP-3 may play a role in Nano-CuO-induced dysregulation of cell junctions in mouse lungs. Thus, we explored the role of MMP-3 in the regulation of cell junction-associated proteins caused by Nano-CuO in mouse lungs. Mice were intratracheally instilled with Nano-CuO (50

µg/mouse) and 1 nmol per mouse of Ambion® *In Vivo* MMP-3 siRNA and sacrificed at day 3 after exposure. Lung tissues were harvested and prepared for Western blot. The results showed that Nano-CuO-induced downregulation of tight and adherens junction-associated proteins was significantly inhibited by MMP-3 siRNA treatment in mouse lungs. These results suggest that MMP-3 plays important roles in the disruption of lung epithelial junctions, which may be further involved in Nano-CuO-induced pulmonary inflammation and injury.

Fibrosis is a pathological wound healing in which excessive accumulation of extracellular matrix components replaces normal parenchymal tissues (Mo et al. 2020b; Wynn 2004). Fibrosis is a complex process in which many factors are involved. Among them, MMP-3 has been shown to be involved in the development of pulmonary fibrosis (Ra and Parks 2007; Suhaimi et al. 2020; Yamashita et al. 2011; Yamashita et al. 2014; Ye et al. 1996). In lungs of patients with idiopathic pulmonary fibrosis (IPF), elevated MMP-3 level was observed and the level of MMP-3 was related to the severity of pulmonary fibrosis (McKeown et al. 2009; Yamashita et al. 2011). In animal models, adenoviral vector-mediated overexpression of MMP-3 resulted in the development of pulmonary fibrosis in rats, whereas mice lacking MMP-3 expression were protected from bleomycin-induced pulmonary fibrosis (Yamashita et al. 2011). In the current study, Nano-CuO exposure caused enhanced expression of MMP-3 and fibrosis in mouse lung tissues, thus, we further studied the role of MMP-3 in Nano-CuO-induced lung fibrosis. Mice were intratracheally instilled with Nano-CuO (50 µg/mouse) and 1 nmol per mouse of Ambion® *In Vivo* MMP-3 siRNA. The mice were repeatedly

administrated with MMP-3 siRNA at days 7, 14, and 21 through oral pharyngeal aspiration. At day 28 after Nano-CuO exposure, mice were sacrificed, and lungs were harvested. The trichrome staining results showed that Nano-CuO exposure caused the development of fibrosis in mouse lungs at day 28 after exposure, which was significantly attenuated by MMP-3 siRNA treatment. The results were further confirmed by measurement of hydroxyproline content and fibrosis-related proteins in mouse lungs. The increased hydroxyproline content caused by Nano-CuO exposure was significantly reduced by MMP-3 siRNA treatment. Furthermore, MMP-3 knockdown also significantly decreased the expression of fibrosis-related proteins in mouse lungs, such as α -SMA, Col1A1, and fibronectin. These results suggest that MMP-3 is involved in Nano-CuO-induced pulmonary fibrosis in mice.

Chronic inflammation or injury plays an important role in the development of lung fibrosis. In our previous studies, exposure to metal nanoparticles, such as nickel and cobalt nanoparticles, caused extensive chronic lung inflammation and injury, which was involved in the subsequent fibrosis (Mo et al. 2020b; Wan et al. 2017). In present study, Nano-CuO exposure also induced chronic inflammation in mouse lungs. We then explored the role of MMP-3 in Nano-CuO-induced chronic pulmonary injury. The results showed that MMP-3 knockdown significantly alleviated the chronic pulmonary inflammation caused by Nano-CuO, suggesting that MMP-3 plays a role in Nano-CuO-induced chronic lung injury, which may further promote the development of lung fibrosis.

Although MMP-3 promoting the development of pulmonary fibrosis was confirmed in this study, the detailed mechanisms of MMP-3-induced fibrosis still

need to be further investigated. Indeed, MMP-3 has shown multiple functions in the development of pulmonary fibrosis (Chulia-Peris et al. 2022). For example, our published study demonstrated that MMP-3 promoted the occurrence of epithelial-mesenchymal transition in human lung epithelial BEAS-2B cells (Zhang et al. 2021b), which plays a crucial role in the development of fibrosis (Rygiel et al. 2008; Zeisberg et al. 2007). Concretely, MMP-3 can cleave adherens junction-associated protein E-cadherin, which further activates the β -catenin pathway and induces epithelial-mesenchymal transition (Yamashita et al. 2011). In addition, MMP-3 could cleave kinds of extracellular matrix molecules into bioactive fragments, such as OPN, which further promotes migration and activation of proinflammatory cells and fibroblasts (Agnihotri et al. 2001; Sorokin 2010). Similarly, MMP-3 could cleave collagen XVIII, an epithelial basement membrane proteoglycan, and generate a biological active endostatin to inhibit the repair and proliferation and to increase the apoptosis of lung distal epithelial cells, which may contribute to the initiation of pulmonary fibrosis (Heljasvaara et al. 2005; Richter et al. 2009). Furthermore, it is also reported that MMP-3 can activate TGF- β 1 from its latent form (Chulia-Peris et al. 2022; Maeda et al. 2002). However, another study showed no difference in the active TGF- β 1 level in BALF between wild-type and MMP-3 KO mice after bleomycin administration (Yamashita et al. 2011). Therefore, further study is needed to fully understand the role of MMP-3 in the development of pulmonary fibrosis.

Taken together, this study showed that Nano-CuO exposure induced upregulation of MMP-3, lung inflammation, injury, and fibrosis in mice, and

knocking down of MMP-3 significantly alleviated Nano-CuO-induced lung inflammation, injury, and fibrosis. The results also showed that MMP-3 siRNA treatment significantly attenuated Nano-CuO-induced damage to lung epithelial barrier and chronic inflammation, which are considered important factors for fibrosis development. However, other mechanisms underlying Nano-CuO-caused pulmonary inflammation and fibrosis may present and need to be investigated in future.

CHAPTER V: SUMMARY AND CONCLUSION

Summary

In this study, we investigated Nano-CuO-induced pulmonary inflammation and fibrosis and explored the potential mechanisms involved in these effects, especially explored whether Nano-CuO exposure could cause dysregulation of MMP-3 and its roles in Nano-CuO-induced pulmonary inflammation and fibrosis.

We firstly determined the expression of MMP-3 in lung epithelial cells after Nano-CuO exposure. Exposure to Nano-CuO caused increased expression and activity of MMP-3 in BEAS-2B cells. To explore the potential signaling pathways that were involved in Nano-CuO-caused MMP-3 expression, the role of ROS and MAPKs pathway were examined *in vitro* after Nano-CuO exposure. Exposure of BEAS-2B cells to Nano-CuO caused a dose- and a time- dependent increase in ROS production, which was abolished by pretreatment of cells with ROS scavengers or inhibitors. Pretreatment of the cells with Mito-TEMPO, a specific mitochondrial ROS inhibitor, inhibited the CuO-induced ROS, suggesting that mitochondria was the potential source of Nano-CuO-induced ROS generation, which was further confirmed in BEAS-2B ρ^0 cells, which lack mitochondrial DNA and dysfunction in oxidative phosphorylation. In BEAS-2B ρ^0 cells, Nano-CuO-

induced ROS generation was significantly attenuated. Nano-CuO-induced ROS further activated MAPKs pathway, reflected by increased phosphorylation of p38, Erk1/2, and JNK. Pretreatment of cells with ROS inhibitor suppressed Nano-CuO-induced activation of MAPKs pathway, which was further confirmed in BEAS-2B ρ^0 cells. Pretreatment of cells with ROS inhibitors or scavengers, and MAPKs inhibitors significantly inhibited Nano-CuO-induced MMP-3 expression, indicating that increased MMP-3 expression and activity caused by Nano-CuO exposure was through Nano-CuO-caused oxidative stress and activation of MAPKs pathway. Then we explored the expression of cell junction-associated proteins after Nano-CuO exposure and the role of MMP-3 in this process. Nano-CuO exposure caused significant downregulation of cell junction-associated proteins, such as ZO-1, occludin, claudin-1, and E-cadherin. MMP-3 siRNA transfection significantly restored the reduced expression of ZO-1, occludin, claudin-1, and E-cadherin caused by Nano-CuO. These results demonstrated that exposure of human lung epithelial cells BEAS-2B to Nano-CuO caused MMP-3 upregulation, which further induced the disruption of tight and adherens junctions.

The role of MMP-3 in Nano-CuO-induced activation of MRC-5 fibroblasts was investigated in a triple co-culture system. Exposure to Nano-CuO caused increases in MMP-3 protein and activity and OPN expression in BEAS-2B and U937* cells, but not in MRC-5 cells. Nano-CuO also caused increased production of cleaved-OPN fragment. MMP-3 siRNA transfection was performed to explore the role of MMP-3 in Nano-CuO-induced increased cleaved-OPN. MMP-3 siRNA transfection in BEAS-2B and U937* cells significantly abolished the production of

cleaved-OPN. Conditioned media from Nano-CuO-exposed BEAS-2B, or U937*, or the co-culture of BEAS-2B and U937* were collected to culture MRC-5 fibroblasts. These conditioned media caused activation of unexposed MRC-5 fibroblasts, which were reflected by increased expression of α -SMA, Col1A1, and fibronectin. However, direct exposure to Nano-CuO did not activate MRC-5 fibroblasts. Then a triple co-culture system, consisting of human lung epithelial BEAS-2B cells, U937* macrophages, and MRC-5 fibroblasts, was established. Exposure of BEAS-2B and U937* cells to Nano-CuO caused activation of unexposed MRC-5 fibroblasts in the triple co-culture system. Transfection of MMP-3 siRNA in BEAS-2B and U937* cells significantly inhibited the activation of MRC-5 fibroblasts, suggesting that MMP-3 may play a key role in Nano-CuO-induced activation of MRC-5 fibroblasts. In addition, pretreatment of GRGDSP peptides, a peptide interrupting the binding of MMP-3-cleaved OPN to its receptors, attenuated the activation of MRC-5 fibroblasts, suggesting that MMP-3-cleaved OPN is involved in Nano-CuO-induced activation of MRC-5 fibroblasts in the triple co-culture system.

The role of MMP-3 in Nano-CuO-induced lung inflammation, injury, and fibrosis was further examined *in vivo*. In mice, Nano-CuO exposure induced persistent increase in MMP-3 expression from day 1 to day 42 post-exposure. Nano-CuO exposure significantly reduced the expression of tight junction-associated proteins, such as occludin and ZO-1, and adherens protein E-cadherin in mouse lungs. Nano-CuO exposure induced pulmonary inflammation, injury, and fibrosis in mice which were confirmed by elevated cellular and biochemical

constituents in BALF, and H&E and trichrome stainings. Knocking down MMP-3 inhibited Nano-CuO-induced downregulation of cell junction-associated proteins in mouse lungs. MMP-3 knockdown also ameliorated Nano-CuO-induced pulmonary inflammation, injury, and fibrosis in mice. These results suggesting that MMP-3 plays important roles in Nano-CuO-induced pulmonary inflammation, injury, and fibrosis in mice.

Conclusion

Overall, this dissertation work showed that exposure to Nano-CuO caused ROS generation which further led to MMP-3 production in lung epithelial cells and macrophages, which disrupted cell junction-associated proteins, initiating and promoting Nano-CuO-induced lung inflammation, injury, and fibrosis. This study highlighted the role of MMP-3 in Nano-CuO-induced lung epithelial junction disruption, and the subsequent inflammation and fibrosis. Nano-CuO-induced MMP-3 activation and lung inflammation and fibrosis can be related to the alterations in human lung diseases, such as IPF. Findings in this study could provide new therapeutic strategies to treat the patients with these lung diseases. Findings in this study could also provide insights into the interventions that prevent metal nanoparticle-induced lung injury and fibrosis. Finally, findings in this study also provided the scientific basis to establish the exposure limits of Nano-CuO or other metal oxide nanoparticles.

REFERENCES

- Agnihotri, R., H. C. Crawford, H. Haro, L. M. Matrisian, M. C. Havrda, and L. Liaw. 2001. "Osteopontin, a Novel Substrate for Matrix Metalloproteinase-3 (Stromelysin-1) and Matrix Metalloproteinase-7 (Matrilysin)." *J Biol Chem* 276: 28261-28267. doi:10.1074/jbc.M103608200.
- Akerlund, E., M. S. Islam, S. McCarrick, E. Alfaro-Moreno, and H. L. Karlsson. 2019. "Inflammation and (Secondary) Genotoxicity of Ni and NiO Nanoparticles." *Nanotoxicology* 13: 1060-1072. doi:10.1080/17435390.2019.1640908.
- Akhtar, M. J., S. Kumar, H. A. Alhadlaq, S. A. Alrokayan, K. M. Abu-Salah, and M. Ahamed. 2016. "Dose-Dependent Genotoxicity of Copper Oxide Nanoparticles Stimulated by Reactive Oxygen Species in Human Lung Epithelial Cells." *Toxicol Ind Health* 32: 809-821. doi:10.1177/0748233713511512.
- Apte, S. S., and W. C. Parks. 2015. "Metalloproteinases: A Parade of Functions in Matrix Biology and an Outlook for the Future." *Matrix Biol* 44-46: 1-6. doi:10.1016/j.matbio.2015.04.005.
- Armstrong, C. W., L. W. Moore, Jr., R. L. Hackler, G. B. Miller, Jr., and R. B. Stroube. 1983. "An Outbreak of Metal Fume Fever. Diagnostic Use of Urinary Copper and Zinc Determinations." *J Occup Med* 25: 886-888.
- Balkowiec, M., R. B. Maksym, and P. K. Wlodarski. 2018. "The Bimodal Role of Matrix Metalloproteinases and Their Inhibitors in Etiology and Pathogenesis of Endometriosis (Review)." *Mol Med Rep* 18: 3123-3136. doi:10.3892/mmr.2018.9303.
- Barosova, H., B. B. Karakocak, D. Septiadi, A. Petri-Fink, V. Stone, and B. Rothen-Rutishauser. 2020. "An in Vitro Lung System to Assess the Proinflammatory Hazard of Carbon Nanotube Aerosols." *Int J Mol Sci* 21. doi:10.3390/ijms21155335.
- Bassiouni, W., M. A. M. Ali, and R. Schulz. 2021. "Multifunctional Intracellular Matrix Metalloproteinases: Implications in Disease." *FEBS J* 288: 7162-7182. doi:10.1111/febs.15701.
- Berrier, A. L., and K. M. Yamada. 2007. "Cell-Matrix Adhesion." *J Cell Physiol* 213: 565-573. doi:10.1002/jcp.21237.
- Bhat, A. A., S. Uppada, I. W. Achkar, S. Hashem, S. K. Yadav, M. Shanmugakonar, H. A. Al-Naemi, M. Haris, and S. Uddin. 2018. "Tight Junction Proteins and Signaling Pathways in Cancer and Inflammation: A Functional Crosstalk." *Front Physiol* 9: 1942. doi:10.3389/fphys.2018.01942.
- Bhaumik, A., A. M. Shearin, R. Patel, and K. Ghosh. 2014. "Significant Enhancement of Optical Absorption through Nano-Structuring of Copper Based Oxide Semiconductors: Possible Future Materials for Solar Energy Applications." *Phys Chem Chem Phys* 16: 11054-11066. doi:10.1039/c4cp00827h.
- Blin, N., and D. W. Stafford. 1976. "A General Method for Isolation of High Molecular Weight DNA from Eukaryotes." *Nucleic Acids Res* 3: 2303-2308. doi:10.1093/nar/3.9.2303.

- Bonnans, C., J. Chou, and Z. Werb. 2014. "Remodelling the Extracellular Matrix in Development and Disease." *Nat Rev Mol Cell Biol* 15: 786-801. doi:10.1038/nrm3904.
- Bonner, J. C. 2010. "Mesenchymal Cell Survival in Airway and Interstitial Pulmonary Fibrosis." *Fibrogenesis Tissue Repair* 3: 15. doi:10.1186/1755-1536-3-15.
- Brew, K., D. Dinakarpandian, and H. Nagase. 2000. "Tissue Inhibitors of Metalloproteinases: Evolution, Structure and Function." *Biochim Biophys Acta* 1477: 267-283. doi:10.1016/s0167-4838(99)00279-4.
- Brune, K., J. Frank, A. Schwingshackl, J. Finigan, and V. K. Sidhaye. 2015. "Pulmonary Epithelial Barrier Function: Some New Players and Mechanisms." *Am J Physiol Lung Cell Mol Physiol* 308: L731-745. doi:10.1152/ajplung.00309.2014.
- Buckley, A., and J. R. Turner. 2018. "Cell Biology of Tight Junction Barrier Regulation and Mucosal Disease." *Cold Spring Harb Perspect Biol* 10. doi:10.1101/cshperspect.a029314.
- Burdo, T. H., M. R. Wood, and H. S. Fox. 2007. "Osteopontin Prevents Monocyte Recirculation and Apoptosis." *J Leukoc Biol* 81: 1504-1511. doi:10.1189/jlb.1106711.
- Cappellini, F., S. Di Bucchianico, V. Karri, S. Latvala, M. Malmlof, M. Kippler, K. Elihn, J. Hedberg, I. Odnevall Wallinder, P. Gerde, and H. L. Karlsson. 2020. "Dry Generation of Ceo2 Nanoparticles and Deposition onto a Co-Culture of A549 and Thp-1 Cells in Air-Liquid Interface-Dosimetry Considerations and Comparison to Submerged Exposure." *Nanomaterials (Basel)* 10. doi:10.3390/nano10040618.
- Carlier, F. M., C. de Fays, and C. Pilette. 2021. "Epithelial Barrier Dysfunction in Chronic Respiratory Diseases." *Front Physiol* 12: 691227. doi:10.3389/fphys.2021.691227.
- Chang, C., and Z. Werb. 2001. "The Many Faces of Metalloproteases: Cell Growth, Invasion, Angiogenesis and Metastasis." *Trends Cell Biol* 11: S37-43. doi:10.1016/s0962-8924(01)02122-5.
- Chen, C. M., M. L. Wu, Y. C. Ho, P. Y. Gung, M. H. Tsai, A. N. Orekhov, I. A. Sobenin, P. Lin, and S. F. Yet. 2020. "Exposure to Zinc Oxide Nanoparticles Disrupts Endothelial Tight and Adherens Junctions and Induces Pulmonary Inflammatory Cell Infiltration." *Int J Mol Sci* 21. doi:10.3390/ijms21103437.
- Chen, I. C., I. L. Hsiao, H. C. Lin, C. H. Wu, C. Y. Chuang, and Y. J. Huang. 2016. "Influence of Silver and Titanium Dioxide Nanoparticles on in Vitro Blood-Brain Barrier Permeability." *Environ Toxicol Pharmacol* 47: 108-118. doi:10.1016/j.etap.2016.09.009.
- Cho, W. S., R. Duffin, C. A. Poland, S. E. Howie, W. MacNee, M. Bradley, I. L. Megson, and K. Donaldson. 2010. "Metal Oxide Nanoparticles Induce Unique Inflammatory Footprints in the Lung: Important Implications for Nanoparticle Testing." *Environ Health Perspect* 118: 1699-1706. doi:10.1289/ehp.1002201.
- Cho, W. S., R. Duffin, C. A. Poland, A. Duschl, G. J. Oostingh, W. Macnee, M. Bradley, I. L. Megson, and K. Donaldson. 2012. "Differential Pro-Inflammatory Effects of Metal Oxide Nanoparticles and Their Soluble Ions in Vitro and in Vivo; Zinc and Copper Nanoparticles, but Not Their Ions, Recruit Eosinophils to the Lungs." *Nanotoxicology* 6: 22-35. doi:10.3109/17435390.2011.552810.
- Christensen, B., L. Schack, E. Klaning, and E. S. Sorensen. 2010. "Osteopontin Is Cleaved at Multiple Sites Close to Its Integrin-Binding Motifs in Milk and Is a Novel Substrate for Plasmin and Cathepsin D." *J Biol Chem* 285: 7929-7937. doi:10.1074/jbc.M109.075010.
- Christensen, B., and E. S. Sorensen. 2014. "Osteopontin Is Highly Susceptible to Cleavage in Bovine Milk and the Proteolytic Fragments Bind the Alpha(v)beta(3)-Integrin Receptor." *J Dairy Sci* 97: 136-146. doi:10.3168/jds.2013-7223.

- Chulia-Peris, L., C. Carreres-Rey, M. Gabasa, J. Alcaraz, J. Carretero, and J. Pereda. 2022. "Matrix Metalloproteinases and Their Inhibitors in Pulmonary Fibrosis: Emmprin/Cd147 Comes into Play." *Int J Mol Sci* 23. doi:10.3390/ijms23136894.
- Cobos-Correa, A., J. B. Trojanek, S. Diemer, M. A. Mall, and C. Schultz. 2009. "Membrane-Bound FRET Probe Visualizes Mmp12 Activity in Pulmonary Inflammation." *Nat Chem Biol* 5: 628-630. doi:10.1038/nchembio.196.
- Costa, P. M., I. Gosens, A. Williams, L. Farcas, D. Pantano, D. M. Brown, V. Stone, F. R. Cassee, S. Halappanavar, and B. Fadeel. 2018. "Transcriptional Profiling Reveals Gene Expression Changes Associated with Inflammation and Cell Proliferation Following Short-Term Inhalation Exposure to Copper Oxide Nanoparticles." *J Appl Toxicol* 38: 385-397. doi:10.1002/jat.3548.
- Craig, V. J., L. Zhang, J. S. Hagood, and C. A. Owen. 2015. "Matrix Metalloproteinases as Therapeutic Targets for Idiopathic Pulmonary Fibrosis." *Am J Respir Cell Mol Biol* 53: 585-600. doi:10.1165/rcmb.2015-0020TR.
- Crapo, J. D., B. E. Barry, P. Gehr, M. Bachofen, and E. R. Weibel. 1982. "Cell Number and Cell Characteristics of the Normal Human Lung." *Am Rev Respir Dis* 126: 332-337. doi:10.1164/arrd.1982.126.2.332.
- Crawford, H. C., L. M. Matrisian, and L. Liaw. 1998. "Distinct Roles of Osteopontin in Host Defense Activity and Tumor Survival During Squamous Cell Carcinoma Progression in Vivo." *Cancer Res* 58: 5206-5215.
- Cui, N., M. Hu, and R. A. Khalil. 2017. "Biochemical and Biological Attributes of Matrix Metalloproteinases." *Prog Mol Biol Transl Sci* 147: 1-73. doi:10.1016/bs.pmbts.2017.02.005.
- Darby, I. A., and T. D. Hewitson. 2007. "Fibroblast Differentiation in Wound Healing and Fibrosis." *Int Rev Cytol* 257: 143-179. doi:10.1016/S0074-7696(07)57004-X.
- Denhardt, D. T., M. Noda, A. W. O'Regan, D. Pavlin, and J. S. Berman. 2001. "Osteopontin as a Means to Cope with Environmental Insults: Regulation of Inflammation, Tissue Remodeling, and Cell Survival." *J Clin Invest* 107: 1055-1061. doi:10.1172/JCI12980.
- Dong, J., and Q. Ma. 2015. "Advances in Mechanisms and Signaling Pathways of Carbon Nanotube Toxicity." *Nanotoxicology* 9: 658-676. doi:10.3109/17435390.2015.1009187.
- Dong, J., and Q. Ma. 2016. "Myofibroblasts and Lung Fibrosis Induced by Carbon Nanotube Exposure." *Part Fibre Toxicol* 13: 60. doi:10.1186/s12989-016-0172-2.
- Dong, J., and Q. Ma. 2017. "Osteopontin Enhances Multi-Walled Carbon Nanotube-Triggered Lung Fibrosis by Promoting Tgf-Beta1 Activation and Myofibroblast Differentiation." *Part Fibre Toxicol* 14: 18. doi:10.1186/s12989-017-0198-0.
- Evans, P., H. Matsunaga, and M. Kiguchi. 2008. "Large-Scale Application of Nanotechnology for Wood Protection." *Nat Nanotechnol* 3: 577. doi:10.1038/nnano.2008.286.
- Fahmy, B., and S. A. Cormier. 2009. "Copper Oxide Nanoparticles Induce Oxidative Stress and Cytotoxicity in Airway Epithelial Cells." *Toxicol In Vitro* 23: 1365-1371. doi:10.1016/j.tiv.2009.08.005.
- Fernandez-Moreno, M., T. Hermida-Gomez, M. E. Gallardo, A. Dalmao-Fernandez, I. Rego-Perez, R. Garesse, and F. J. Blanco. 2016. "Generating Rho-0 Cells Using Mesenchymal Stem Cell Lines." *PLoS One* 11: e0164199. doi:10.1371/journal.pone.0164199.
- Ferrero-Miliani, L., O. H. Nielsen, P. S. Andersen, and S. E. Girardin. 2007. "Chronic Inflammation: Importance of Nod2 and Nalp3 in Interleukin-1beta Generation." *Clin Exp Immunol* 147: 227-235. doi:10.1111/j.1365-2249.2006.03261.x.
- Fingleton, B. 2017. "Matrix Metalloproteinases as Regulators of Inflammatory Processes." *Biochim Biophys Acta Mol Cell Res* 1864: 2036-2042. doi:10.1016/j.bbamcr.2017.05.010.

- François Carlier, C. P. 2022. "The Memory of Airway Epithelium Damage in Smokers and Copd Patients." *European Respiratory Society* 8.
- Fujita, K., M. Fukuda, H. Fukui, M. Horie, S. Endoh, K. Uchida, M. Shichiri, Y. Morimoto, A. Ogami, and H. Iwahashi. 2015. "Intratracheal Instillation of Single-Wall Carbon Nanotubes in the Rat Lung Induces Time-Dependent Changes in Gene Expression." *Nanotoxicology* 9: 290-301. doi:10.3109/17435390.2014.921737.
- Future Markets Inc. . 2015. "The Global Market for Copper Oxide Nanoparticles, 2010-2025." Available online: <https://www.futuremarketsinc.com/>. doi:<http://www.futuremarketsinc.com/global-market-copper-oxide-nanoparticles-2010-2025>.
- Garcia-de-Alba, C., C. Becerril, V. Ruiz, Y. Gonzalez, S. Reyes, J. Garcia-Alvarez, M. Selman, and A. Pardo. 2010. "Expression of Matrix Metalloproteases by Fibrocytes: Possible Role in Migration and Homing." *Am J Respir Crit Care Med* 182: 1144-1152. doi:10.1164/rccm.201001-0028OC.
- Gelzo, M., S. Cacciapuoti, B. Pinchera, A. De Rosa, G. Cerneria, F. Scialo, M. Comegna, M. Mormile, G. Fabbrocini, R. Parrella, G. Corso, I. Gentile, and G. Castaldo. 2022. "Matrix Metalloproteinases (Mmp) 3 and 9 as Biomarkers of Severity in Covid-19 Patients." *Sci Rep* 12: 1212. doi:10.1038/s41598-021-04677-8.
- Giannandrea, M., and W. C. Parks. 2014. "Diverse Functions of Matrix Metalloproteinases During Fibrosis." *Dis Model Mech* 7: 193-203. doi:10.1242/dmm.012062.
- Gomez, D. E., D. F. Alonso, H. Yoshiji, and U. P. Thorgeirsson. 1997. "Tissue Inhibitors of Metalloproteinases: Structure, Regulation and Biological Functions." *Eur J Cell Biol* 74: 111-122.
- Gomis-Ruth, F. X., K. Maskos, M. Betz, A. Bergner, R. Huber, K. Suzuki, N. Yoshida, H. Nagase, K. Brew, G. P. Bourenkov, H. Bartunik, and W. Bode. 1997. "Mechanism of Inhibition of the Human Matrix Metalloproteinase Stromelysin-1 by Timp-1." *Nature* 389: 77-81. doi:10.1038/37995.
- Gosens, I., F. R. Cassee, M. Zanella, L. Manodori, A. Brunelli, A. L. Costa, B. G. Bokkers, W. H. de Jong, D. Brown, D. Hristozov, and V. Stone. 2016. "Organ Burden and Pulmonary Toxicity of Nano-Sized Copper (II) Oxide Particles after Short-Term Inhalation Exposure." *Nanotoxicology* 10: 1084-1095. doi:10.3109/17435390.2016.1172678.
- Gross, J., and C. M. Lapiere. 1962. "Collagenolytic Activity in Amphibian Tissues: A Tissue Culture Assay." *Proc Natl Acad Sci U S A* 48: 1014-1022. doi:10.1073/pnas.48.6.1014.
- Guo, R., H. Sakamoto, S. Sugiura, and M. Ogawa. 2007. "Endothelial Cell Motility Is Compatible with Junctional Integrity." *J Cell Physiol* 211: 327-335. doi:10.1002/jcp.20937.
- Hashiguchi, K., and Q. M. Zhang-Akiyama. 2009. "Establishment of Human Cell Lines Lacking Mitochondrial DNA." *Methods Mol Biol* 554: 383-391. doi:10.1007/978-1-59745-521-3_23.
- Hatipoglu, O. F., E. Uctepe, G. Opoku, H. Wake, K. Ikemura, T. Ohtsuki, J. Inagaki, M. Gunduz, E. Gunduz, S. Watanabe, T. Nishinaka, H. Takahashi, and S. Hirohata. 2021. "Osteopontin Silencing Attenuates Bleomycin-Induced Murine Pulmonary Fibrosis by Regulating Epithelial-Mesenchymal Transition." *Biomed Pharmacother* 139: 111633. doi:10.1016/j.biopha.2021.111633.
- He, H., Z. Zou, B. Wang, G. Xu, C. Chen, X. Qin, C. Yu, and J. Zhang. 2020. "Copper Oxide Nanoparticles Induce Oxidative DNA Damage and Cell Death Via Copper Ion-Mediated P38 Mapk Activation in Vascular Endothelial Cells." *Int J Nanomedicine* 15: 3291-3302. doi:10.2147/IJN.S241157.

- Heijink, I. H., J. A. Noordhoek, W. Timens, A. J. van Oosterhout, and D. S. Postma. 2014. "Abnormalities in Airway Epithelial Junction Formation in Chronic Obstructive Pulmonary Disease." *Am J Respir Crit Care Med* 189: 1439-1442. doi:10.1164/rccm.201311-1982LE.
- Heljasvaara, R., P. Nyberg, J. Luostarinen, M. Parikka, P. Heikkilä, M. Rehn, T. Sorsa, T. Salo, and T. Pihlajaniemi. 2005. "Generation of Biologically Active Endostatin Fragments from Human Collagen XVIII by Distinct Matrix Metalloproteases." *Exp Cell Res* 307: 292-304. doi:10.1016/j.yexcr.2005.03.021.
- Helluin, O., C. Chan, G. Vilaire, S. Mousa, W. F. DeGrado, and J. S. Bennett. 2000. "The Activation State of Alpha_vBeta₃ Regulates Platelet and Lymphocyte Adhesion to Intact and Thrombin-Cleaved Osteopontin." *J Biol Chem* 275: 18337-18343. doi:10.1074/jbc.M001529200.
- Henry, M. T., K. McMahon, A. J. Mackarel, K. Prikk, T. Sorsa, P. Maisi, R. Sepper, M. X. Fitzgerald, and C. M. O'Connor. 2002. "Matrix Metalloproteinases and Tissue Inhibitor of Metalloproteinase-1 in Sarcoidosis and Ipf." *Eur Respir J* 20: 1220-1227. doi:10.1183/09031936.02.00022302.
- Herrera, I., J. Cisneros, M. Maldonado, R. Ramirez, B. Ortiz-Quintero, E. Anso, N. S. Chandel, M. Selman, and A. Pardo. 2013. "Matrix Metalloproteinase (Mmp)-1 Induces Lung Alveolar Epithelial Cell Migration and Proliferation, Protects from Apoptosis, and Represses Mitochondrial Oxygen Consumption." *J Biol Chem* 288: 25964-25975. doi:10.1074/jbc.M113.459784.
- Horie, M., K. Shimizu, and Y. Tabei. 2018. "Validation of Metallothionein, Interleukin-8, and Heme Oxygenase-1 as Markers for the Evaluation of Cytotoxicity Caused by Metal Oxide Nanoparticles." *Toxicol Mech Methods* 28: 630-638. doi:10.1080/15376516.2018.1486931.
- Hu, G., and J. W. Christman. 2019. "Editorial: Alveolar Macrophages in Lung Inflammation and Resolution." *Front Immunol* 10: 2275. doi:10.3389/fimmu.2019.02275.
- Hussain, S., S. Sangtian, S. M. Anderson, R. J. Snyder, J. D. Marshburn, A. B. Rice, J. C. Bonner, and S. Garantziotis. 2014. "Inflammasome Activation in Airway Epithelial Cells after Multi-Walled Carbon Nanotube Exposure Mediates a Profibrotic Response in Lung Fibroblasts." *Part Fibre Toxicol* 11: 28. doi:10.1186/1743-8977-11-28.
- Hynes, R. 2009. "The Extracellular Matrix: Not Just Pretty Fibrils." *Science* 326: 1216-1219. doi:10.1126/science.1176009.
- Hynes, R. O. 2002. "Integrins: Bidirectional, Allosteric Signaling Machines." *Cell* 110: 673-687. doi:10.1016/s0092-8674(02)00971-6.
- Ilves, M., P. A. S. Kinaret, J. Ndika, P. Karisola, V. Marwah, V. Fortino, Y. Fedutik, M. Correia, N. Ehrlich, K. Loeschner, A. Besinis, J. Vassallo, R. D. Handy, H. Wolff, K. Savolainen, D. Greco, and H. Alenius. 2019. "Surface Pegylation Suppresses Pulmonary Effects of CuO in Allergen-Induced Lung Inflammation." *Part Fibre Toxicol* 16: 28. doi:10.1186/s12989-019-0309-1.
- Jablonska-Trypuc, A., M. Matejczyk, and S. Rosochacki. 2016. "Matrix Metalloproteinases (Mmps), the Main Extracellular Matrix (Ecm) Enzymes in Collagen Degradation, as a Target for Anticancer Drugs." *J Enzyme Inhib Med Chem* 31: 177-183. doi:10.3109/14756366.2016.1161620.
- Jantzen, K., M. Roursgaard, C. Desler, S. Loft, L. J. Rasmussen, and P. Moller. 2012. "Oxidative Damage to DNA by Diesel Exhaust Particle Exposure in Co-Cultures of Human Lung Epithelial Cells and Macrophages." *Mutagenesis* 27: 693-701. doi:10.1093/mutage/ges035.

- Jing, X., J. H. Park, T. M. Peters, and P. S. Thorne. 2015. "Toxicity of Copper Oxide Nanoparticles in Lung Epithelial Cells Exposed at the Air-Liquid Interface Compared with in Vivo Assessment." *Toxicol In Vitro* 29: 502-511. doi:10.1016/j.tiv.2014.12.023.
- Juganson, K., A. Ivask, I. Blinova, M. Mortimer, and A. Kahru. 2015. "Nanoe-Tox: New and in-Depth Database Concerning Ecotoxicity of Nanomaterials." *Beilstein J Nanotechnol* 6: 1788-1804. doi:10.3762/bjnano.6.183.
- Kabadi, P. K., A. L. Rodd, A. E. Simmons, N. J. Messier, R. H. Hurt, and A. B. Kane. 2019. "A Novel Human 3d Lung Microtissue Model for Nanoparticle-Induced Cell-Matrix Alterations." *Part Fibre Toxicol* 16: 15. doi:10.1186/s12989-019-0298-0.
- Karlsson, H. L., P. Cronholm, J. Gustafsson, and L. Moller. 2008. "Copper Oxide Nanoparticles Are Highly Toxic: A Comparison between Metal Oxide Nanoparticles and Carbon Nanotubes." *Chem Res Toxicol* 21: 1726-1732. doi:10.1021/tx800064j.
- Karlsson, H. L., J. Gustafsson, P. Cronholm, and L. Moller. 2009. "Size-Dependent Toxicity of Metal Oxide Particles--a Comparison between Nano- and Micrometer Size." *Toxicol Lett* 188: 112-118. doi:10.1016/j.toxlet.2009.03.014.
- Kasper, J., M. I. Hermanns, C. Bantz, M. Maskos, R. Stauber, C. Pohl, R. E. Unger, and J. C. Kirkpatrick. 2011. "Inflammatory and Cytotoxic Responses of an Alveolar-Capillary Coculture Model to Silica Nanoparticles: Comparison with Conventional Monocultures." *Part Fibre Toxicol* 8: 6. doi:10.1186/1743-8977-8-6.
- Keller, U., A. Prudova, U. Eckhard, B. Fingleton, and C. M. Overall. 2013. "Systems-Level Analysis of Proteolytic Events in Increased Vascular Permeability and Complement Activation in Skin Inflammation." *Sci Signal* 6: rs2. doi:10.1126/scisignal.2003512.
- Kennon, A. M., and J. A. Stewart, Jr. 2021. "Rage Differentially Altered in Vitro Responses in Vascular Smooth Muscle Cells and Adventitial Fibroblasts in Diabetes-Induced Vascular Calcification." *Front Physiol* 12: 676727. doi:10.3389/fphys.2021.676727.
- Khaliullin, T. O., E. R. Kisin, A. R. Murray, N. Yanamala, M. R. Shurin, D. W. Gutkin, L. M. Fatkhutdinova, V. E. Kagan, and A. A. Shvedova. 2017. "Mediation of the Single-Walled Carbon Nanotubes Induced Pulmonary Fibrogenic Response by Osteopontin and Tgf-Beta1." *Exp Lung Res* 43: 311-326. doi:10.1080/01902148.2017.1377783.
- Klein, S. G., J. Hennen, T. Serchi, B. Blomeke, and A. C. Gutleb. 2011. "Potential of Coculture in Vitro Models to Study Inflammatory and Sensitizing Effects of Particles on the Lung." *Toxicol In Vitro* 25: 1516-1534. doi:10.1016/j.tiv.2011.09.006.
- Ko, J. W., N. R. Shin, J. W. Park, S. H. Park, I. C. Lee, J. S. Kim, J. C. Kim, K. S. Ahn, and I. S. Shin. 2018. "Copper Oxide Nanoparticles Induce Collagen Deposition Via Tgf-Beta1/Smad3 Signaling in Human Airway Epithelial Cells." *Nanotoxicology* 12: 239-250. doi:10.1080/17435390.2018.1432778.
- Kon, S., Y. Nakayama, N. Matsumoto, K. Ito, M. Kanayama, C. Kimura, H. Kouro, D. Ashitomi, T. Matsuda, and T. Uede. 2014. "A Novel Cryptic Binding Motif, Lrskrsfsqvsdeqy, in the C-Terminal Fragment of Mmp-3/7-Cleaved Osteopontin as a Novel Ligand for Alpha9beta1 Integrin Is Involved in the Anti-Type Ii Collagen Antibody-Induced Arthritis." *PLoS One* 9: e116210. doi:10.1371/journal.pone.0116210.
- Kulkarni, T., J. de Andrade, Y. Zhou, T. Luckhardt, and V. J. Thannickal. 2016. "Alveolar Epithelial Disintegrality in Pulmonary Fibrosis." *Am J Physiol Lung Cell Mol Physiol* 311: L185-191. doi:10.1152/ajplung.00115.2016.
- Lai, X., H. Zhao, Y. Zhang, K. Guo, Y. Xu, S. Chen, and J. Zhang. 2018. "Intranasal Delivery of Copper Oxide Nanoparticles Induces Pulmonary Toxicity and Fibrosis in C57bl/6 Mice." *Sci Rep* 8: 4499. doi:10.1038/s41598-018-22556-7.

- Lakatos, H. F., H. A. Burgess, T. H. Thatcher, M. R. Redonnet, E. Hernady, J. P. Williams, and P. J. Sime. 2006. "Oropharyngeal Aspiration of a Silica Suspension Produces a Superior Model of Silicosis in the Mouse When Compared to Intratracheal Instillation." *Exp Lung Res* 32: 181-199. doi:10.1080/01902140600817465.
- Lappi-Blanco, E., S. T. Lehtonen, R. Sormunen, H. M. Merikallio, Y. Soini, and R. L. Kaarteenaho. 2013. "Divergence of Tight and Adherens Junction Factors in Alveolar Epithelium in Pulmonary Fibrosis." *Hum Pathol* 44: 895-907. doi:10.1016/j.humpath.2012.08.016.
- Laronha, H., and J. Caldeira. 2020. "Structure and Function of Human Matrix Metalloproteinases." *Cells* 9. doi:10.3390/cells9051076.
- Leckband, D., and A. Prakasam. 2006. "Mechanism and Dynamics of Cadherin Adhesion." *Annu Rev Biomed Eng* 8: 259-287. doi:10.1146/annurev.bioeng.8.061505.095753.
- Lee, J. Y., H. Y. Choi, H. J. Ahn, B. G. Ju, and T. Y. Yune. 2014. "Matrix Metalloproteinase-3 Promotes Early Blood-Spinal Cord Barrier Disruption and Hemorrhage and Impairs Long-Term Neurological Recovery after Spinal Cord Injury." *Am J Pathol* 184: 2985-3000. doi:10.1016/j.ajpath.2014.07.016.
- Leitner, L., K. Schuch, A. Jurets, B. K. Itariu, M. Keck, V. Grablowitz, O. C. Aszmann, G. Prager, G. Staffler, M. Zeyda, and T. M. Stulnig. 2015. "Immunological Blockade of Adipocyte Inflammation Caused by Increased Matrix Metalloproteinase-Cleaved Osteopontin in Obesity." *Obesity (Silver Spring)* 23: 779-785. doi:10.1002/oby.21024.
- Li, N., L. Wang, F. Shi, P. Yang, K. Sun, J. Zhang, X. Yang, X. Li, F. Shen, H. Liu, Y. Jin, and S. Yao. 2021. "Silica Nanoparticle Induces Pulmonary Fibroblast Transdifferentiation Via Macrophage Route: Potential Mechanism Revealed by Proteomic Analysis." *Toxicol In Vitro* 76: 105220. doi:10.1016/j.tiv.2021.105220.
- Lin, Y. H., C. J. Huang, J. R. Chao, S. T. Chen, S. F. Lee, J. J. Yen, and H. F. Yang-Yen. 2000. "Coupling of Osteopontin and Its Cell Surface Receptor Cd44 to the Cell Survival Response Elicited by Interleukin-3 or Granulocyte-Macrophage Colony-Stimulating Factor." *Mol Cell Biol* 20: 2734-2742. doi:10.1128/MCB.20.8.2734-2742.2000.
- Lin, Y. H., and H. F. Yang-Yen. 2001. "The Osteopontin-Cd44 Survival Signal Involves Activation of the Phosphatidylinositol 3-Kinase/Akt Signaling Pathway." *J Biol Chem* 276: 46024-46030. doi:10.1074/jbc.M105132200.
- Lindsey, M. L., F. A. Zouein, Y. Tian, R. Padmanabhan Iyer, and L. E. de Castro Bras. 2015. "Osteopontin Is Proteolytically Processed by Matrix Metalloproteinase 9." *Can J Physiol Pharmacol* 93: 879-886. doi:10.1139/cjpp-2015-0019.
- Liu, Y., H. Wei, J. Tang, J. Yuan, M. Wu, C. Yao, K. Hosoi, S. Yu, X. Zhao, Y. Han, and G. Chen. 2020. "Dysfunction of Pulmonary Epithelial Tight Junction Induced by Silicon Dioxide Nanoparticles Via the Ros/Erk Pathway and Protein Degradation." *Chemosphere* 255: 126954. doi:10.1016/j.chemosphere.2020.126954.
- Livak, K. J., and T. D. Schmittgen. 2001. "Analysis of Relative Gene Expression Data Using Real-Time Quantitative Pcr and the 2(-Delta Delta C(T)) Method." *Methods* 25: 402-408. doi:10.1006/meth.2001.1262.
- Long, G., Y. Mo, Q. Zhang, and M. Jiang. 2019. "Analysis of Nanomaterial Toxicity by Western Blot." *Methods Mol Biol* 1894: 161-169. doi:10.1007/978-1-4939-8916-4_10.
- Longano, D., N. Ditaranto, N. Cioffi, F. Di Niso, T. Sibillano, A. Ancona, A. Conte, M. A. Del Nobile, L. Sabbatini, and L. Torsi. 2012. "Analytical Characterization of Laser-Generated Copper Nanoparticles for Antibacterial Composite Food Packaging." *Anal Bioanal Chem* 403: 1179-1186. doi:10.1007/s00216-011-5689-5.
- Loret, T., E. Peyret, M. Dubreuil, O. Aguerre-Chariol, C. Bressot, O. le Bihan, T. Amodeo, B. Trouiller, A. Braun, C. Egles, and G. Lacroix. 2016. "Air-Liquid Interface Exposure to

- Aerosols of Poorly Soluble Nanomaterials Induces Different Biological Activation Levels Compared to Exposure to Suspensions." *Part Fibre Toxicol* 13: 58. doi:10.1186/s12989-016-0171-3.
- Luo, C., Y. Li, L. Yang, Y. Zheng, J. Long, J. Jia, S. Xiao, and J. Liu. 2014. "Activation of Erk and P53 Regulates Copper Oxide Nanoparticle-Induced Cytotoxicity in Keratinocytes and Fibroblasts." *Int J Nanomedicine* 9: 4763-4772. doi:10.2147/IJN.S67688.
- Maeda, S., D. D. Dean, R. Gomez, Z. Schwartz, and B. D. Boyan. 2002. "The First Stage of Transforming Growth Factor Beta1 Activation Is Release of the Large Latent Complex from the Extracellular Matrix of Growth Plate Chondrocytes by Matrix Vesicle Stromelysin-1 (Mmp-3)." *Calcif Tissue Int* 70: 54-65. doi:10.1007/s002230010032.
- Mangum, J., E. Bermudez, M. Sar, and J. Everitt. 2004. "Osteopontin Expression in Particle-Induced Lung Disease." *Exp Lung Res* 30: 585-598. doi:10.1080/01902140490476346.
- Mangum, J. B., E. A. Turpin, A. Antao-Menezes, M. F. Cesta, E. Bermudez, and J. C. Bonner. 2006. "Single-Walled Carbon Nanotube (Swcnt)-Induced Interstitial Fibrosis in the Lungs of Rats Is Associated with Increased Levels of Pdgf Mrna and the Formation of Unique Intercellular Carbon Structures That Bridge Alveolar Macrophages in Situ." *Part Fibre Toxicol* 3: 15. doi:10.1186/1743-8977-3-15.
- Manke, A., L. Wang, and Y. Rojanasakul. 2013. "Mechanisms of Nanoparticle-Induced Oxidative Stress and Toxicity." *Biomed Res Int* 2013: 942916. doi:10.1155/2013/942916.
- Maqsood, A., A. Hisham, K. Ponmurugan, and A. Naif. 2014. "Synthesis, Characterization, and Antimicrobial Activity of Copper Oxide Nanoparticles." *Journal of Nanomaterials*, 10.1155/2014/637858. doi:10.1155/2014/637858.
- McKeown, S., A. G. Richter, C. O'Kane, D. F. McAuley, and D. R. Thickett. 2009. "Mmp Expression and Abnormal Lung Permeability Are Important Determinants of Outcome in Ipf." *Eur Respir J* 33: 77-84. doi:10.1183/09031936.00060708.
- Michael J. Derelanko, M. A. H. (2001). Fundamental Inhalation Toxicology. In: M. A. H. Michael J. Derelanko ed. Handbook of Toxicology. Boca Raton: CRC Press, 67.
- Mittal, R., A. P. Patel, L. H. Debs, D. Nguyen, K. Patel, M. Grati, J. Mittal, D. Yan, P. Chapagain, and X. Z. Liu. 2016. "Intricate Functions of Matrix Metalloproteinases in Physiological and Pathological Conditions." *J Cell Physiol* 231: 2599-2621. doi:10.1002/jcp.25430.
- Mo, Y., R. Wan, S. Chien, D. J. Tollerud, and Q. Zhang. 2009a. "Activation of Endothelial Cells after Exposure to Ambient Ultrafine Particles: The Role of NADPH Oxidase." *Toxicol Appl Pharmacol* 236: 183-193. doi:10.1016/j.taap.2009.01.017.
- Mo, Y., R. Wan, J. Wang, S. Chien, D. J. Tollerud, and Q. Zhang. 2009b. "Diabetes Is Associated with Increased Sensitivity of Alveolar Macrophages to Urban Particulate Matter Exposure." *Toxicology* 262: 130-137. doi:10.1016/j.tox.2009.05.019.
- Mo, Y., R. Wan, and Q. Zhang. 2012. "Application of Reverse Transcription-Pcr and Real-Time Pcr in Nanotoxicity Research." *Methods Mol Biol* 926: 99-112. doi:10.1007/978-1-62703-002-1_7.
- Mo, Y., J. Chen, D. M. Humphrey, Jr., R. A. Fodah, J. M. Warawa, and G. W. Hoyle. 2015. "Abnormal Epithelial Structure and Chronic Lung Inflammation after Repair of Chlorine-Induced Airway Injury." *Am J Physiol Lung Cell Mol Physiol* 308: L168-178. doi:10.1152/ajplung.00226.2014.
- Mo, Y., M. Jiang, Y. Zhang, R. Wan, J. Li, C. J. Zhong, H. Li, S. Tang, and Q. Zhang. 2019. "Comparative Mouse Lung Injury by Nickel Nanoparticles with Differential Surface Modification." *J Nanobiotechnology* 17: 2. doi:10.1186/s12951-018-0436-0.

- Mo, Y., Y. Zhang, L. Mo, R. Wan, M. Jiang, and Q. Zhang. 2020a. "The Role of Mir-21 in Nickel Nanoparticle-Induced Mmp-2 and Mmp-9 Production in Mouse Primary Monocytes: In Vitro and in Vivo Studies." *Environ Pollut* 267: 115597. doi:10.1016/j.envpol.2020.115597.
- Mo, Y., Y. Zhang, R. Wan, M. Jiang, Y. Xu, and Q. Zhang. 2020b. "Mir-21 Mediates Nickel Nanoparticle-Induced Pulmonary Injury and Fibrosis." *Nanotoxicology* 14: 1175-1197. doi:10.1080/17435390.2020.1808727.
- Mo, Y., Y. Zhang, Y. Zhang, J. Yuan, L. Mo, and Q. Zhang. 2021. "Nickel Nanoparticle-Induced Cell Transformation: Involvement of DNA Damage and DNA Repair Defect through Hif-1alpha/Mir-210/Rad52 Pathway." *J Nanobiotechnology* 19: 370. doi:10.1186/s12951-021-01117-7.
- Mori, R., T. J. Shaw, and P. Martin. 2008. "Molecular Mechanisms Linking Wound Inflammation and Fibrosis: Knockdown of Osteopontin Leads to Rapid Repair and Reduced Scarring." *J Exp Med* 205: 43-51. doi:10.1084/jem.20071412.
- Msebawi, M. S., Z. Leman, S. Shamsudin, S. M. Tahir, C. N. Aiza Jaafar, A. H. M. Ariff, N. I. Zahari, and A. Abdellatif. 2021. "Production of Aluminum Aa6061 Hybrid Nanocomposite from Waste Metal Using Hot Extrusion Process: Strength Performance and Prediction by Rsm and Random Forest." *Materials (Basel)* 14. doi:10.3390/ma14206102.
- Muller, L., M. Riediker, P. Wick, M. Mohr, P. Gehr, and B. Rothen-Rutishauser. 2010. "Oxidative Stress and Inflammation Response after Nanoparticle Exposure: Differences between Human Lung Cell Monocultures and an Advanced Three-Dimensional Model of the Human Epithelial Airways." *J R Soc Interface* 7 Suppl 1: S27-40. doi:10.1098/rsif.2009.0161.focus.
- Nagase, H., and J. F. Woessner, Jr. 1999. "Matrix Metalloproteinases." *J Biol Chem* 274: 21491-21494. doi:10.1074/jbc.274.31.21491.
- Nagase, H., and K. Brew. 2002. "Engineering of Tissue Inhibitor of Metalloproteinases Mutants as Potential Therapeutics." *Arthritis Res* 4 Suppl 3: S51-61. doi:10.1186/ar573.
- Naz, S., A. Gul, and M. Zia. 2020. "Toxicity of Copper Oxide Nanoparticles: A Review Study." *IET Nanobiotechnol* 14: 1-13. doi:10.1049/iet-nbt.2019.0176.
- Nerusu, K. C., R. L. Warner, N. Bhagavathula, S. D. McClintock, K. J. Johnson, and J. Varani. 2007. "Matrix Metalloproteinase-3 (Stromelysin-1) in Acute Inflammatory Tissue Injury." *Exp Mol Pathol* 83: 169-176. doi:10.1016/j.yexmp.2007.04.003.
- Netea, M. G., F. Balkwill, M. Chonchol, F. Cominelli, M. Y. Donath, E. J. Giamarellos-Bourboulis, D. Golenbock, M. S. Gresnigt, M. T. Heneka, H. M. Hoffman, R. Hotchkiss, L. A. B. Joosten, D. L. Kastner, M. Korte, E. Latz, P. Libby, T. Mandrup-Poulsen, A. Mantovani, K. H. G. Mills, K. L. Nowak, L. A. O'Neill, P. Pickkers, T. van der Poll, P. M. Ridker, J. Schalkwijk, D. A. Schwartz, B. Siegmund, C. J. Steer, H. Tilg, J. W. M. van der Meer, F. L. van de Veerdonk, and C. A. Dinarello. 2017. "A Guiding Map for Inflammation." *Nat Immunol* 18: 826-831. doi:10.1038/ni.3790.
- Nielsen, T. B., J. Yan, B. Luna, and B. Spellberg. 2018. "Murine Oropharyngeal Aspiration Model of Ventilator-Associated and Hospital-Acquired Bacterial Pneumonia." *J Vis Exp*, 10.3791/57672. doi:10.3791/57672.
- O'Regan, A., and J. S. Berman. 2000. "Osteopontin: A Key Cytokine in Cell-Mediated and Granulomatous Inflammation." *Int J Exp Pathol* 81: 373-390. doi:10.1046/j.1365-2613.2000.00163.x.
- O'Regan, A. 2003. "The Role of Osteopontin in Lung Disease." *Cytokine Growth Factor Rev* 14: 479-488. doi:10.1016/s1359-6101(03)00055-8.
- Ohta, H., S. Chiba, M. Ebina, M. Furuse, and T. Nukiwa. 2012. "Altered Expression of Tight Junction Molecules in Alveolar Septa in Lung Injury and Fibrosis." *Am J Physiol Lung Cell Mol Physiol* 302: L193-205. doi:10.1152/ajplung.00349.2010.

- Ophascharoensuk, V., C. M. Giachelli, K. Gordon, J. Hughes, R. Pichler, P. Brown, L. Liaw, R. Schmidt, S. J. Shankland, C. E. Alpers, W. G. Couser, and R. J. Johnson. 1999. "Obstructive Uropathy in the Mouse: Role of Osteopontin in Interstitial Fibrosis and Apoptosis." *Kidney Int* 56: 571-580. doi:10.1046/j.1523-1755.1999.00580.x.
- Pang, X., K. Gong, X. Zhang, S. Wu, Y. Cui, and B. Z. Qian. 2019. "Osteopontin as a Multifaceted Driver of Bone Metastasis and Drug Resistance." *Pharmacol Res* 144: 235-244. doi:10.1016/j.phrs.2019.04.030.
- Pardo, A., K. Gibson, J. Cisneros, T. J. Richards, Y. Yang, C. Becerril, S. Yousem, I. Herrera, V. Ruiz, M. Selman, and N. Kaminski. 2005. "Up-Regulation and Profibrotic Role of Osteopontin in Human Idiopathic Pulmonary Fibrosis." *PLoS Med* 2: e251. doi:10.1371/journal.pmed.0020251.
- Park, J. W., I. C. Lee, N. R. Shin, C. M. Jeon, O. K. Kwon, J. W. Ko, J. C. Kim, S. R. Oh, I. S. Shin, and K. S. Ahn. 2016. "Copper Oxide Nanoparticles Aggravate Airway Inflammation and Mucus Production in Asthmatic Mice Via Mapk Signaling." *Nanotoxicology* 10: 445-452. doi:10.3109/17435390.2015.1078851.
- Park, Y. H., D. Kim, J. Dai, and Z. Zhang. 2015. "Human Bronchial Epithelial Beas-2b Cells, an Appropriate in Vitro Model to Study Heavy Metals Induced Carcinogenesis." *Toxicol Appl Pharmacol* 287: 240-245. doi:10.1016/j.taap.2015.06.008.
- Pokutta, S., and W. I. Weis. 2007. "Structure and Mechanism of Cadherins and Catenins in Cell-Cell Contacts." *Annu Rev Cell Dev Biol* 23: 237-261. doi:10.1146/annurev.cellbio.22.010305.104241.
- Puntorieri, V., L. A. McCaig, C. J. Howlett, L. J. Yao, J. F. Lewis, C. M. Yamashita, and R. A. Veldhuizen. 2016. "Lack of Matrix Metalloproteinase 3 in Mouse Models of Lung Injury Ameliorates the Pulmonary Inflammatory Response in Female but Not in Male Mice." *Exp Lung Res* 42: 365-379. doi:10.1080/01902148.2016.1231243.
- Ra, H. J., and W. C. Parks. 2007. "Control of Matrix Metalloproteinase Catalytic Activity." *Matrix Biol* 26: 587-596. doi:10.1016/j.matbio.2007.07.001.
- Rangaswami, H., A. Bulbule, and G. C. Kundu. 2006. "Osteopontin: Role in Cell Signaling and Cancer Progression." *Trends Cell Biol* 16: 79-87. doi:10.1016/j.tcb.2005.12.005.
- Rao, V. H., G. E. Lees, C. E. Kashtan, D. C. Delimont, R. Singh, D. T. Meehan, G. Bhattacharya, B. R. Berridge, and D. Cosgrove. 2005. "Dysregulation of Renal Mmp-3 and Mmp-7 in Canine X-Linked Alport Syndrome." *Pediatr Nephrol* 20: 732-739. doi:10.1007/s00467-004-1805-5.
- Ren, G., D. Hu, E. W. Cheng, M. A. Vargas-Reus, P. Reip, and R. P. Allaker. 2009. "Characterisation of Copper Oxide Nanoparticles for Antimicrobial Applications." *Int J Antimicrob Agents* 33: 587-590. doi:10.1016/j.ijantimicag.2008.12.004.
- Richter, A. G., S. McKeown, S. Rathinam, L. Harper, P. Rajesh, D. F. McAuley, R. Heljasvaara, and D. R. Thickett. 2009. "Soluble Endostatin Is a Novel Inhibitor of Epithelial Repair in Idiopathic Pulmonary Fibrosis." *Thorax* 64: 156-161. doi:10.1136/thx.2008.102814.
- Rothen-Rutishauser, B., F. Blank, C. Muhlfeld, and P. Gehr. 2008. "In Vitro Models of the Human Epithelial Airway Barrier to Study the Toxic Potential of Particulate Matter." *Expert Opin Drug Metab Toxicol* 4: 1075-1089. doi:10.1517/17425255.4.8.1075.
- Rothen-Rutishauser, B. M., S. G. Kiama, and P. Gehr. 2005. "A Three-Dimensional Cellular Model of the Human Respiratory Tract to Study the Interaction with Particles." *Am J Respir Cell Mol Biol* 32: 281-289. doi:10.1165/rcmb.2004-0187OC.
- Russell, R. E., A. Thorley, S. V. Culpitt, S. Dodd, L. E. Donnelly, C. Demattos, M. Fitzgerald, and P. J. Barnes. 2002. "Alveolar Macrophage-Mediated Elastolysis: Roles of Matrix Metalloproteinases, Cysteine, and Serine Proteases." *Am J Physiol Lung Cell Mol Physiol* 283: L867-873. doi:10.1152/ajplung.00020.2002.

- Rygiel, K. A., H. Robertson, H. L. Marshall, M. Pekalski, L. Zhao, T. A. Booth, D. E. Jones, A. D. Burt, and J. A. Kirby. 2008. "Epithelial-Mesenchymal Transition Contributes to Portal Tract Fibrogenesis During Human Chronic Liver Disease." *Lab Invest* 88: 112-123. doi:10.1038/labinvest.3700704.
- Ryman-Rasmussen, J. P., E. W. Tewksbury, O. R. Moss, M. F. Cesta, B. A. Wong, and J. C. Bonner. 2009. "Inhaled Multiwalled Carbon Nanotubes Potentiate Airway Fibrosis in Murine Allergic Asthma." *Am J Respir Cell Mol Biol* 40: 349-358. doi:10.1165/rcmb.2008-0276OC.
- Samitas, K., E. Zervas, S. Vittorakis, M. Semitekolou, T. Alissafi, A. Bossios, H. Gogos, E. Economidou, J. Lotvall, G. Xanthou, V. Panoutsakopoulou, and M. Gaga. 2011. "Osteopontin Expression and Relation to Disease Severity in Human Asthma." *Eur Respir J* 37: 331-341. doi:10.1183/09031936.00017810.
- Samitas, K., E. Zervas, G. Xanthou, V. Panoutsakopoulou, and M. Gaga. 2013. "Osteopontin Is Increased in the Bronchoalveolar Lavage Fluid and Bronchial Tissue of Smoking Asthmatics." *Cytokine* 61: 713-715. doi:10.1016/j.cyto.2012.12.028.
- Scatena, M., M. Almeida, M. L. Chaisson, N. Fausto, R. F. Nicosia, and C. M. Giachelli. 1998. "Nf-Kappab Mediates Alphavbeta3 Integrin-Induced Endothelial Cell Survival." *J Cell Biol* 141: 1083-1093. doi:10.1083/jcb.141.4.1083.
- Scatena, M., L. Liaw, and C. M. Giachelli. 2007. "Osteopontin: A Multifunctional Molecule Regulating Chronic Inflammation and Vascular Disease." *Arterioscler Thromb Vasc Biol* 27: 2302-2309. doi:10.1161/ATVBAHA.107.144824.
- Schor, H., G. G. Vaday, and O. Lider. 2000. "Modulation of Leukocyte Behavior by an Inflamed Extracellular Matrix." *Dev Immunol* 7: 227-238. doi:10.1155/2000/51902.
- Semenzin, E., V. Subramanian, L. Pizzol, A. Zabeo, W. Fransman, C. Oksef, D. Hristozov, and A. Marcomini. 2019. "Controlling the Risks of Nano-Enabled Products through the Life Cycle: The Case of Nano Copper Oxide Paint for Wood Protection and Nano-Pigments Used in the Automotive Industry." *Environ Int* 131: 104901. doi:10.1016/j.envint.2019.06.011.
- Senger, D. R., S. R. Ledbetter, K. P. Claffey, A. Papadopoulos-Sergiou, C. A. Peruzzi, and M. Detmar. 1996. "Stimulation of Endothelial Cell Migration by Vascular Permeability Factor/Vascular Endothelial Growth Factor through Cooperative Mechanisms Involving the Alphavbeta3 Integrin, Osteopontin, and Thrombin." *Am J Pathol* 149: 293-305.
- Senger, D. R., and C. A. Perruzzi. 1996. "Cell Migration Promoted by a Potent Grgds-Containing Thrombin-Cleavage Fragment of Osteopontin." *Biochim Biophys Acta* 1314: 13-24. doi:10.1016/s0167-4889(96)00067-5.
- Shay, G., C. C. Lynch, and B. Fingleton. 2015. "Moving Targets: Emerging Roles for Mmps in Cancer Progression and Metastasis." *Matrix Biol* 44-46: 200-206. doi:10.1016/j.matbio.2015.01.019.
- Simoës, D. C., G. Xanthou, K. Petrochilou, V. Panoutsakopoulou, C. Roussos, and C. Gratziou. 2009. "Osteopontin Deficiency Protects against Airway Remodeling and Hyperresponsiveness in Chronic Asthma." *Am J Respir Crit Care Med* 179: 894-902. doi:10.1164/rccm.200807-1081OC.
- Snyder-Talkington, B. N., D. Schwegler-Berry, V. Castranova, Y. Qian, and N. L. Guo. 2013. "Multi-Walled Carbon Nanotubes Induce Human Microvascular Endothelial Cellular Effects in an Alveolar-Capillary Co-Culture with Small Airway Epithelial Cells." *Part Fibre Toxicol* 10: 35. doi:10.1186/1743-8977-10-35.
- Snyder-Talkington, B. N., C. Dong, X. Zhao, J. Dymacek, D. W. Porter, M. G. Wolfarth, V. Castranova, Y. Qian, and N. L. Guo. 2015. "Multi-Walled Carbon Nanotube-Induced Gene Expression in Vitro: Concordance with in Vivo Studies." *Toxicology* 328: 66-74. doi:10.1016/j.tox.2014.12.012.

- Sodek, J., B. Ganss, and M. D. McKee. 2000. "Osteopontin." *Crit Rev Oral Biol Med* 11: 279-303. doi:10.1177/10454411000110030101.
- Soltani, A., B. Khorramdel Vahed, A. Mardoukhi, and M. Mantysalo. 2016. "Laser Sintering of Copper Nanoparticles on Top of Silicon Substrates." *Nanotechnology* 27: 035203. doi:10.1088/0957-4484/27/3/035203.
- Sorokin, L. 2010. "The Impact of the Extracellular Matrix on Inflammation." *Nat Rev Immunol* 10: 712-723. doi:10.1038/nri2852.
- Sternlicht, M. D., A. Lochter, C. J. Sympson, B. Huey, J. P. Rougier, J. W. Gray, D. Pinkel, M. J. Bissell, and Z. Werb. 1999. "The Stromal Proteinase Mmp3/Stromelysin-1 Promotes Mammary Carcinogenesis." *Cell* 98: 137-146. doi:10.1016/s0092-8674(00)81009-0.
- Sternlicht, M. D., and Z. Werb. 2001. "How Matrix Metalloproteinases Regulate Cell Behavior." *Annu Rev Cell Dev Biol* 17: 463-516. doi:10.1146/annurev.cellbio.17.1.463.
- Strauch, B. M., R. K. Niemand, N. L. Winkelbeiner, and A. Hartwig. 2017. "Comparison between Micro- and Nanosized Copper Oxide and Water Soluble Copper Chloride: Interrelationship between Intracellular Copper Concentrations, Oxidative Stress and DNA Damage Response in Human Lung Cells." *Part Fibre Toxicol* 14: 28. doi:10.1186/s12989-017-0209-1.
- Suhaimi, S. A., S. C. Chan, and R. Rosli. 2020. "Matrix Metalloproteinase 3 Polymorphisms: Emerging Genetic Markers in Human Breast Cancer Metastasis." *J Breast Cancer* 23: 1-9. doi:10.4048/jbc.2020.23.e17.
- Szalay, G., M. Sauter, M. Haberland, U. Zuegel, A. Steinmeyer, R. Kandolf, and K. Klingel. 2009. "Osteopontin: A Fibrosis-Related Marker Molecule in Cardiac Remodeling of Enterovirus Myocarditis in the Susceptible Host." *Circ Res* 104: 851-859. doi:10.1161/CIRCRESAHA.109.193805.
- Takahashi, F., K. Takahashi, T. Okazaki, K. Maeda, H. Ienaga, M. Maeda, S. Kon, T. Uede, and Y. Fukuchi. 2001. "Role of Osteopontin in the Pathogenesis of Bleomycin-Induced Pulmonary Fibrosis." *Am J Respir Cell Mol Biol* 24: 264-271. doi:10.1165/ajrcmb.24.3.4293.
- Takahashi, K., F. Takahashi, K. K. Tanabe, H. Takahashi, and Y. Fukuchi. 1998. "The Carboxyl-Terminal Fragment of Osteopontin Suppresses Arginine-Glycine-Aspartic Acid-Dependent Cell Adhesion." *Biochem Mol Biol Int* 46: 1081-1092. doi:10.1080/15216549800204632.
- Tal Ben-Moshe, I. D., Brian Berkowitz. 2009. "Oxidation of Organic Pollutants in Aqueous Solutions by Nanosized Copper Oxide Catalysts." *Applied Catalysis B: Environmental* 85: 207-211. doi:10.1016/j.apcatb.2008.07.020.
- Tan, T. K., G. Zheng, T. T. Hsu, S. R. Lee, J. Zhang, Y. Zhao, X. Tian, Y. Wang, Y. M. Wang, Q. Cao, Y. Wang, V. W. Lee, C. Wang, D. Zheng, S. I. Alexander, E. Thompson, and D. C. Harris. 2013. "Matrix Metalloproteinase-9 of Tubular and Macrophage Origin Contributes to the Pathogenesis of Renal Fibrosis Via Macrophage Recruitment through Osteopontin Cleavage." *Lab Invest* 93: 434-449. doi:10.1038/labinvest.2013.3.
- Taylor, M. D., J. R. Roberts, A. F. Hubbs, M. J. Reasor, and J. M. Antonini. 2002. "Quantitative Image Analysis of Drug-Induced Lung Fibrosis Using Laser Scanning Confocal Microscopy." *Toxicol Sci* 67: 295-302. doi:10.1093/toxsci/67.2.295.
- Tepass, U. 2003. "Claudin Complexities at the Apical Junctional Complex." *Nat Cell Biol* 5: 595-597. doi:10.1038/ncb0703-595.
- Thompson, E. A., B. C. Sayers, E. E. Glista-Baker, K. A. Shipkowski, A. J. Taylor, and J. C. Bonner. 2014. "Innate Immune Responses to Nanoparticle Exposure in the Lung." *J Environ Immunol Toxicol* 1: 150-156. doi:10.7178/jeit.23.

- Tran, S., A. Ksajikian, J. Overbey, P. Li, and Y. Li. 2022. "Pathophysiology of Pulmonary Fibrosis in the Context of Covid-19 and Implications for Treatment: A Narrative Review." *Cells* 11. doi:10.3390/cells11162489.
- van den Berge, M., K. Steiling, W. Timens, P. S. Hiemstra, P. J. Sterk, I. H. Heijink, G. Liu, Y. O. Alekseyev, M. E. Lenburg, A. Spira, and D. S. Postma. 2014. "Airway Gene Expression in Copd Is Dynamic with Inhaled Corticosteroid Treatment and Reflects Biological Pathways Associated with Disease Activity." *Thorax* 69: 14-23. doi:10.1136/thoraxjnl-2012-202878.
- Van Hove, I., E. Lefevere, L. De Groef, J. Sergeys, M. Salinas-Navarro, C. Libert, R. Vandenbroucke, and L. Moons. 2016. "Mmp-3 Deficiency Alleviates Endotoxin-Induced Acute Inflammation in the Posterior Eye Segment." *Int J Mol Sci* 17. doi:10.3390/ijms17111825.
- Venter, C., and C. Niesler. 2018. "A Triple Co-Culture Method to Investigate the Effect of Macrophages and Fibroblasts on Myoblast Proliferation and Migration." *Biotechniques* 64: 52-58. doi:10.2144/btn-2017-0100.
- Verhoecx, K., P. Cotter, I. Lopez-Exposito, C. Kleiveland, T. Lea, A. Mackie, T. Requena, D. Swiatecka, and H. Wichers. (2015). *The Impact of Food Bioactives on Health: In Vitro and Ex Vivo Models*. Cham (CH).
- Visse, R., and H. Nagase. 2003. "Matrix Metalloproteinases and Tissue Inhibitors of Metalloproteinases: Structure, Function, and Biochemistry." *Circ Res* 92: 827-839. doi:10.1161/01.RES.0000070112.80711.3D.
- Wan, J., G. Zhang, X. Li, X. Qiu, J. Ouyang, J. Dai, and S. Min. 2021. "Matrix Metalloproteinase 3: A Promoting and Destabilizing Factor in the Pathogenesis of Disease and Cell Differentiation." *Front Physiol* 12: 663978. doi:10.3389/fphys.2021.663978.
- Wan, R., Y. Mo, X. Zhang, S. Chien, D. J. Tollerud, and Q. Zhang. 2008. "Matrix Metalloproteinase-2 and -9 Are Induced Differently by Metal Nanoparticles in Human Monocytes: The Role of Oxidative Stress and Protein Tyrosine Kinase Activation." *Toxicol Appl Pharmacol* 233: 276-285. doi:10.1016/j.taap.2008.08.022.
- Wan, R., Y. Mo, S. Chien, Y. Li, Y. Li, D. J. Tollerud, and Q. Zhang. 2011. "The Role of Hypoxia Inducible Factor-1alpha in the Increased Mmp-2 and Mmp-9 Production by Human Monocytes Exposed to Nickel Nanoparticles." *Nanotoxicology* 5: 568-582. doi:10.3109/17435390.2010.537791.
- Wan, R., Y. Mo, L. Feng, S. Chien, D. J. Tollerud, and Q. Zhang. 2012. "DNA Damage Caused by Metal Nanoparticles: Involvement of Oxidative Stress and Activation of Atm." *Chem Res Toxicol* 25: 1402-1411. doi:10.1021/tx200513t.
- Wan, R., Y. Mo, Z. Zhang, M. Jiang, S. Tang, and Q. Zhang. 2017. "Cobalt Nanoparticles Induce Lung Injury, DNA Damage and Mutations in Mice." *Part Fibre Toxicol* 14: 38. doi:10.1186/s12989-017-0219-z.
- Wang, K. X., and D. T. Denhardt. 2008. "Osteopontin: Role in Immune Regulation and Stress Responses." *Cytokine Growth Factor Rev* 19: 333-345. doi:10.1016/j.cytogfr.2008.08.001.
- Wang, P., X. Nie, Y. Wang, Y. Li, C. Ge, L. Zhang, L. Wang, R. Bai, Z. Chen, Y. Zhao, and C. Chen. 2013. "Multiwall Carbon Nanotubes Mediate Macrophage Activation and Promote Pulmonary Fibrosis through Tgf-Beta/Smad Signaling Pathway." *Small* 9: 3799-3811. doi:10.1002/smll.201300607.
- Wang, Y., X. Y. Zi, J. Su, H. X. Zhang, X. R. Zhang, H. Y. Zhu, J. X. Li, M. Yin, F. Yang, and Y. P. Hu. 2012a. "Cuprous Oxide Nanoparticles Selectively Induce Apoptosis of Tumor Cells." *Int J Nanomedicine* 7: 2641-2652. doi:10.2147/IJN.S31133.
- Wang, Z., N. Li, J. Zhao, J. C. White, P. Qu, and B. Xing. 2012b. "Cuo Nanoparticle Interaction with Human Epithelial Cells: Cellular Uptake, Location, Export, and Genotoxicity." *Chem Res Toxicol* 25: 1512-1521. doi:10.1021/tx3002093.

- Warner, R. L., L. Beltran, E. M. Younkin, C. S. Lewis, S. J. Weiss, J. Varani, and K. J. Johnson. 2001. "Role of Stromelysin 1 and Gelatinase B in Experimental Acute Lung Injury." *Am J Respir Cell Mol Biol* 24: 537-544. doi:10.1165/ajrcmb.24.5.4160.
- Woessner, J. F., Jr. 1998. "Role of Matrix Proteases in Processing Enamel Proteins." *Connect Tissue Res* 39: 69-73; discussion 141-149. doi:10.3109/03008209809023913.
- Wottrich, R., S. Diabate, and H. F. Krug. 2004. "Biological Effects of Ultrafine Model Particles in Human Macrophages and Epithelial Cells in Mono- and Co-Culture." *Int J Hyg Environ Health* 207: 353-361. doi:10.1078/1438-4639-00300.
- Wu, Z., P. Shi, H. K. Lim, Y. Ma, M. I. Setyawati, D. Bitounis, P. Demokritou, K. W. Ng, and C. Y. Tay. 2020. "Inflammation Increases Susceptibility of Human Small Airway Epithelial Cells to Pneumonic Nanotoxicity." *Small* 16: e2000963. doi:10.1002/sml.202000963.
- Wynn, T. 2008. "Cellular and Molecular Mechanisms of Fibrosis." *J Pathol* 214: 199-210. doi:10.1002/path.2277.
- Wynn, T. A. 2004. "Fibrotic Disease and the T(H)1/T(H)2 Paradigm." *Nat Rev Immunol* 4: 583-594. doi:10.1038/nri1412.
- Wynn, T. A., and T. R. Ramalingam. 2012. "Mechanisms of Fibrosis: Therapeutic Translation for Fibrotic Disease." *Nat Med* 18: 1028-1040. doi:10.1038/nm.2807.
- Xia, T., R. F. Hamilton, J. C. Bonner, E. D. Crandall, A. Elder, F. Fazlollahi, T. A. Girtsman, K. Kim, S. Mitra, S. A. Ntim, G. Orr, M. Tagmount, A. J. Taylor, D. Telesca, A. Tolic, C. D. Vulpe, A. J. Walker, X. Wang, F. A. Witzmann, N. Wu, Y. Xie, J. I. Zink, A. Nel, and A. Holian. 2013. "Interlaboratory Evaluation of in Vitro Cytotoxicity and Inflammatory Responses to Engineered Nanomaterials: The Niehs Nano Go Consortium." *Environ Health Perspect* 121: 683-690. doi:10.1289/ehp.1306561.
- Xu, L., M. Dan, A. Shao, X. Cheng, C. Zhang, R. A. Yokel, T. Takemura, N. Hanagata, M. Niwa, and D. Watanabe. 2015. "Silver Nanoparticles Induce Tight Junction Disruption and Astrocyte Neurotoxicity in a Rat Blood-Brain Barrier Primary Triple Coculture Model." *Int J Nanomedicine* 10: 6105-6118. doi:10.2147/IJN.S85265.
- Xu, M., Y. Wang, Z. Mu, S. Li, and H. Li. 2021. "Dissolution of Copper Oxide Nanoparticles Is Controlled by Soil Solution Ph, Dissolved Organic Matter, and Particle Specific Surface Area." *Sci Total Environ* 772: 145477. doi:10.1016/j.scitotenv.2021.145477.
- Yamashita, C. M., L. Dolgonos, R. L. Zemans, S. K. Young, J. Robertson, N. Briones, T. Suzuki, M. N. Campbell, J. Gauldie, D. C. Radisky, D. W. Riches, G. Yu, N. Kaminski, C. A. McCulloch, and G. P. Downey. 2011. "Matrix Metalloproteinase 3 Is a Mediator of Pulmonary Fibrosis." *Am J Pathol* 179: 1733-1745. doi:10.1016/j.ajpath.2011.06.041.
- Yamashita, C. M., D. C. Radisky, Y. Aschner, and G. P. Downey. 2014. "The Importance of Matrix Metalloproteinase-3 in Respiratory Disorders." *Expert Rev Respir Med* 8: 411-421. doi:10.1586/17476348.2014.909288.
- Ye, S., P. Eriksson, A. Hamsten, M. Kurkinen, S. E. Humphries, and A. M. Henney. 1996. "Progression of Coronary Atherosclerosis Is Associated with a Common Genetic Variant of the Human Stromelysin-1 Promoter Which Results in Reduced Gene Expression." *J Biol Chem* 271: 13055-13060. doi:10.1074/jbc.271.22.13055.
- Yokasaki, Y., and D. Sheppard. 2000. "Mapping of the Cryptic Integrin-Binding Site in Osteopontin Suggests a New Mechanism by Which Thrombin Can Regulate Inflammation and Tissue Repair." *Trends Cardiovasc Med* 10: 155-159. doi:10.1016/s1050-1738(00)00055-4.
- Yu, G., E. Kovkova-Naumovski, P. Jara, A. Parwani, D. Kass, V. Ruiz, C. Lopez-Otin, I. O. Rosas, K. F. Gibson, S. Cabrera, R. Ramirez, S. A. Yousem, T. J. Richards, L. J. Chensny, M. Selman, N. Kaminski, and A. Pardo. 2012. "Matrix Metalloproteinase-19 Is a Key Regulator of Lung

- Fibrosis in Mice and Humans." *Am J Respir Crit Care Med* 186: 752-762. doi:10.1164/rccm.201202-0302OC.
- Yu, M., Y. Mo, R. Wan, S. Chien, X. Zhang, and Q. Zhang. 2010. "Regulation of Plasminogen Activator Inhibitor-1 Expression in Endothelial Cells with Exposure to Metal Nanoparticles." *Toxicol Lett* 195: 82-89. doi:10.1016/j.toxlet.2010.02.010.
- Yuan, J., Y. Zhang, Y. Zhang, Y. Mo, and Q. Zhang. 2021. "Effects of Metal Nanoparticles on Tight Junction-Associated Proteins Via Hif-1alpha/Mir-29b/Mmps Pathway in Human Epidermal Keratinocytes." *Part Fibre Toxicol* 18: 13. doi:10.1186/s12989-021-00405-2.
- Yuksel, H., M. Ocalan, and O. Yilmaz. 2021. "E-Cadherin: An Important Functional Molecule at Respiratory Barrier between Defence and Dysfunction." *Front Physiol* 12: 720227. doi:10.3389/fphys.2021.720227.
- Zeisberg, E. M., O. Tarnavski, M. Zeisberg, A. L. Dorfman, J. R. McMullen, E. Gustafsson, A. Chandraker, X. Yuan, W. T. Pu, A. B. Roberts, E. G. Neilson, M. H. Sayegh, S. Izumo, and R. Kalluri. 2007. "Endothelial-to-Mesenchymal Transition Contributes to Cardiac Fibrosis." *Nat Med* 13: 952-961. doi:10.1038/nm1613.
- Zhang, Q., Y. Kusaka, K. Sato, K. Nakakuki, N. Kohyama, and K. Donaldson. 1998. "Differences in the Extent of Inflammation Caused by Intratracheal Exposure to Three Ultrafine Metals: Role of Free Radicals." *J Toxicol Environ Health A* 53: 423-438. doi:10.1080/009841098159169.
- Zhang, Q., Y. Kusaka, X. Zhu, K. Sato, Y. Mo, T. Kluz, and K. Donaldson. 2003. "Comparative Toxicity of Standard Nickel and Ultrafine Nickel in Lung after Intratracheal Instillation." *J Occup Health* 45: 23-30. doi:10.1539/joh.45.23.
- Zhang, Q., M. Zheng, C. E. Betancourt, L. Liu, A. Sitikov, N. Sladojevic, Q. Zhao, J. H. Zhang, J. K. Liao, and R. Wu. 2021a. "Increase in Blood-Brain Barrier (Bbb) Permeability Is Regulated by Mmp3 Via the Erk Signaling Pathway." *Oxid Med Cell Longev* 2021: 6655122. doi:10.1155/2021/6655122.
- Zhang, S., Q. An, T. Wang, S. Gao, and G. Zhou. 2018. "Autophagy- and Mmp-2/9-Mediated Reduction and Redistribution of Zo-1 Contribute to Hyperglycemia-Increased Blood-Brain Barrier Permeability During Early Reperfusion in Stroke." *Neuroscience* 377: 126-137. doi:10.1016/j.neuroscience.2018.02.035.
- Zhang, Y., Y. Mo, J. Yuan, Y. Zhang, L. Mo, and Q. Zhang. 2021b. "Mmp-3 Activation Is Involved in Copper Oxide Nanoparticle-Induced Epithelial-Mesenchymal Transition in Human Lung Epithelial Cells." *Nanotoxicology* 15: 1380-1402. doi:10.1080/17435390.2022.2030822.
- Zhao, M., L. Wang, M. Wang, S. Zhou, Y. Lu, H. Cui, A. C. Racanelli, L. Zhang, T. Ye, B. Ding, B. Zhang, J. Yang, and Y. Yao. 2022. "Targeting Fibrosis, Mechanisms and Cilinical Trials." *Signal Transduct Target Ther* 7: 206. doi:10.1038/s41392-022-01070-3.
- Zhao, X., J. Y. Y. Kwan, K. Yip, P. P. Liu, and F. F. Liu. 2020. "Targeting Metabolic Dysregulation for Fibrosis Therapy." *Nat Rev Drug Discov* 19: 57-75. doi:10.1038/s41573-019-0040-5.
- Zihni, C., C. Mills, K. Matter, and M. S. Balda. 2016. "Tight Junctions: From Simple Barriers to Multifunctional Molecular Gates." *Nat Rev Mol Cell Biol* 17: 564-580. doi:10.1038/nrm.2016.80.
- Zou, J., Y. Li, J. Yu, L. Dong, A. N. Husain, L. Shen, and C. R. Weber. 2020. "Idiopathic Pulmonary Fibrosis Is Associated with Tight Junction Protein Alterations." *Biochim Biophys Acta Biomembr* 1862: 183205. doi:10.1016/j.bbamem.2020.183205.

CURRICULUM VITAE

Yuanbao Zhang

Address: Department of Epidemiology and Population Health
School of Public Health and Information Sciences
University of Louisville
511 S. Floyd St.
MDR-room 205
Louisville, KY 40202

E-Mail: Y0ZHAN66@louisville.edu

Education

- ❖ Doctor of Philosophy in Public Health Sciences - Environmental Health, 08/2018-Now
University of Louisville
- ❖ Master of Science – Environmental and Occupational Health, 09/2012-06/2015
Beijing Municipal Institute of Labor Protection
- ❖ Bachelor of Medicine - Preventive Medicine, 09/2007-06/2012
Anhui Medical University

Fellowships

- ❖ 2018-2020 GRA, Department of Environmental and Occupational Health Sciences, University of Louisville
- ❖ 2015-2018 Research fellowship, Beijing Municipal institute of Labour protection

Professional Experience

- ❖ University of Louisville, 2018-Now
 1. Investigated the mechanisms underlying Nano-CuO-induced pulmonary fibrosis

2. Explored the roles of MMP-3 in metal oxide nanoparticle-induced pulmonary toxicity in vitro and in vivo
 3. Examined the toxic effects of metal oxide nanoparticles on BEAS-2B and U937 cells
- ❖ Beijing Municipal Institute of Labor Protection, 2012-2015
 1. Examined the exposure characteristic of metal oxide nanoparticles in workplace
 2. Explored the biological safety assessment of manufactured nanomaterials
 3. Participated in establishing the standard exposure assessment method of nanoparticles

Honors

- ❖ 1st place, Graduate Student Award, Research!Louisville, University of Louisville (2021)

Publications

- ❖ Book Chapters
 1. Zhao P, **Zhang YB**. The Overview of Methods of Nanoparticle Exposure Assessment. *Methods Mol Biol.* 2019;1894:353-367.
- ❖ Journal Articles
 1. Yuan J, Mo Y, **Zhang YB**, Zhang Y, Zhang Q. Nickel nanoparticles induce epithelial-mesenchymal transition in human bronchial epithelial cells via the HIF-1 α /HDAC3 pathway. *Nanotoxicology*, 2022, in press.
 2. Yuan JL, Mo L, Mo YQ, **Zhang YB**, Zhang Y, Zhang QW. A protective role of autophagy in fine airborne particulate matter-induced apoptosis in LN-229 cells. *Toxicology.* 2022;477:153271.
 3. **Zhang YB**, Mo YQ, Yuan JL, Zhang Y, Mo L, Zhang QW. MMP-3 activation is involved in copper oxide nanoparticle-induced epithelial-mesenchymal transition in human lung epithelial cells. *Nanotoxicology.* 2021;15(10):1380-1402.
 4. Mo YQ, Zhang Y, **Zhang YB**, Yuan JL, Mo L, Zhang QW. Nickel nanoparticle-induced cell transformation: involvement of DNA damage and DNA repair defect through HIF-1 α /miR-210/Rad52 pathway. *J Nanobiotechnology.* 2021;19(1):370.
 5. Yuan JL, Zhang Y, **Zhang YB**, Mo YQ, Zhang QW. Effects of metal nanoparticles on tight junction-associated proteins via HIF-1 α /miR-

- 29b/MMPs pathway in human epidermal keratinocytes. Part Fibre Toxicol. 2021;18(1):13.
6. Wang YQ, Chen R, Zhou XF, Jin SB, **Zhang YB**, Xu ZZ, Guo L, Tang SC. Risk Assessment of Nanoparticle Exposure in a Calcium Carbonate Manufacturing Workshop with Six Control Banding Tools. J Nanosci Nanotechnol. 2020;20(6):3610-3619.
 7. Tang SC, Zhu P, Yu M, **Zhang YB**. Application of control banding to occupational hazard management in nanotechnology industry. Journal of Environmental and Occupational Medicine, 2017, 34(6): 555 - 549.
 8. Xu ZZ, Zhao P, **Zhang YB**, Tang SC . Research progress review in the toxic effects of the engineering nanomaterials on the typical organisms. Journal of safety and environment, 2017, 02-0786-07.
 9. **Zhang YB**, Xu ZZ, Tang SC, Zhao P. Research progress on the measurement methods of ambient ultrafine (nano) particles. Asian Journal of Ecotoxicology. 2017, 12(5): 64-71.
 10. **Zhang YB**, Zhao P, Xu ZZ, Tang SC. Research progress of nanoparticles impact on male reproductive system. Asian Journal of Ecotoxicology, 2016, 11(1):111-116.
 11. Xing ML, **Zhang YB**, Zou H, Chang B, Tang SC, Zhang MB. Exposure characteristics of ferric oxide nanoparticles released during activities for manufacturing ferric oxide nanomaterials. Inhal Toxicol. 2015;27(3):138-148.
 12. **Zhang YB**, Fu ZH, Wang YQ, Zhao P, Xing ML, Zhang MB, Tang SC. An analysis of characteristics of exposure to nanoparticles in a workplace manufacturing iron oxide nanoparticle. Zhonghua Lao Dong Wei Sheng Zhi Ye Bing Za Zhi. 2015;33(6):427-429.
 13. Wang YQ, **Zhang YB**, Zhao P, Xu ZZ, Tang SC. Exposure patterns and Health Effects of Nanometer Calcium Carbonate in a Manufacturer. Journal of Environmental and Occupational Medicine. 2015, 32(10):903-908.

Manuscripts in preparation:

1. **Zhang YB**, Mo Y, Yuan J, Zhang Y, Zhang Q. MMP-3-mediated cleavage of osteopontin is involved in copper oxide nanoparticle-induced activation of fibroblasts.
2. **Zhang YB**, Mo Y, Yuan J, Zhang Y, Zhang Q. MMP-3 mediates copper oxide nanoparticle-induced pulmonary inflammation and fibrosis.

Presentations

1. **Zhang YB**, Mo YQ, Yuan JL, Zhang QW. MMP-3-mediated cleavage of osteopontin is involved in copper oxide nanoparticle-induced activation of fibroblasts, Research!Louisville, September, 2022
2. Mo YQ, Yuan JL, **Zhang YB**, Zhang QW. Nickel nanoparticles induce epithelial-mesenchymal transition in human bronchial epithelial cells via the HIF-1 α /HDAC3 pathway, Research!Louisville, September, 2022
3. **Zhang YB**, Mo YQ, Yuan JL, Zhang QW. MMP-3 activation is involved in copper oxide nanoparticle-induced epithelial-mesenchymal transition in human lung epithelial cells, Research!Louisville, October, 2021
4. Mo YQ, **Zhang YB**, Yuan JL, Zhang QW. Nickel nanoparticle-induced cell transformation: involvement of DNA damage and DNA repair defect through HIF-1 α /miR-210/Rad52 pathway, Research!Louisville, October, 2021
5. Yuan JL, Mo YQ, **Zhang YB**, Zhang QW. The role of mitochondrial ROS generation and JNK activation in fine airborne particulate matter (PM_{2.5}) - induced autophagy and apoptosis in LN-229 cell, Research!Louisville, October, 2021

Volunteer and community Work

1. 2022 Leader Judge, Kentucky Science & Engineering Fair, KY
2. 2019-2021 Judge, Kentucky Science Fair, KY